YMEP 2021-071

URSA PROPERTY

Mayo Mining District, Yukon Territory
NTS: 105O12

Latitude 63° 44' N, Longitude 133° 55' W

2021 - Sample # Ursa 009

Prepared for:

SNOWLINE GOLD Corp.
Field work performed on Aug. 30th, 2021
Airborne survey performed between Sept. 8th and Sept. 14th, 2021
Submitted of March 9th, 222

By: Jérôme de Pasquale

Owner:
SENOA GOLD Corp.

Summary

The Ursa project sits in the Selwyn Basin and shares similar stratigraphy with world-class base metal districts such as Howard's Pass (400.7 Mt @ 4.5% Zn, 1.5% Pb) and the Anvil district (120 Mt @ 5.6% Zn, 3.7% Pb, 45 g/t Ag) as well as important gold deposits (Jennings, 1986; Emsbo, 2000).

In 2021, a helicopter-supported airborne VTEM survey was conducted over the Ursa property. Survey lines were flown in a southwest to northeast orientation at 200 metre line spacings and tie lines flown perpendicular to the traverse lines at 2000 metre line spacings. Multiple southeast-northwest trends have been identified, consistent with stratigraphic and structural control. These data provide a baseline for tracking prospective sulphide rich shale horizons. The VTEM survey results raise questions that require data re-interpretation and potentially additional geology and structural mapping.

A field visit, combining soil sampling and XRF measurements, was conducted to evaluate the influence of the rock-size fraction in the elemental distribution. Fine and coarse fractions of rocky soils were analysed separately by geochemical analysis. Sixty elements were analyzed including Rare Earth Elements (REE). The fine rock fraction analysis returned significant higher values than the coarse fraction in silver and various base metal elements of interest as well as elements considered as pathfinders. These preliminary observations suggest that sampling at the Ursa property necessitates a well-established protocol to provide relevant and interpretable data. It also suggests that the potential of the property may have been overlooked by previous operators, as non-mineralized cherty layers and other resistant units provide easier targets for rock sampling, thus introducing a bias towards non-mineralized rocks. Additionally, the presence of high zinc, silver and base metal values suggest that historical stream and sediment data showing similar anomalies are likely reliable.

Contents

Table of figures

Table of tables

Table of photos

1 INTRODUCTION

Senoa Gold's "Ursa" property is located on the west side of the Hess River, east of the Rogue River in the central Yukon Territory, 250 km east of Mayo, 25 km from the Northwest Territories border.

The claims were staked to cover a large multi-base metal stream anomaly along a southeast-northwest trend running parallel to geological bedding and structures.

The 2021 exploration program consisted of 439 km Airborne VTEM survey and field work to define an experimental methodology based on X-Ray Fluorescence (XRF) in-situ field measurement and geochemical analysis.

The current report described the 2021 exploration program and results.

2 WORK HISTORY

1981, Noranda Exploration Company Ltd.
- Staking
- Bedrock mapping

1991-1992, Kennecott Canada Inc.
- Staking
- Bedrock mapping
- Geochemical survey

2008, 18526 Yukon Inc.
- Staking
- Silt/stream sediment sampling
- Prospecting/rock sampling

2011, Golden Predator Corp.
- Silt/stream sediment sampling

2012, Golden Predator Corp.
- Soil sampling

2013, 18526 Yukon Inc.
- Soil sampling

2017, Rio Tinto
- Cursory visit
- Soil and rock sampling

3 PROPERTY INFORMATION

The Ursa property presently consists of 367 quartz claims. All claims are registered with the Mayo Mining Recorder in the name of Senoa Gold Corp. (Table 1 and Figure 1).

Claim Name	Grant number	Owner
UR 1 - 200	YE51401 - YE51600	Senoa Gold Corp. 100%
UR 201 - 360	YE51801 - YE51960	Senoa Gold Corp. 100%
F 637	YD106651	Senoa Gold Corp. 100%
F 639	YD106653	Senoa Gold Corp. 100%
F 641	YD106655	Senoa Gold Corp. 100%
F 643	YD106657	Senoa Gold Corp. 100%
F 749	YD106763	Senoa Gold Corp. 100%
F 751	YD106765	Senoa Gold Corp. 100%
F 753	YD106767	Senoa Gold Corp. 100%

Table 1: Ursa Claim Tenure Information

3.1 LOCATION AND ACCESS

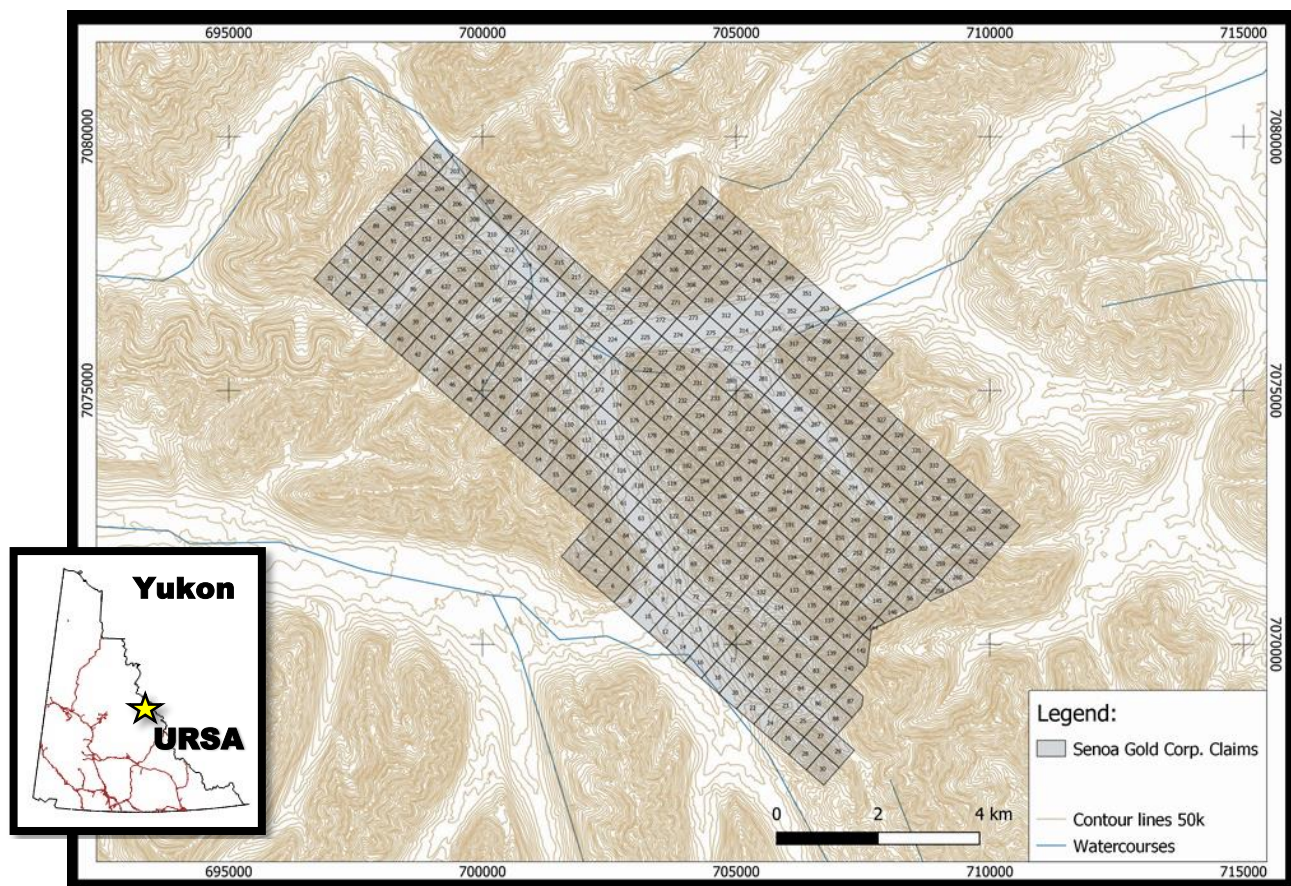*Figure 1: Ursa Project Claim Map*

The Ursa property is located 344 km east of Mayo, 12 km east of the Rogue River 17 km west of the Hess River watershed, 65 km north-west of the MacMillan pass, in the Mayo Mining District, on NTS105O10, 105O11, 105O14, 105O15 at 63° 44' N latitude, 130° 55' W longitude.

Algae Lake sits in the north-east corner of the claim block. The lake is suitable for float planes.

Access to the 2021 field program was provided by Horizon Helicopter out of the Anthill Lake base camp. Fireweed Zinc provided accommodation for the geophysics crew from their camp at Macmillan Pass.

3.2 CLIMATE

(From *Ecoregions of the Yukon Territory: Biophysical properties of Yukon landscapes*, Smith C. A. S. et al., 2004)

This ecoregion is located on the western slopes of the continental divide between the Yukon and Northwest Territories. Seasonal variations and the effect of elevation result in a complex climate. Mean annual temperatures are believed to range from –5 to –8°C. Mean temperatures are expected to be near –20°C in January, and 5 to 10°C in July.

Summer temperatures are lower in summer at the higher elevations. Temperature extremes in January in the valley floors can range from –55 to 3°C, but over the higher terrain temperatures would probably range from –30 to –5°C. In July, extremes would range from –5 to 30°C in the valley floor and from –5 to 15°C over higher terrain. Frost can be expected at any time of the year.

Seasonal variations and the effect of elevation result in a complex climate. Precipitation is moderate and locally heavy with annual amounts of 600 to 700 mm. The winter months have mean amounts of 30 to 50 mm with the least amounts from February to April. The wettest months are July and August with rainfall amounts of 60 to 90 mm.

The Selwyn Mountains Ecoregion is in the widespread discontinuous permafrost zone. Soils in this rugged, high-elevation ecoregion have formed under the influence of a relatively moist, continental climate on a variety of geologic parent materials. Mountain summits and ridges are characterized by bedrock outcrops and shallow soil over bedrock. Coarse colluvium associated with felsenmeer supports Regosol formation. North facing slopes and seepage areas tend to be underlain by permafrost.

3.3 PHYSIOGRAPHY

(From *Ecoregions of the Yukon Territory: Biophysical properties of Yukon landscapes*, Smith et al., 2004)

The Ursa property is located within the Taiga Cordillera Ecozone.

Elevations rise from 1,200 m to 2140 m. Lakes are found occasionally throughout the ecoregion but are more common in the broader valleys between the Hess and Logan mountains. Alpine landforms such as horns and arêtes are common in this area. Significant accumulations of glacial sediments are present only in the bottoms of major valleys where moraine and glaciofluvial deposits can be found.

Upper slopes and side valleys are blanketed with Holocene colluvium deposits of various thickness and particle size. This ecoregion is located on the western slopes of the continental divide between the Yukon and Northwest Territories.

There are some extensive wetlands in major valley systems. Sedge-dominated wetlands, or fens, are often without permafrost.

Valleys and middle to lower slopes are forested Alpine ridges and peaks are sparsely vegetated. The vegetation composition of alpine areas varies greatly within short distances due to microtopography, microclimate and changes in bedrock lithology. The more nutrient-rich limestones and carbonate-rich shales host different plant assemblages, including more forbs (dryas, anemone and gentian) than the more acidic bedrock types. Lichen-grass communities with lots of exposed soil and rock dominate the most extreme sites at high elevations. Dwarf shrub communities are common on slopes and ridges between 1,200 and 1,800 m, occupying slightly moister sites than the lichen dominated communities. White mountain heather, crowberry and alpine blueberry, grass, sagewort, gentian, feathermoss, Cetraria and reindeer lichens are the typical plants found in these areas.

Photo 1: Ursa landscape and geomorphology. On the front, the black shale unit forms scree slopes and saddles. An outfitter lodge (Rogue River Outfitters) is located at the far end of the Algae Lake (right side, background).

Rock lichen colonizes scree slopes (Photo 1). Shrub birch–willow communities dominate much of the subalpine including many colluvial slopes, coarser deposits of subalpine valleys, and gentle moraine slopes in the northern part of the ecoregion along the Northwest Territories border (Department of Renewable Resources, 1981). Shrub birch has an understory of alpine blueberry, crowberry, feathermoss and lichens, with willow on moister sites.

On dry southerly exposures, sparse patches of fir krummholz form. Black spruce predominates at lower elevations through much of the ecoregion. In the valleys, patches of white and black spruce, subalpine fir, and mixed stands are interspersed with shrubland and wetlands.

3.4 GEOLOGY

Most of the geology is extracted from *Geology of the Northeastern Niddery Lake Map Area, East-Central Yukon and Adjacent Northwest Territories,* Cecile (2000).

Cecile has two Earn Group formations (Misfortune and Thor hills), which, combined, are "roughly equivalent" with the Portrait Lake Formation of the Earn Group elsewhere (Figure 2). The Misfortune Formation is continuous with the Canol formation and is included in the lower part of the Earn Group (Moynihan, D., pers. Comm.).

Both the upper Misfortune and Canol formations are interpreted as deep-water, organic-rich shales deposited during the early stage of foredeep basin development ('starved-basin facies').
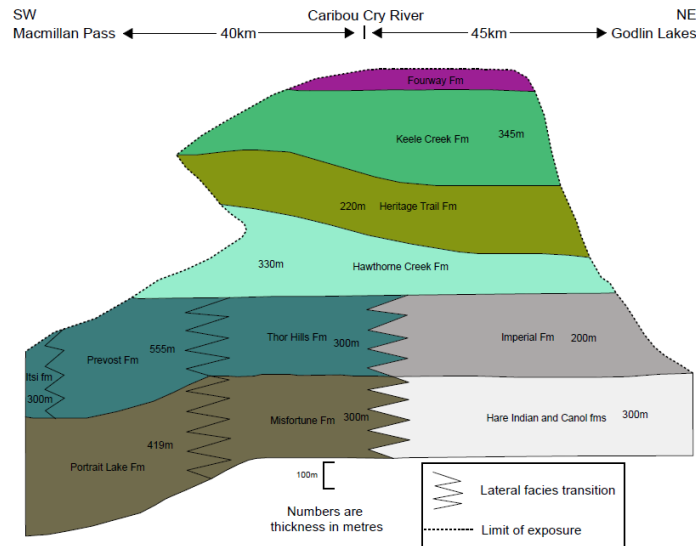
Figure 2: Schematic relationships among Earn Group (and equivalent units) and Tsichu Group in the western Mackenzie Mountains. Adapted from Gordey and Anderson (1993) and Cecile (2000), with additional Sekwi Project data (extracted from Martel. E. et al., 2011)

The type-section is described as follow:

- the lower member consists of 170 m of black shale with limonitic weathering and minor siltstone. In the upper part of the lower member are 10 to 20 percent lithic sandstone with chert, quartz, and argillite clasts.
- The upper member is a more resistant white-ish weathering, black siliceous shale with minor (centimetre to metre scale) lithic sandstone and chert pebble conglomerate.

To the northeast, the Misfortune Formation lithologies becomes more siliceous and contains chert successions to the southwest.

3.4.1   Regional Geology

The Selwyn Basin is a large northwest trending Paleozoic deep water sedimentary basin that extends for 1000's of km from Alaska, through the Yukon and western Northwest Territories (NWT) and into northern British Columbia (Goodfellow, 2007). The Selwyn Basin is mainly composed of black shales and cherts of Ordovician to Devonian age. It is unconformably underlain by Hadrynian-Cambrian-age basement grit rocks that form part of the continental margin. Lithologies consist of a lower section of Early Ordovician to Early Devonian mudstones, siltstones, carbonates, chert, and minor sandstone (Figure 3). The upper section consists of Devonian to Mississippian and Early Triassic mudstones and siltstones, with more abundant sandstones and conglomerates. The Selwyn Basin rocks were deformed and metamorphosed during the Mesozoic. Cretaceous granitoid intrusions also occurred during this tectonic event. Except for fold and thrust deformation and metamorphism to greenschist facies, the Selwyn Basin is relatively well preserved (Goodfellow, 2007).
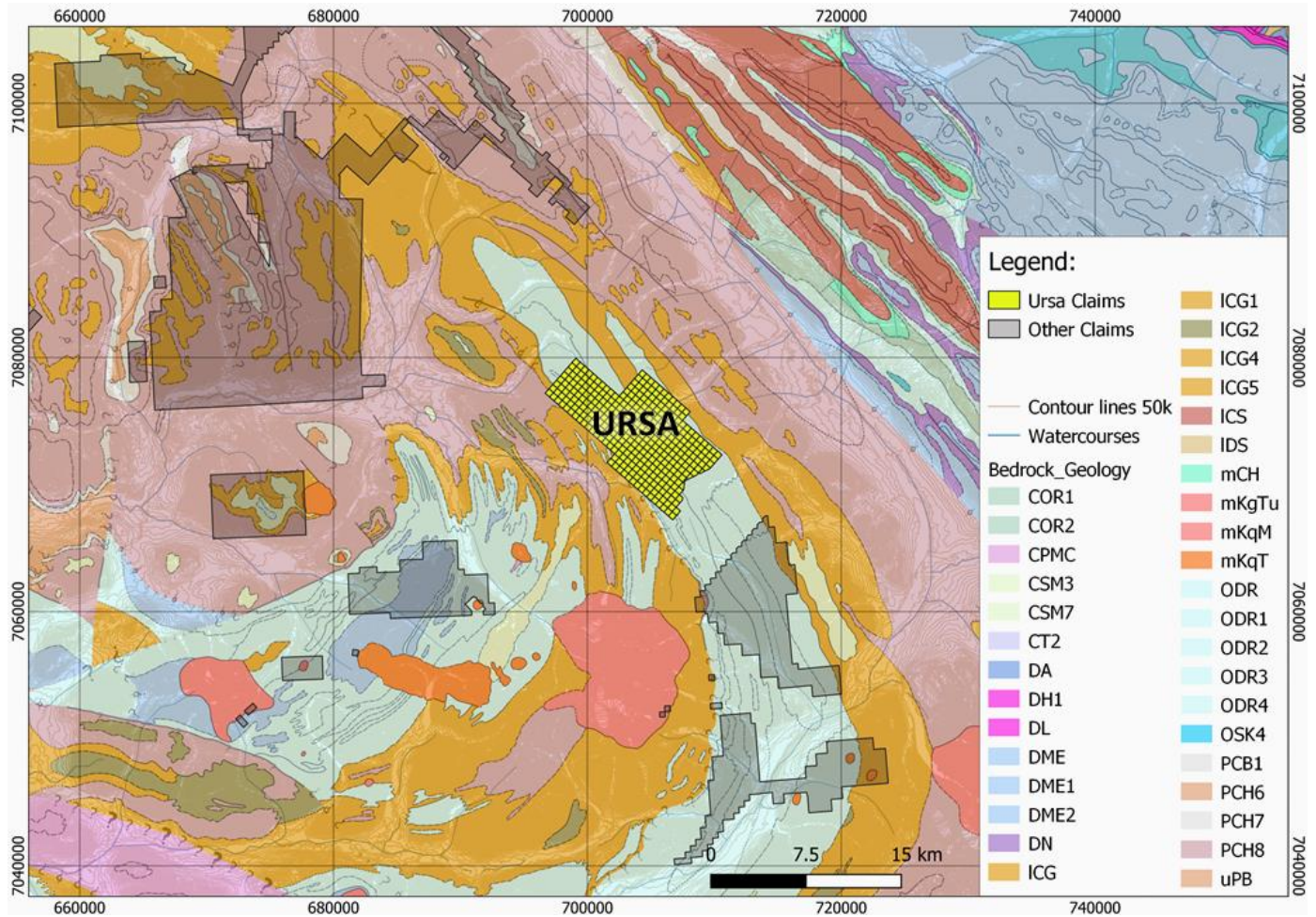
Figure 3: Ursa claim block and Regional Geology map (for detailed legend, see Figure 5)

3.4.2   Local Geology

According to the Yukon Bedrock Geology map (2016), two main formations from the Road River Group are encountered at the Ursa Property. The formations are described by Cecile as follow:

- Steel Formation: thin to thick bedded, siliceous, dark grey mudstone that weathers yellowish brown, dull olive grey, or dark yellowish brown. Thin bedding and lack of shallow-water features suggest deposition of the Steel Formation in relatively deep water.
- Gull Lake Formation: green and maroon argillites with quartzite and limestone. The Gull Lake Formation in the Niddery Lake map area is considered to be a relatively deep-water unit on the basis of its graded bedding, dominance of fine grain size, and its facies position.

The Steel formations lie within the Rogue Décollement Complex. In the Rogue Décollement Complex shortening is intense (80%) and accommodated along numerous inter-stratal décollements. Because of composition and competency differences, strain varies widely from unit to unit. In order to restore and characterize the stratigraphy of units, Cecile defined "tectonostratigraphic units" where type traverse is measured through a nearly continuous exposure over part of the décollement complex using biostratigraphy and lithological characteristics, together with distinct special features like bioturbation, rare limestone occurrences, and observations of actual structures, structural cross-sections. From the structural cross-sections, stratigraphic successions were established and a composite type section of the Elmer Creek Formation, as well as a reference section for the Steel Formation, were compiled.
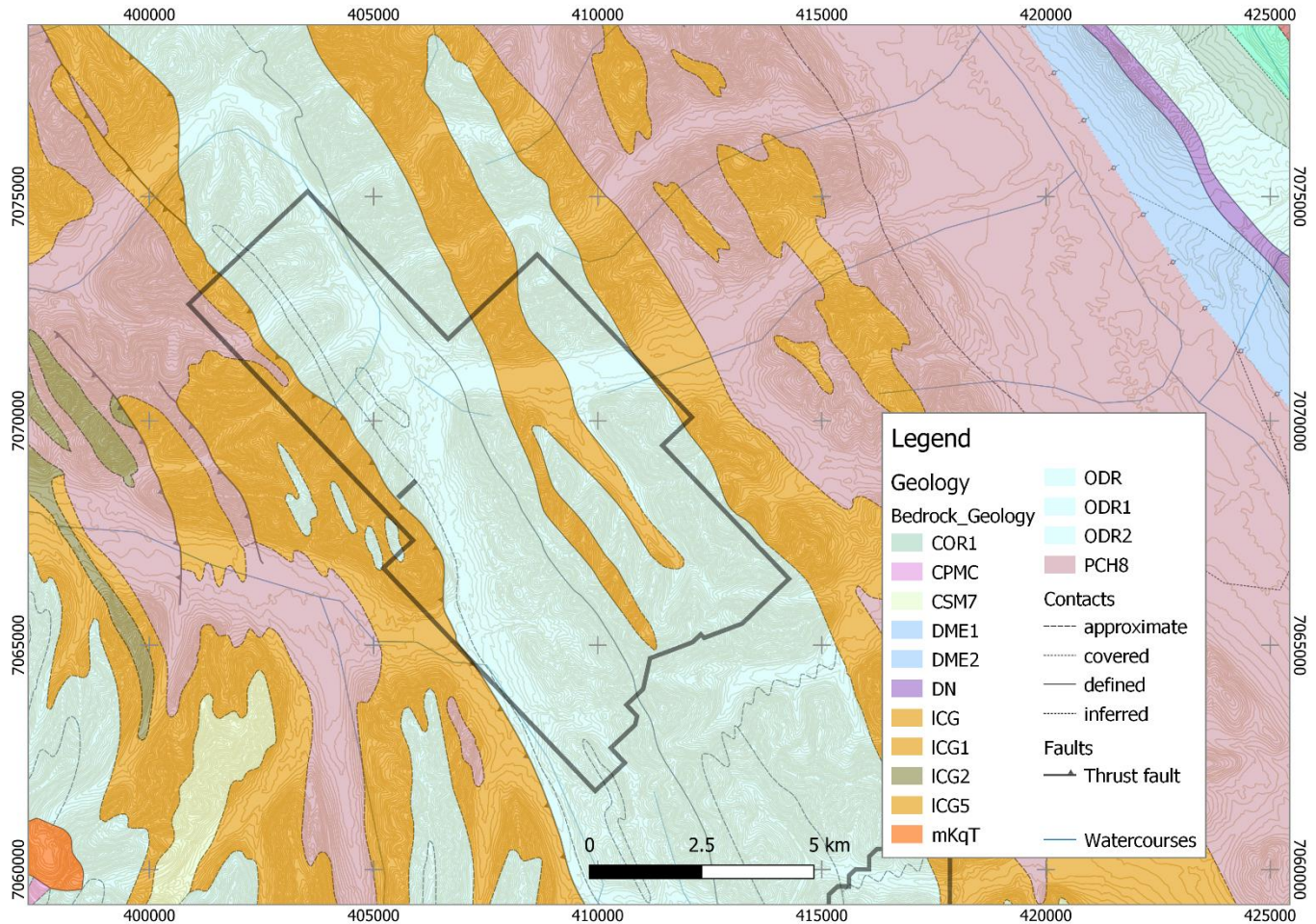
Figure 4: Ursa Property Geology Map. YGS, 2021 (for detailed legend, see Figure 5).

Tectonostratigraphic map unit concept (from Cecile, M.P., 2000):

"Although the stratigraphy can be locally resolved for the décollement complex, for practical mapping purposes, map units in the Rogue Décollement must include a mixture of formational units. Because of the dominance of shallow local detachments, large areas of the décollement complex are dominated by structural repetitions of one formation. To accommodate this circumstance the "tectonostratigraphic map unit" was established. A tectonostratigraphic map unit is here defined as an area of outcrop with complex structural repetition that contains more than 50 per cent of the formation from which it derives its name and includes some outcrops of older and younger units repeated in fold hinges or on thrust faults. In practice, most areas mapped in the study area as the Elmer Creek Tectonostratigraphic Unit are more than 80 per cent Elmer Creek Formation, and more than 60 per cent of the Steel Tectonostratigraphic Unit is Steel Formation."

On the east side of the Ursa property, geology consists in a sequence of heavily folded carbonaceous black shales and cherts. The carbonaceous, passive margin shales have been compressed into a tight anticlinorium and later intruded in their vicinities by felsic plutons. In the Ursa area, these plutons are members of the Tombstone plutonic suite.

To clarify the terminology used by Cecile (2000) and the apparent discrepancy with the actual Yukon bedrock Geology map, the original "Dc" unit from Cecile was assigned to the Earn Group/Misfortune Formation. It is currently assigned to the Road River/Steel Formation. However, the Rogue decollement Complex justify the tectonostratigraphic method used by Cecile justify the presence of slabs of Earn Group within the Road River Group.

Photo 2: Rusty weathering, pyritic siltstone (Steel Formation) at the Ursa Property. This unit is less recessive than the black shale and forms relief in the landscape.

mKgM: MAYO SUITE: Hbl > Bt (± Cpx) quartz monzonite or monzodiorite

mKgTu: TUNGSTEN SUITE: K-feldspar porphyritic Bt monzogranite and leucogranite

mKgT: TOMBSTONE SUITE: quartz monzonite, granodiorite, quartz diorite

CT2: TSICHU/KENO HILL: black to silvery shale or carbonaceous phyllite

CPMC: MOUNT CHRISTIE: burrowed, interbedded greenish grey cherty shale and green shale

DME: EARN: black siliceous shale and chert

DME1: EARN: laminated slate, fine to medium-grained chert-quartz arenite and wacke

DME2: EARN: silvery blue weathering black shale, argillite, cherty argillite and chert

DN: NATLA: dark grey weathering, platy, thin-bedded, recessive sooty limestone

DH1: HEADLESS: buff-brown weathering argillaceous to silty, fine-grained limestone

DL: LANDRY: thin to very thick bedded, resistant, crypto-grained limestone

DA: ARNICA: dark grey to black commonly laminated dolostone

IDC: CAMSELL: grey, black, and white weathering dolostone

ODR: ROAD RIVER - SELWYN: black shale and chert, dolomitic siltstone, calcareous shale, buff platy limestone

ODR1: DUO LAKE/ELMER CREEK - SELWYN: black graptolitic shale and black chert

ODR2: STEEL - SELWYN: rusty dark green to orange buff weathering argillite and dolomitic siltstone

ODR3: SAPPER - SELWYN: blue-grey weathering, black limestone

ODR4: ROAD RIVER - SELWYN: black shale, limestone, limestone conglomerate

OSK4: MOUNT KINDLE: thick-bedded dolostone and limestone, fetid limestone

CSM3: DEMPSTER: mafic volcanic flows, tuff and hyaloclastic breccia

CSM7: MARMOT: basic lapilli tuff, breccia, flows, sills, and dikes

COR1: RABBITKETTLE: thin-bedded, silty limestone and grey lustrous calcareous phyllite

COR2: RABBITKETTLE: thin-bedded, silty limestone and grey lustrous calcareous phyllite

mCH: HESS RIVER: shale, black, pyritic, unfossiliferous

ICG: GULL LAKE: undivided - shale, siltstone, sandstone, conglomerate, limestone

ICG1: GULL LAKE: shale, siltstone and mudstone, minor quartz sandstone

ICG2: GULL LAKE: mafic metavolcanic and volcaniclastic rocks

ICG4: GULL LAKE: conglomerate, quartzite, argillite, brown-weathering sandstone

ICG5: GULL LAKE: shale, limestone, limestone conglomerate (incl. Ordovician strata)

ICS: SEKWI: limestone, locally wavy bedded and nodular

PCB1: BACKBONE: thick-bedded, medium to coarse-grained orthoquartzite

PCH6: YUSEZYU: upper - brown to pale green shale, quartz-rich sandstone, grit, pebble conglomerate

PCH7: ALGAE: grey weathering, very fine crystalline limestone, locally sandy

PCH8: NARCHILLA: interbedded maroon and apple-green slate, siltstone, sandstone

uPB: BLUEFLOWER: undivided fine-grained siliciclastic and carbonate rocks, locally conglomerate

Figure 5: Yukon Bedrock Geology Legend from YGS, 2016
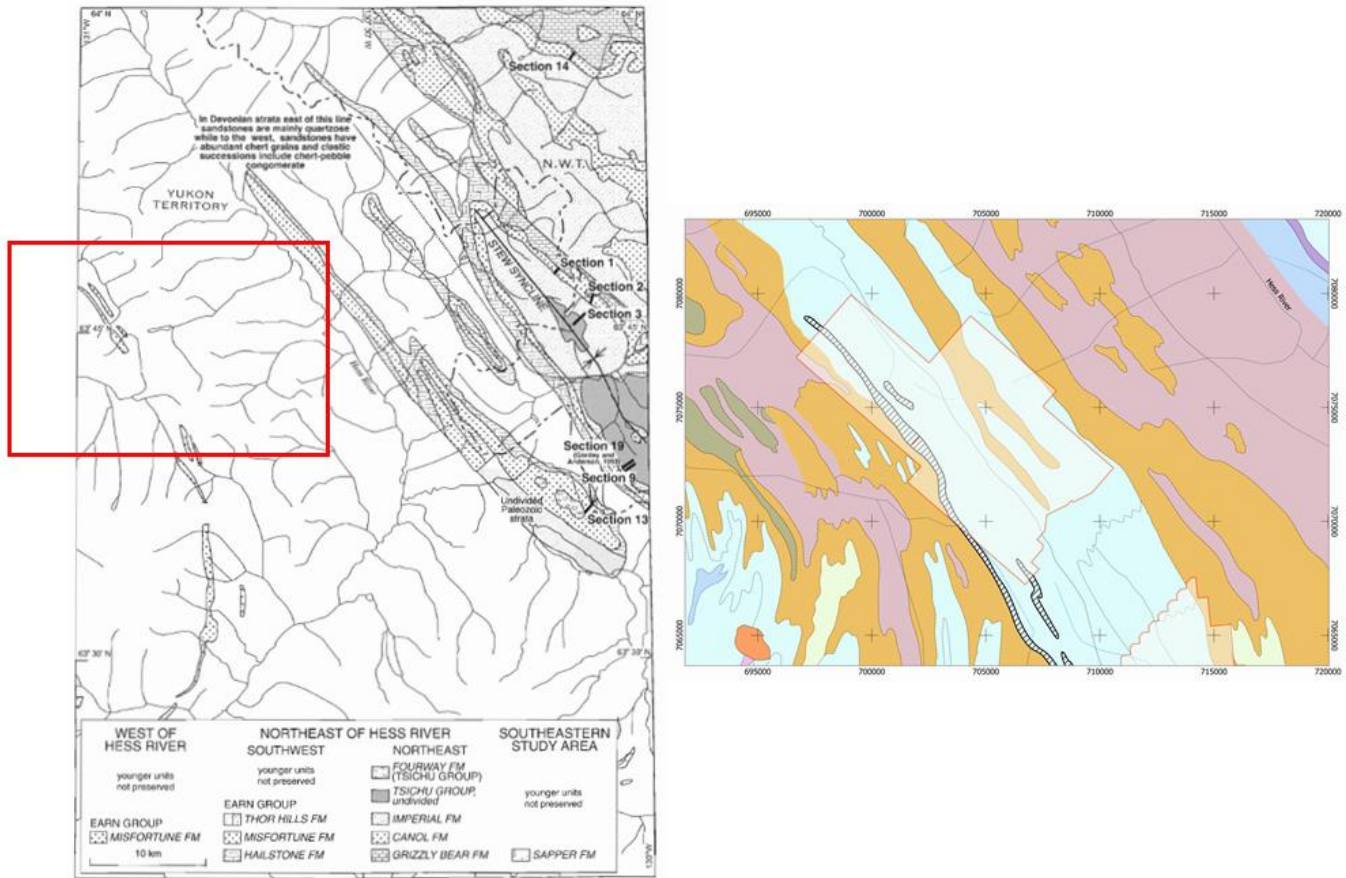
Figure 6: Comparison map between Cecile's interpretation and actual Yukon Bedrock Geology map. The red rectangle on the left mal corresponds to the boundaries of the map of the property map on the right side. The claim block area is shown by transparency. The dash polygons on the map correspond to the original mapped "Dc Unit" by Cecile named Earn Group/Misfortune.

3.5 MINERALIZATION

The Selwyn Basin is known for SEDEX deposit potential, hosting twelve major deposits with proven reserves in four major districts, including the giant Howards Pass deposits at 180 Mt indicated (Kirkham et al., 2012) and past producers Faro, Vangorda and Grum. The deposits are richer in Zn, Pb, and Ag and generally Cu and Au poor.

Stratiform barite deposits and Ni-Mo SEDEX showings also occur in the basin (Goodfellow, 2007). Cretaceous age Zn-Pb and W skarns, vein Ag-Pb and intrusive-related Au deposits also occur throughout the Selwyn Basin (Carne et al., 2013). Recent discoveries of Carlin-style gold mineralization have been made 100km northwest of the survey area along the northern margin of Selwyn Basin (Arehart et al., 2013).

3.5.1 Historic mineralization

The mineralization at Ursa was discovered during field mapping in 1980 by Cecile (1981). It was subsequently staked by Noranda in August of 1981 and again by Kennecott Canada Inc. in July of 1991 (Yukon Minfile, 1994).

The mineralization observed by Cecile (1981) is in the Lower to Middle Devonian Misfortune Formation limestone interstratified with black shale.

Mineralization consists of witherite and norsethite (BaMg(CO$_3$)$_2$ with traces of copper staining that occur as thin beds in limestone. While rare, the barium carbonate mineral norsethite has also been observed at the Tom and Jason deposits at Macmillan Pass (Gardner, 1985).

Note: The "Misfortune Formation" terminology is no longer used. It was assigned to the Earn Group by Cecile (2000). The actual Road River/Steel Formation constitutes the upper Road River Group, at the lower contact of the Earn Group (Figure 6).

Cecile mentions: *"the most interesting stratigraphic target may be the Lower to Middle Devonian Hailstone Formation, which shows metal anomalies in more than one place (Hailstone and Hess). This formation is laterally time equivalent to the Misfortune Formation farther southwest. The Misfortune Formation is host to the Ursa mineralization and to one zinc zap anomaly. Neither the Hailstone nor the Misfortune Formation are well exposed in the area and a geochemical program targeting their interpreted outcrop area could be productive."*

3.5.2   Mineralization types

3.5.2.1   Base metal target

The west side of the Ursa property covers a 14-km trend of elevated to highly anomalous zinc, silver, copper, molybdenum, nickel, and vanadium thought to be associated with Devonian age enriched black shales.
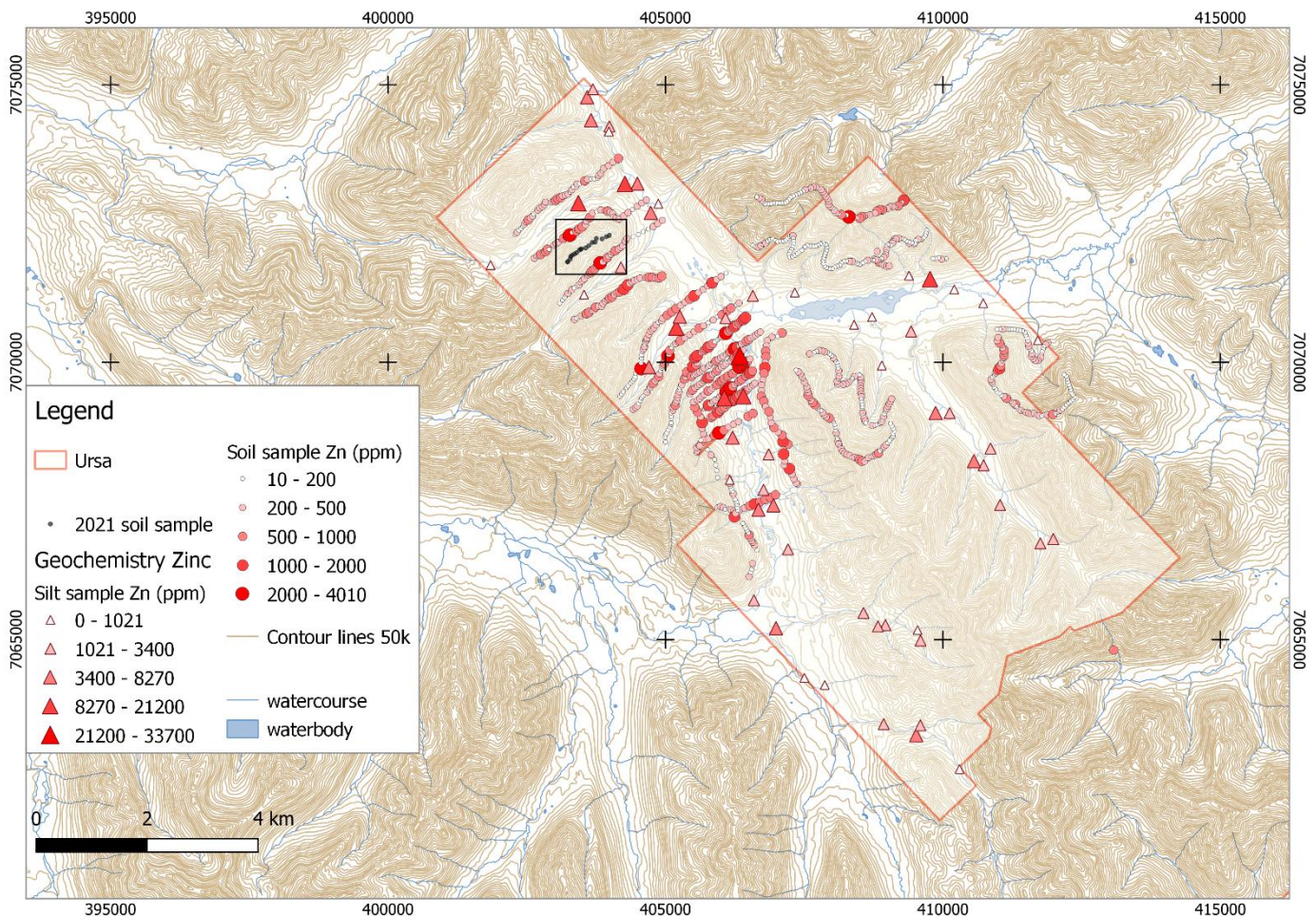
Figure 7: Ursa Zn Geochemistry. All values are given in ppm, the box corresponds to the 2021 work area.

Of 45 historic stream sediment samples draining the length of the trend, 44 returned concentrations exceeding 0.1% Zn, with 8 of these samples exceeding 1% Zn to a maximum of 3.4% Zn (Figure 7). Concentrations of up to 0.48% Ni, up to 0.18% Cu and up to 118.5 ppm Mo were also returned by this stream sediment sampling along the trend.
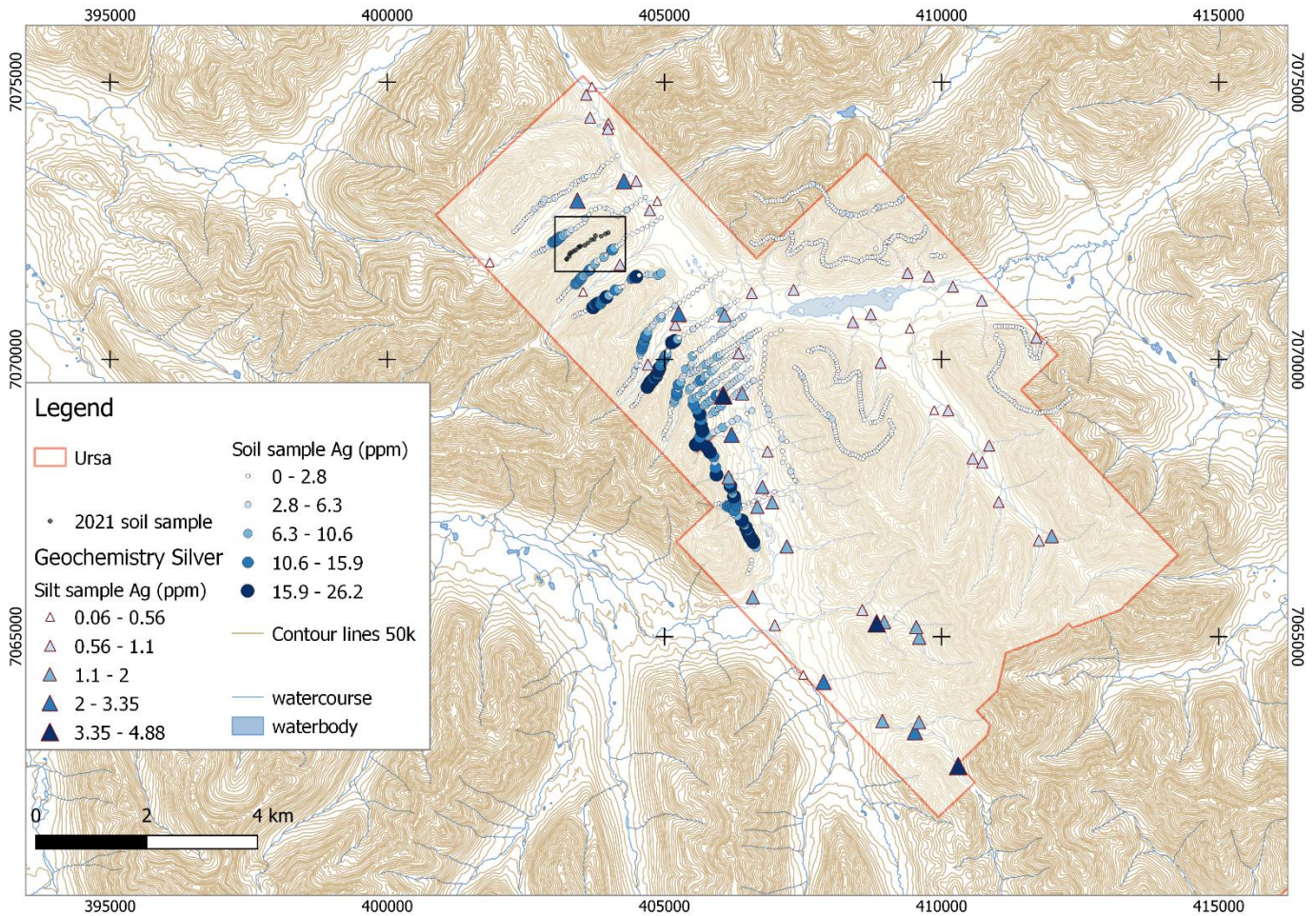
Figure 8: Ursa Ag Geochemistry. All values are given in ppm, the box corresponds to the 2021 work area.

Historic, first-pass contour soil sampling along a subsection of the trend revealed a zone 500 m to 1,500 m wide along the length of the 6.7-km subsection wherein soils consistently exceed 5 g/t Ag. A 2.7 km-long, 43-sample contour soil line within this subsection had a median concentration of 14.8 g/t (0.43 oz/ton) silver (Figure 8).

3.5.2.2   Gold target

The east side of the Ursa property covers a 9-kilometer trend of elevated gold in stream sediments and soils (Figure 7) in a sequence of heavily folded carbonaceous black shales and cherts. Gold was discovered in black shale hosted pyrite nodules by previous operators 18526 Yukon Inc. and Golden Predator while assessing for Carlin-style gold potential.

No major carbonate units were encountered, but subsequent analysis of field data by Snowline's technical team determined that Ursa's geological setting is similar to Russia's Sukhoi Log deposit with resources estimated at 1100 t Au at an average grade of 2.45 g/t (Distler, 2004) in which gold is hosted in pyritic nodules and masses. The carbonaceous, passive margin shales in both areas have been compressed into a tight anticlinorium and later intruded in their vicinities by felsic plutons. At Ursa, these plutons would be members of the Tombstone plutonic suite that drive the intrusion-related gold targets at Rogue. There has been very little, if any, previous exploration for this deposit type in the Selwyn Basin.
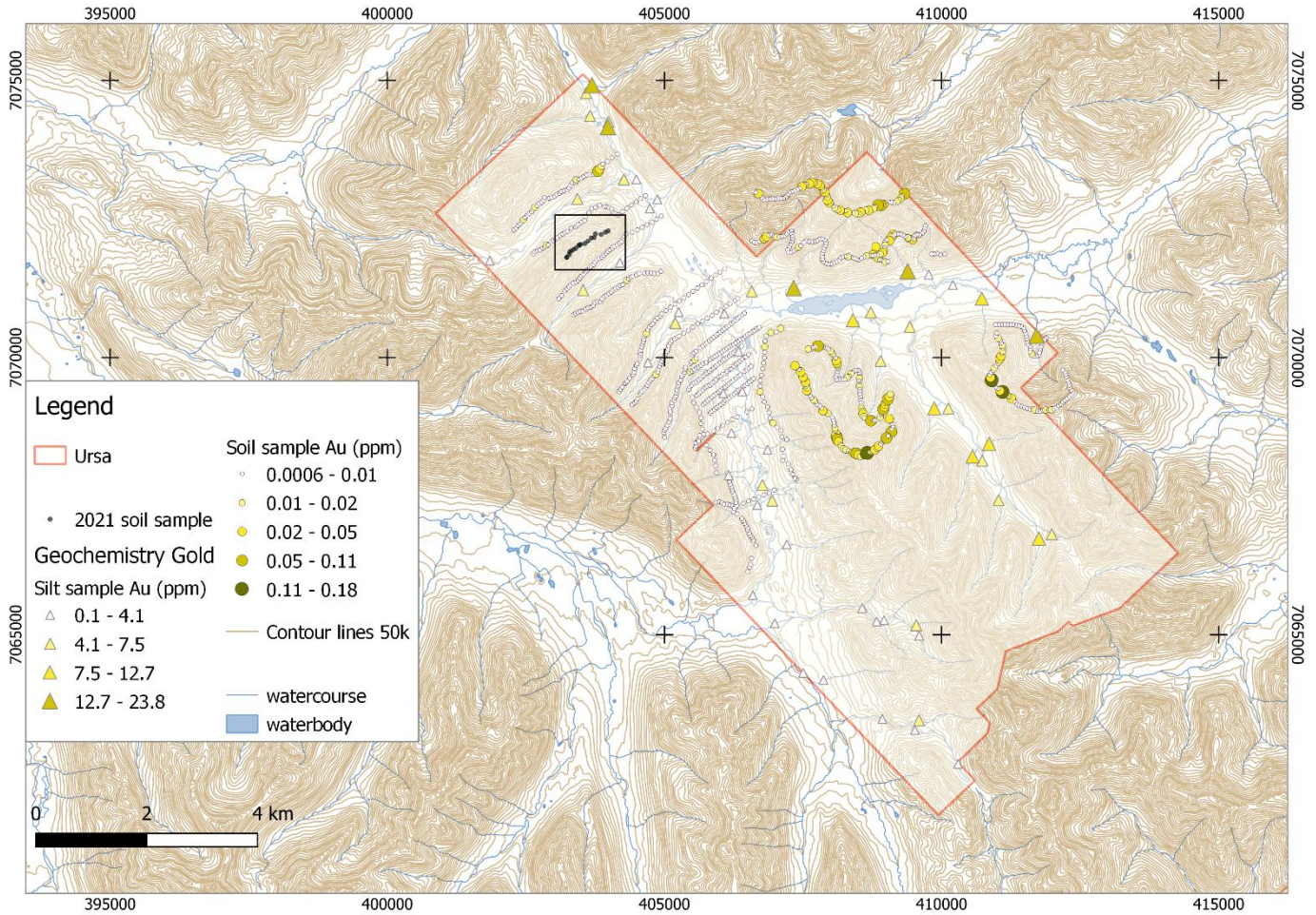
Figure 9: Ursa Au Geochemistry. All values are given in ppm, the box corresponds to the 2021 work area.

4   2021 PROGRAM DESCRIPTION AND RESULTS

4.1   INTRODUCTION

In 2021, the core of the program consisted of a 439 km-line airborne VTEM survey. Fieldwork was limited to an 18-sample geochemical reconnaissance comprising coarse fraction, fine fraction/soil sampling, and X-ray measurement as well as minimal rock sampling.

4.2   SURFACE SAMPLING AND X-RAY SURVEY

The surface sampling was completed in a prospective part of the Ursa base metals trend to gain further insight on the origin of the anomalous zinc, nickel, copper, vanadium and silver values in soil and stream geochemical sampling encountered in historical sampling across a wide area, and to provide context for results of the geophysical surveying and previous geochemical sampling.
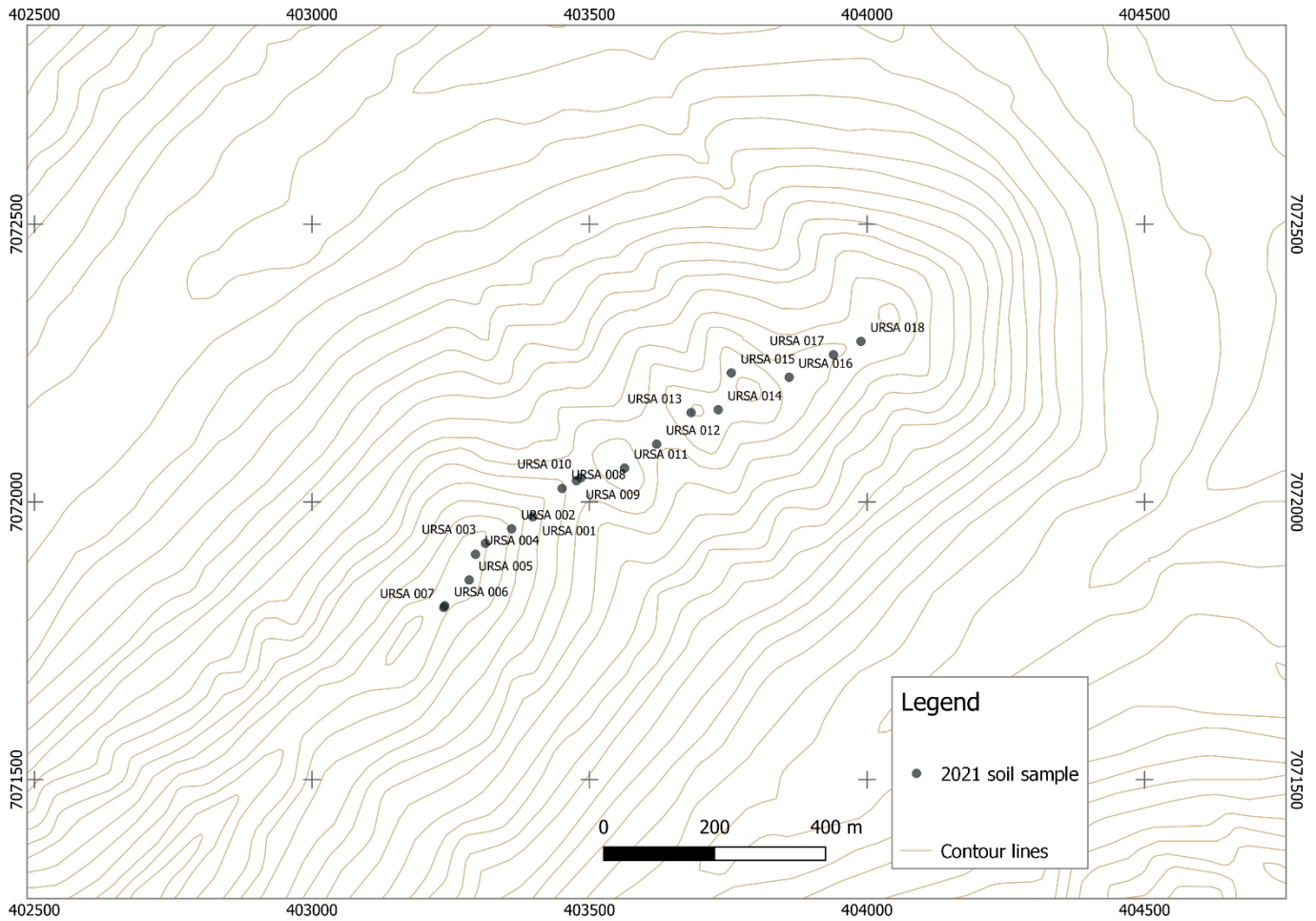
Figure 10 : 2021 soil sample location map.

The samples were analyzed for sixty elements by ALS Minerals with super trace ICP-MS methodology ME-MS61L. The method involves four acid digestion dissolving nearly all minerals in the majority of geological samples and provides extensive coverage of trace elements as well as major element proxies for mineralogy using ICP-MS and ICP-AES analysis. The rare earth elements (REE), which are not fully extracted in the four-acid digestion, have been added to the package (referring as MS61L-REE, ALS Minerals)

A total of 18 coarse fraction/soil and solid rock float were scanned with The REFLEX XRF™ - Olympus VANTA XRF (Photo 3). The coarse fraction was sampled for geochemical analysis on top of a ridge within a "rough" 50 m spacing, alternately targeting resistive and recessive horizons. One rock sample of "cherty" texture black with crosscutting pyritic veinlets was taken.

Photo 3: Scott Berdahl operating the XRF portable analyzer. Left picture illustrate a measurement on solid rock, right picture illustrate measurement on compacted "crumbly" black shale. The XRF measurements were repetitively proceeded in-situ on compacted soil/coarse fraction and solid rock at the sample geo-location.

All along the ridge, the recessive shale unit forms saddle where siliceous unit remains blocky and form scree slopes and outcrops. The method reveals that the historical rock samples were taken from the more competent material and thus, partially missed the more prospective shale unit.

The assays returned consistent anomalous values in silver (up to 24 g/t) and base metals. Other elements such as cerium (Ce), molybdenum (Mo), nickel (Ni), antimony (Sb), selenium (Se), uranium (U), and neodymium (Nd) are also noticeably anomalous.
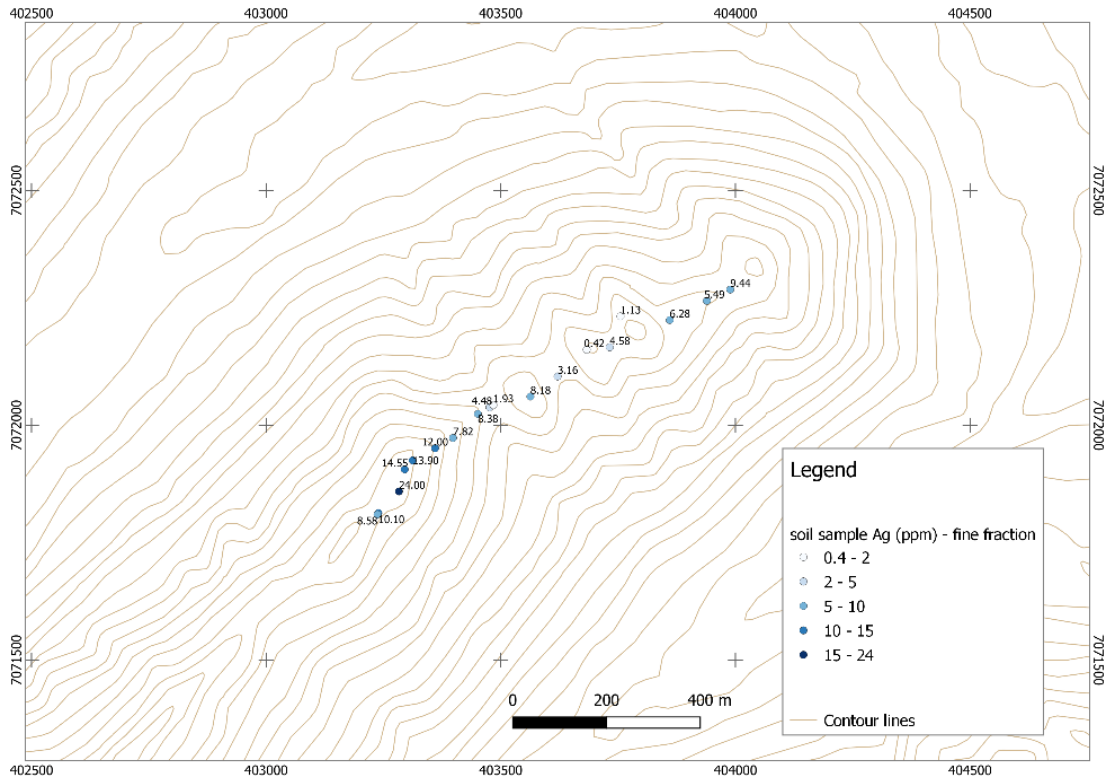
Figure 11: Ursa 2021 Ag geochemistry for fine fraction.
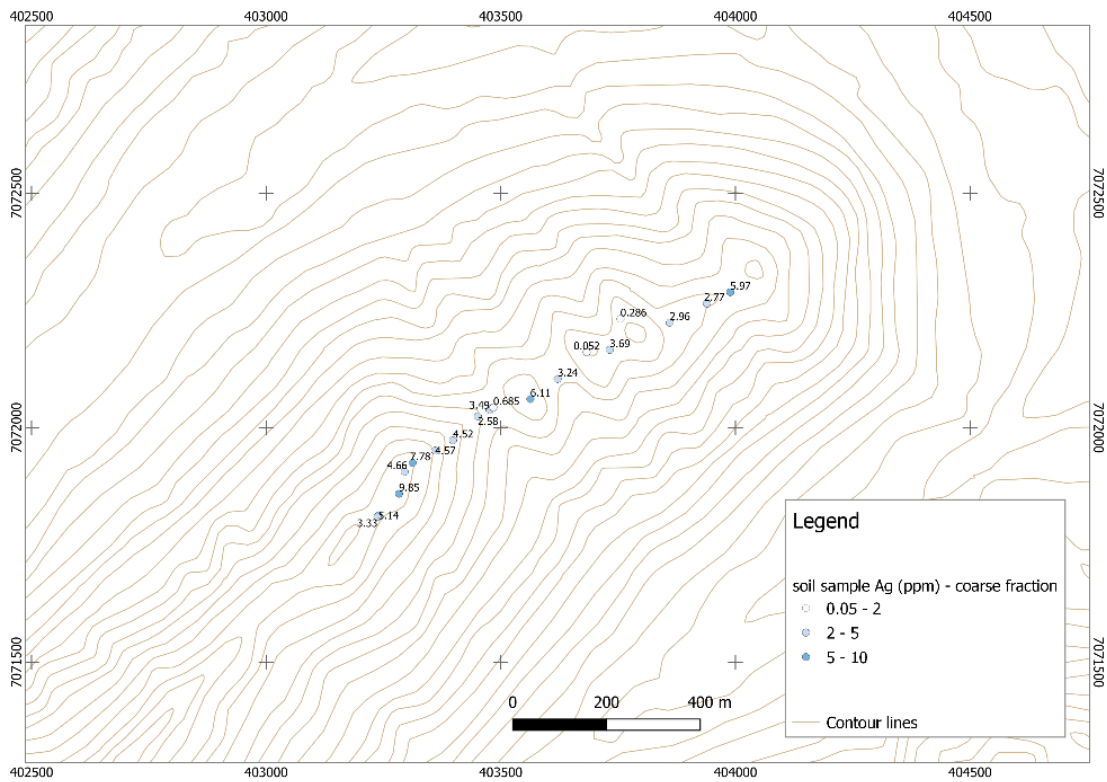
Figure 12: Ursa 2021 Ag geochemistry for coarse fraction.
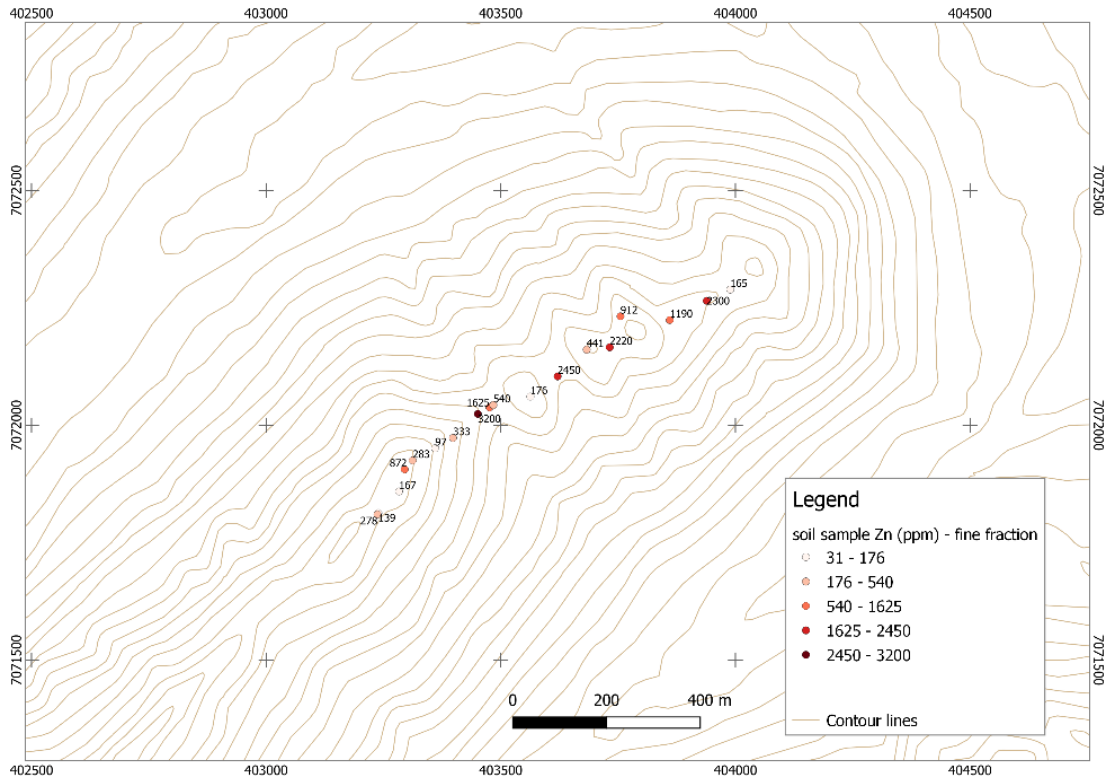
Figure 13: Ursa 2021 Zn geochemistry for fine fraction.
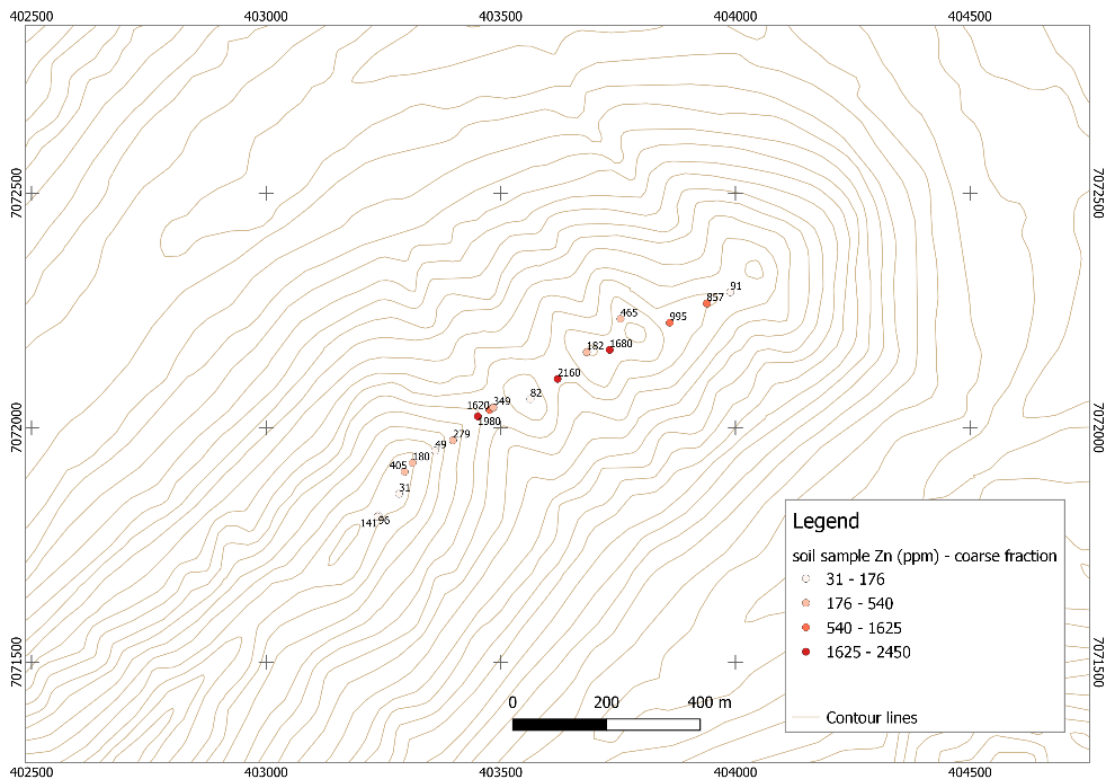
Figure 14: Ursa 2021 Zn geochemistry for coarse fraction.

The Figure 11 to 14 illustrate how the fraction size of the sample biases the overall geochemical analysis. For silver, the values of the fine fraction are 2.5 times higher in average the values of the coarse fraction (up to 8 times higher). For zinc, the ratio is 1.9.

Photo 4: Rock sample C953044 and sample area. Note the conchoidal break and the oxidation on the fracture surface.

Comparing the XRF field value to the assay results (Table 2), the XRF measurement seems to under-estimate the grade for most of the selected elements (ratio average >1). With the exception of the cobalt – extremely over the assay results, the results from the field for the selected elements give an acceptable first estimation of the grade. Copper, nickel, and antimony field measurement are strongly correlated to the lab assay value. However, numerous antimony measurements returned "no values" for common assay value under 10 ppm. It is also noticeable that most of the assay values comprised between 0 to 25 ppm are not capture by the XRF gun (Table 2).

Sample_Num	Ag ppm	Ag ppm	Ratio	As ppm	As ppm	Ratio	Co ppm	Co ppm	Ratio	Cu ppm	Cu ppm	Ratio	Mo ppm	Mo ppm	Ratio	Ni ppm	Ni ppm	Ratio	Sb ppm	Sb ppm	Ratio	Se ppm	Se ppm	Ratio	V ppm	V ppm	Ratio	Zn ppm	Zn ppm	Ratio
Ursa 001	5.00	7.82	1.56	59.00	74.40	1.26	No Value	1.28	N/A	254.00	243.00	0.96	91	122.5	1.35	107.00	109.50	1.02	47.00	65.10	1.39	22.00	23.10	1.05	3115.00	6290.00	2.02	295.00	333.00	1.13
Ursa 001	8.00		0.98	62.00		1.20	37.00		0.03	245.00		0.99	97		1.26	103.00		1.06	55.00		1.18	24.00		0.96	3071.00		2.05	291.00		1.14
	6.00		1.30	60.00		1.24	12.00		0.11	251.00		0.97	93		1.32	106.00		1.03	50.00		1.30	23.00		1.00	3100.00		2.03	293.00		1.14
Ursa 002	4.00	12.00	3.00	18.00	33.30	1.85	66.00	1.05	0.02	80.00	107.00	1.34	11	30.9	2.81	49.00	58.00	1.18	No Value	9.47	N/A	24.00	48.30	2.01	310.00	661.00	2.13	62.00	96.80	1.56
Ursa 002	6.00		2.00	18.00		1.85	71.00		0.01	81.00		1.32	12		2.58	46.00		1.26	No Value		N/A	24.00		2.01	303.00		2.18	62.00		1.56
	4.00		3.00	18.00		1.85	68.00		0.02	80.00		1.34	11		2.81	48.00		1.21	No Value		N/A	24.00		2.01	308.00		2.15	62.00		1.56
Ursa 003	8.00	13.90	1.74	24.00	34.40	1.43	50.00	1.96	0.04	419.00	436.00	1.04	40	69.8	1.75	149.00	180.50	1.21	No Value	21.50	N/A	32.00	42.00	1.31	1439.00	2720.00	1.89	204.00	283.00	1.39
Ursa 003	7.00		1.99	25.00		1.38	42.00		0.05	421.00		1.04	42		1.66	164.00		1.10	No Value		N/A	33.00		1.27	1551.00		1.75	233.00		1.21
	7.00		1.99	24.00		1.43	48.00		0.04	419.00		1.04	41		1.70	154.00		1.17	No Value		N/A	32.00		1.31	1476.00		1.84	213.00		1.33
Ursa 004	6.00	14.55	2.43	43.00	83.80	1.95	No Value	2.63	N/A	372.00	473.00	1.27	39	101	2.59	203.00	263.00	1.30	No Value	26.30	N/A	16.00	28.00	1.75	864.00	1685.00	1.95	589.00	872.00	1.48
Ursa 004	16.00		0.91	53.00		1.58	No Value		N/A	405.00		1.17	46		2.20	227.00		1.16	No Value		N/A	16.00		1.75	961.00		1.75	606.00		1.44
	9.00		1.62	46.00		1.82	No Value		N/A	383.00		1.23	41		2.46	211.00		1.25	No Value		N/A	16.00		1.75	896.00		1.88	595.00		1.47
Ursa 005	8.00	24.00	3.00	70.00	107.00	1.53	325.00	2.25	0.01	120.00	143.00	1.19	17	49.9	2.94	48.00	43.50	0.91	No Value	16.05	N/A	58.00	102.50	1.77	439.00	786.00	1.79	156.00	167.00	1.07
Ursa 005	11.00		2.18	54.00		1.98	193.00		0.01	102.00		1.40	17		2.94	33.00		1.32	30.00		0.54	56.00		1.83	382.00		2.06	100.00		1.67
	9.00		2.67	65.00		1.65	281.00		0.01	114.00		1.25	17		2.94	43.00		1.01	10.00		1.61	57.00		1.80	420.00		1.87	137.00		1.22
Ursa 006	5.00	10.10	2.02	26.00	37.90	1.46	143.00	3.45	0.02	83.00	99.60	1.20	7	14.7	2.10	44.00	39.20	0.89	No Value	6.50	N/A	17.00	26.50	1.56	219.00	458.00	2.09	108.00	139.00	1.29
Ursa 006	6.00		1.68	21.00		1.80	143.00		0.02	79.00		1.26	13		1.13	39.00		1.01	No Value		N/A	16.00		1.66	236.00		1.94	107.00		1.30
	6.00		1.68	25.00		1.52	143.00		0.02	81.00		1.23	9		1.63	42.00		0.93	No Value		N/A	16.00		1.66	225.00		2.04	108.00		1.29
Ursa 007	5.00	8.58	1.72	38.00	72.10	1.90	126.00	2.52	0.02	121.00	174.50	1.44	11	24.4	2.22	60.00	65.80	1.10	No Value	9.47	N/A	18.00	36.00	2.00	288.00	557.00	1.93	193.00	278.00	1.44
Ursa 007	No Value		N/A	37.00		1.95	113.00		0.02	129.00		1.35	13		1.88	56.00		1.18	No Value		N/A	21.00		1.71	267.00		2.09	198.00		1.40
	3.00		2.86	38.00		1.90	122.00		0.02	124.00		1.41	12		2.03	59.00		1.12	No Value		N/A	19.00		1.89	281.00		1.98	195.00		1.43
Ursa 008	No Value	8.38	N/A	68.00	92.10	1.35	118.00	13.35	0.11	274.00	344.00	1.26	65	81	1.25	264.00	373.00	1.41	50.00	67.50	1.35	13.00	14.75	1.13	1575.00	2870.00	1.82	2272.00	3200.00	1.41
Ursa 008	No Value		N/A	65.00		1.42	174.00		0.08	281.00		1.22	59		1.37	282.00		1.32	47.00		1.44	11.00		1.34	1456.00		1.97	2279.00		1.40
	No Value		N/A	67.00		1.37	137.00		0.10	276.00		1.25	63		1.29	270.00		1.38	49.00		1.38	13.00		1.13	1536.00		1.87	2274.00		1.41
Ursa 009	4.00	4.48	1.12	72.00	91.60	1.27	97.00	6.23	0.06	279.00	313.00	1.12	48	68.5	1.43	212.00	240.00	1.13	66.00	68.90	1.04	10.00	10.70	1.07	1093.00	2130.00	1.95	1402.00	1625.00	1.16
Ursa 009	No Value		N/A	76.00		1.21	81.00		0.08	295.00		1.06	52		1.32	226.00		1.06	48.00		1.44	9.00		1.19	1152.00		1.85	1449.00		1.12
	3.00		1.49	73.00		1.25	92.00		0.07	284.00		1.10	49		1.40	217.00		1.11	60.00		1.15	10.00		1.07	1113.00		1.91	1417.00		1.15
Ursa 010	No Value	1.93	N/A	26.00	38.50	1.48	192.00	11.25	0.06	131.00	177.50	1.35	16	30	1.88	64.00	101.50	1.59	No Value	17.35	N/A	10.00	14.35	1.44	300.00	658.00	2.19	361.00	540.00	1.50
Ursa 010	No Value		N/A	23.00		1.67	246.00		0.05	122.00		1.45	13		2.31	69.00		1.47	No Value		N/A	9.00		1.59	241.00		2.73	365.00		1.48
	No Value		N/A	25.00		1.54	210.00		0.05	128.00		1.39	15		2.00	65.00		1.56	No Value		N/A	9.00		1.59	281.00		2.34	363.00		1.49
Ursa 011	6.00	8.18	1.36	29.00	28.70	0.99	312.00	3.91	0.01	95.00	86.90	0.91	11	11.6	1.05	53.00	45.90	0.87	No Value	3.82	N/A	25.00	23.10	0.92	290.00	377.00	1.30	165.00	175.50	1.06
Ursa 011	4.00		2.05	26.00		1.10	244.00		0.02	95.00		0.91	10		1.16	46.00		1.00	No Value		N/A	21.00		1.10	215.00		1.75	152.00		1.15
	5.00		1.64	28.00		1.03	289.00		0.01	95.00		0.91	10		1.16	50.00		0.92	No Value		N/A	24.00		0.96	265.00		1.42	161.00		1.09
Ursa 012	No Value	3.16	N/A	70.00	85.30	1.22	112.00	5.78	0.05	313.00	405.00	1.29	66	79.5	1.20	213.00	255.00	1.20	63.00	52.50	0.83	12.00	12.25	1.02	1099.00	2320.00	2.11	2009.00	2450.00	1.22
Ursa 012	No Value		N/A	68.00		1.25	88.00		0.07	316.00		1.28	68		1.17	206.00		1.24	46.00		1.14	12.00		1.02	1069.00		2.17	1989.00		1.23
	No Value		N/A	69.00		1.24	104.00		0.06	314.00		1.29	67		1.19	211.00		1.21	58.00		0.91	12.00		1.02	1089.00		2.13	2002.00		1.22
Ursa 013	No Value	0.42	N/A	9.00	16.10	1.79	148.00	24.30	0.16	85.00	116.00	1.36	10	14.65	1.47	125.00	176.00	1.41	No Value	5.89	N/A	2.00	2.75	1.38	420.00	965.00	2.30	284.00	441.00	1.55
Ursa 013	No Value		N/A	12.00		1.34	143.00		0.17	77.00		1.51	10		1.47	118.00		1.49	No Value		N/A	No Value		N/A	444.00		2.17	272.00		1.62
	No Value		N/A	10.00		1.61	147.00		0.17	82.00		1.41	10		1.47	123.00		1.43	No Value		N/A	1.00		2.75	428.00		2.25	280.00		1.58
Ursa 014	No Value	4.58	N/A	62.00	70.80	1.14	118.00	7.67	0.07	239.00	314.00	1.31	44	60.5	1.38	290.00	364.00	1.26	No Value	39.10	N/A	19.00	20.50	1.08	1136.00	2420.00	2.13	1716.00	2220.00	1.29
Ursa 014	3.00		1.53	56.00		1.26	87.00		0.09	261.00		1.20	42		1.44	278.00		1.31	42.00		0.93	18.00		1.14	1214.00		1.99	1774.00		1.25
	1.00		4.58	38.00		1.18	108.00		0.07	246.00		1.28	43		1.41	286.00		1.27	14.00		2.79	18.00		1.14	1162.00		2.08	1735.00		1.28
Ursa 015	No Value	1.13	N/A	No Value	17.65	N/A	375.00	33.30	0.09	140.00	150.50	1.08	No Value	9.22	N/A	144.00	179.50	1.25	No Value	8.44	N/A	No Value	3.23	N/A	No Value	190.00	N/A	556.00	912.00	1.64
Ursa 015	No Value		N/A	11.00		1.60	194.00		0.17	127.00		1.19	8		1.15	120.00		1.50	No Value		N/A	No Value		N/A	71.00		2.68	598.00		1.53
	No Value		N/A	4.00		4.41	315.00		0.11	136.00		1.11	3		3.07	136.00		1.32	No Value		N/A	No Value		N/A	24.00		7.92	570.00		1.60
Ursa 016	No Value	6.28	N/A	51.00	63.20	1.24	128.00	11.20	0.09	241.00	246.00	1.02	44	61.9	1.41	215.00	238.00	1.11	61.00	45.20	0.74	9.00	11.10	1.23	1243.00	2520.00	2.03	1022.00	1190.00	1.16
Ursa 016	No Value		N/A	57.00		1.11	140.00		0.08	252.00		0.98	54		1.15	220.00		1.08	59.00		0.77	10.00		1.11	1246.00		2.02	1079.00		1.10
	No Value		N/A	53.00		1.19	132.00		0.08	245.00		1.00	48		1.29	217.00		1.10	60.00		0.75	9.00		1.23	1244.00		2.03	1041.00		1.14
Ursa 017	No Value	5.49	N/A	67.00	87.70	1.31	125.00	9.72	0.08	331.00	402.00	1.21	51	83	1.63	290.00	340.00	1.17	45.00	46.00	1.02	13.00	15.45	1.19	1082.00	2490.00	2.30	1863.00	2300.00	1.23
Ursa 017	No Value		N/A	70.00		1.25	97.00		0.10	355.00		1.13	57		1.46	266.00		1.28	62.00		0.74	13.00		1.19	1200.00		2.08	1783.00		1.29
	No Value		N/A	68.00		1.29	115.00		0.08	339.00		1.19	53		1.57	282.00		1.21	50.00		0.92	13.00		1.19	1121.00		2.22	1836.00		1.25
Ursa 018	No Value	9.44	N/A	18.00	20.40	1.13	116.00	1.80	0.02	99.00	98.60	1.00	11	21.3	1.94	37.00	35.10	0.95	No Value	7.65	N/A	30.00	38.60	1.29	485.00	825.00	1.70	141.00	165.00	1.17
Ursa 018	No Value		N/A	14.00		1.46	76.00		0.02	85.00		1.16	16		1.33	33.00		1.06	No Value		N/A	31.00		1.25	497.00		1.66	126.00		1.31
	No Value		N/A	17.00		1.20	103.00		0.02	94.00		1.05	13		1.64	36.00		0.98	No Value		N/A	30.00		1.29	489.00		1.69	136.00		1.21
Ratio Average			2.00			1.50			0.06			1.19			1.72			1.19			1.15			1.40			2.12			1.33

Table 2: XRF data compared to lab assay results. The white cell columns correspond to the XRF value measured in the field. The pale-yellow cell columns correspond to the lab assay values. The pale-blue columns correspond to the ratio the ratio lab assay/field XRF value. "No values" stand for no value recorded by the XRF gun - "N/A" stands for not applicable.

Element	Ag	As	Co	Cu	Mo	Ni	Sb	Se	V	Zn
Assay/XRF average	2.00	1.50	0.06	1.19	1.72	1.19	1.15	1.40	2.12	1.33
Correlation coefficient assay/XRF average	0.82	0.94	0.47	0.98	0.93	0.99	0.74	0.95	1.00	0.99

Table 3: Summary table showing average ratio between assay values and field portable XRF measurements and correlation coefficient for representative elements.

Overall, the selected elements show high to very high correlation coefficient (Table 3). This tends to validate the use of the XRF field portable as a primary evaluation of the element grade. The risk of misinterpretation is minimized by the consistency of under-estimated values given by the XRF field portable unit, suggesting that with further calibration, the portable XRF could be an accurate and effective field tool for early-stage exploration. However, the collected data set was collected in a restricted area (single ridge) and the observations may not be transferrable for the entire property.

4.3 AIRBORNE VTEM SURVEY

At Ursa, a 461 line-km VTEM and magnetic survey was conducted in early September by Geotech Inc. across most of the northernmost Ursa claim block at a line spacing of 200 m. The survey covers an area of roughly 7,750 ha. It will provide the Company with information on the conductivity and chargeability of rock units underlying the trend of anomalous geochemistry, allowing for better understanding of the underlying geology and potentially mapping out anomalous geophysical targets directly related to base metals or gold mineralisation.

Work performed, results and interpretation are described in detail in the attached Geotech Inc. report.
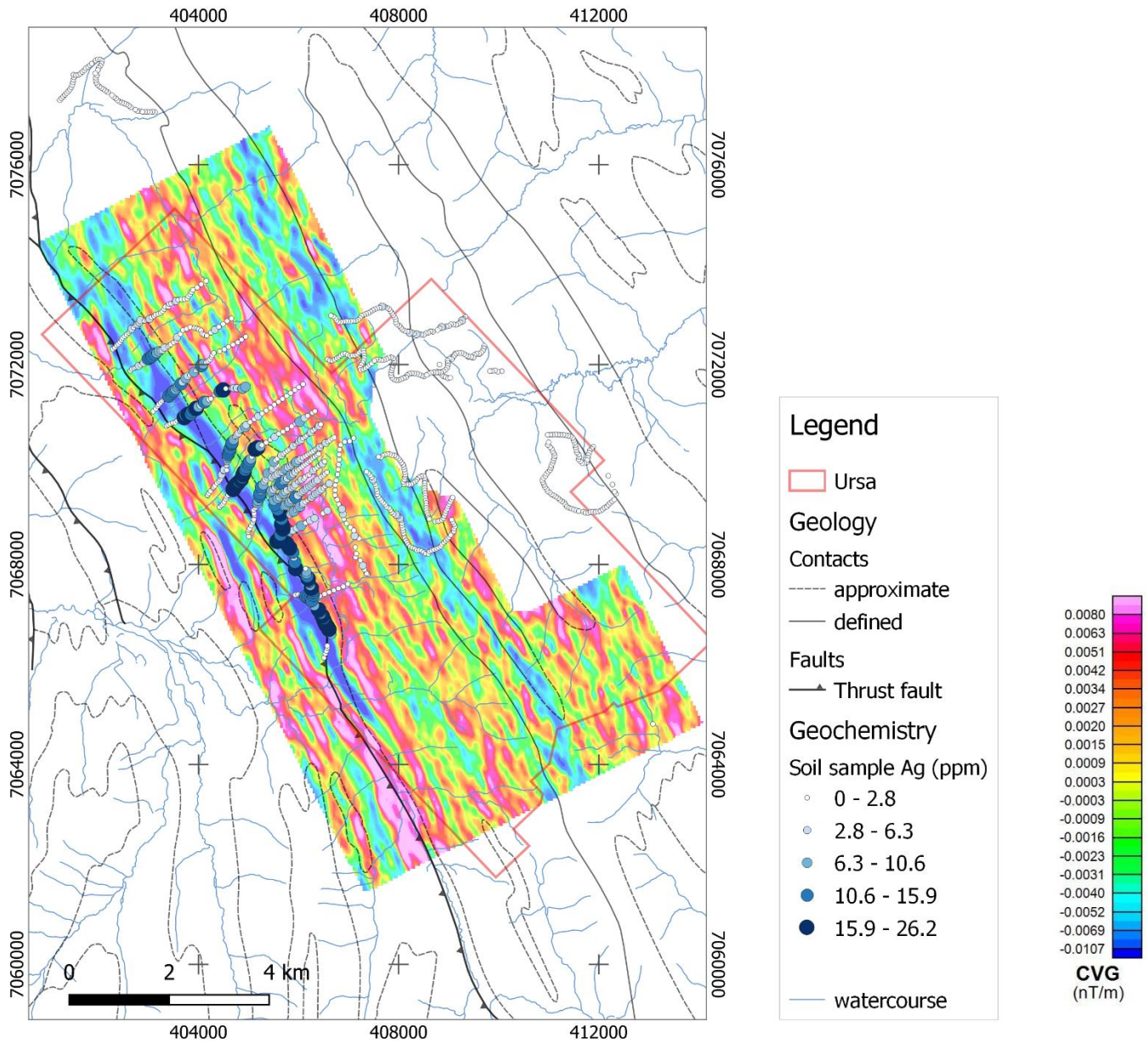
Figure 15: Compilation map correlation showing the correlation between the rate of change of the magnetic field, geological contacts, and the silver geochemistry at the Ursa property. Vivid colours represent the Calculated Vertical Derivative (CVG) of the Total Magnetic Intensity

The magnetic contrast closely correlates with the southeast-northwest thrust fault and the lithology contacts. The higher silver values sit in the footwall of the thrust (Figure 15).
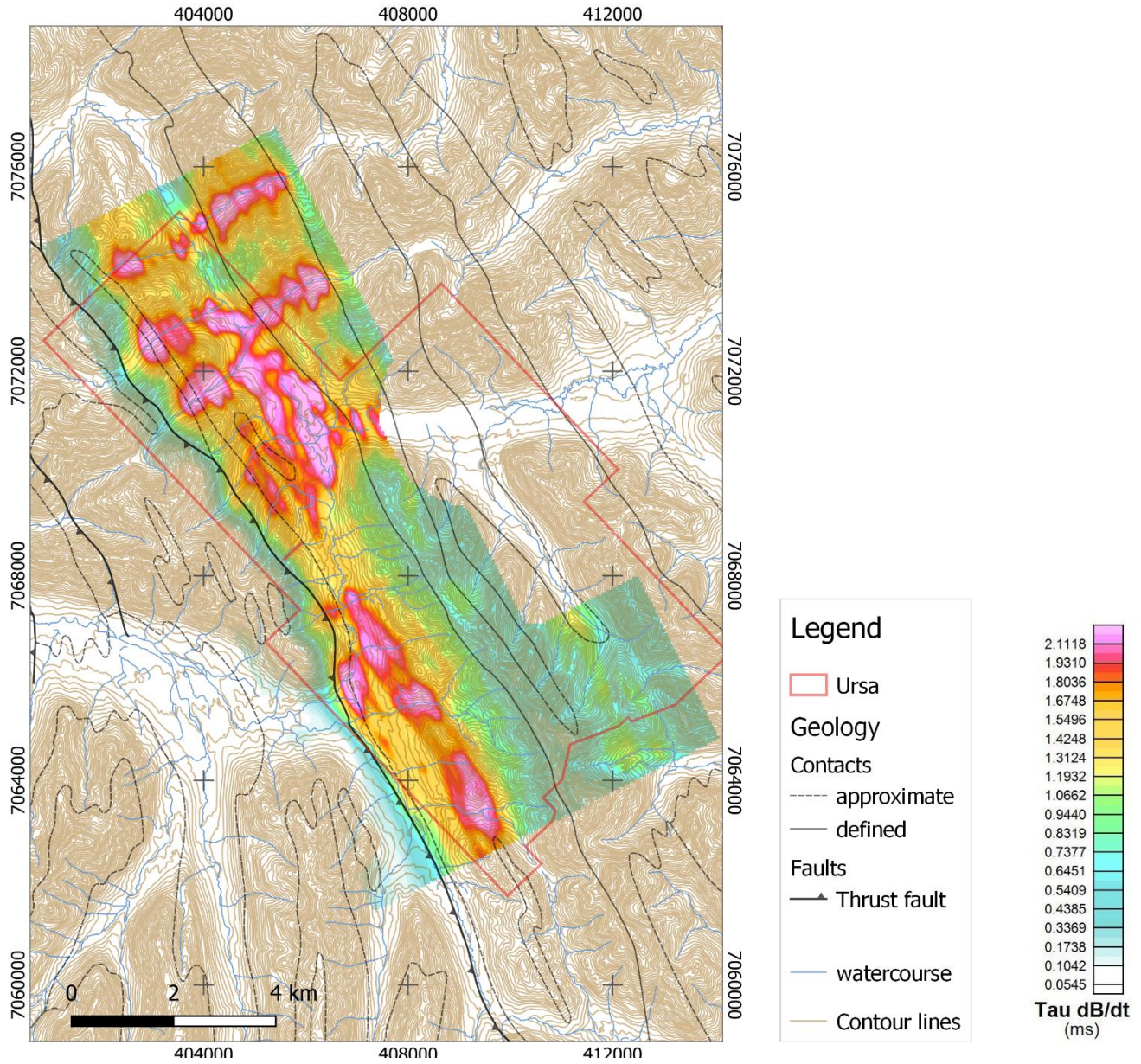
Figure 16: Compilation map showing the correlation between topography and conductivity intensity

Figure 16 shows the strong correlation between the high conductive area and the valley bottom. The NW-SE elongated shape of the anomalies suggests that at least part of the signal is due to physical property of the unit. However, the contrast intensity looks to be heavily biased by topographic effects and/or groundwater content.
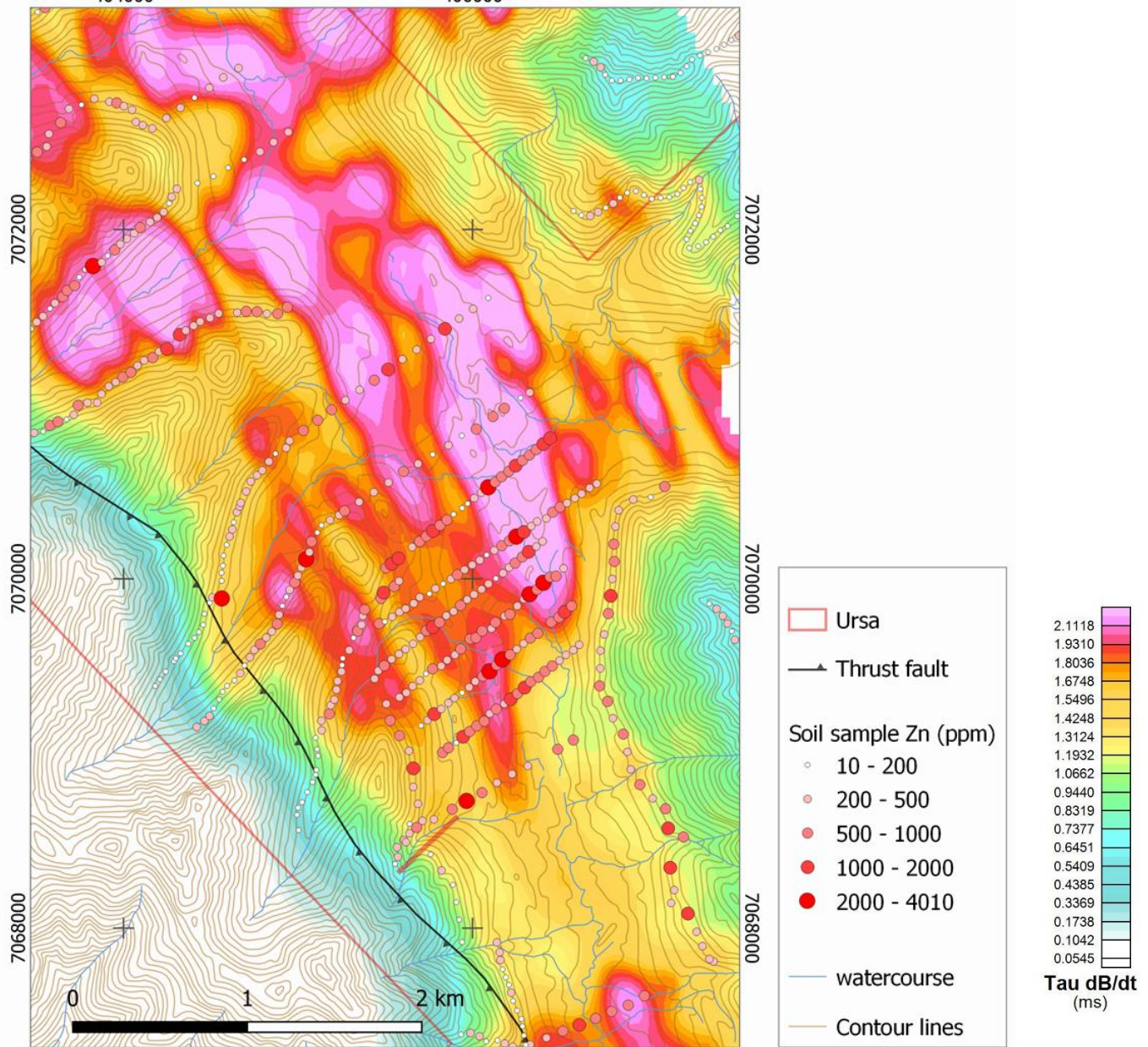
Figure 17: Ursa geophysics and Zn geochemistry distribution.

Zinc values in historical soils show a similar southeast-northwest trend (Figure 17) but also significant concentration within organic-rich swampy areas located at the bottom of the valley. Multiple assumptions can be made:

- Mineralized horizons are more recessive, and the swamps are their landform expression. However, the valley-bottom anomalies are markedly single-element (zinc), compared to the multi-element anomalism encountered in talus fines on hillsides.

- The organic material in swamps selectively concentrates transported zinc, either from depth through groundwater circulation or transported laterally from hillside anomalies (Figure 18).

- The humps in between the swampy area are of glacial material and may selectively mask and/or transport underlying anomalies.
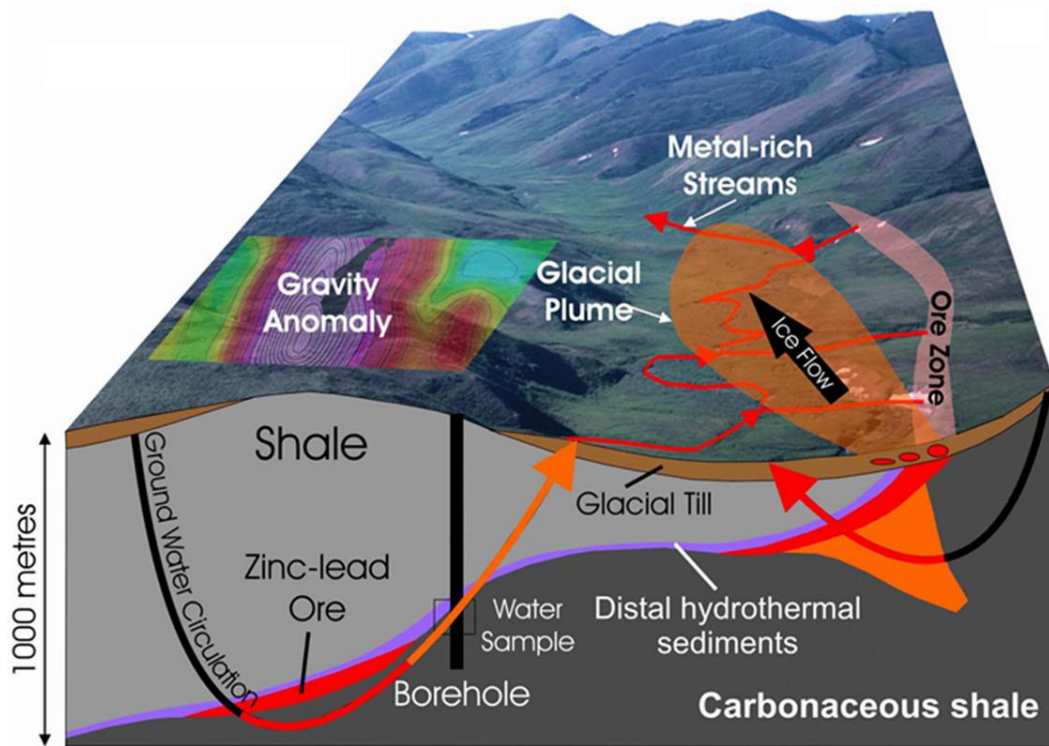
Figure 18: Hypothesis of ground water circulation, extracted from Paradis and Goodfellow (2012).

Figure 18 illustrates how ground water circulation can play a role in zinc migration. The Ursa property shows similarities with the model exposed with the exception of the steepening of the stratigraphy and the intensity of folding resulting of the Rogue decollement.

5 CONCLUSION AND RECOMMENDATION

Historical geochemical data confirmed the potential of the Ursa property for silver and base metals. The distribution of anomalous areas suggests a primary lithological control. High silver and multi-element anomalism seems to correlate with exposed units in the footwall of the thrust fault figuring in the YGS bedrock geology map.

Additional field work is recommended to understand the distribution of the high zinc anomalies. Potentially, surficial geology would help in the interpretation of the valley bottom anomalies. Ground gravity survey lines may also be of use in distinguishing between naturally conductive units and potentially economic mineralization.

Comparison between coarse fraction and fine fraction geochemistry for samples collected at the same location reveals a strong variability. More important, values are consistently more elevated in fine fraction for silver, arsenic, copper, iron, lead, zinc, cobalt, molybdenum as well as elements commonly considered as pathfinders such as bismuth, cadmium, cerium, cesium, stibnite, lanthanum, or tellurium. This confirms that added precaution should be taken in the sampling, and it demonstrates an association between carbon-rich recessive units and anomalous silver and base metal mineralization. A specific protocol should be established to provide consistent data as required for interpretation.

The geochemical assay results confirmed the accuracy of the handheld XRF analyzer for most of the tested elements. Overall, the field value are within a ratio of 1-for-2 with a consistent minimized reading from the XRF portable analyzer. Also, the correlation coefficient for most of the elements tested show high to very high values. The XRF portable analyser proves to be a reliable tool for As, Cu, Mo, Ni, Se, V, and Zn and a decent tool for Ag. This allows exploration program adjustments in the course of the season whilst awaiting the lab assay results, and with further calibration, could allow for much more detailed geochemical mapping at reduced cost.

Geological reconnaissance is recommended to explain the elevated historical gold soil values (up to 0.18 ppm). The airborne VTEM survey covers only part of the high soil and silt samples. Gold bearing pyrite nodules have been reported in the area. The central and south Ursa property remains an attractive gold target and addition prospection and soil line perpendicular to the lithology trend is recommended.

Air magnetic data show strong correlation with the stratigraphic contact including the southeast-northwest trending thrust fault cutting across the western side of the property-low response in the Calculated Vertical Derivative of the Total Magnetic Intensity. It is worth noting that the geochemical anomaly (e.g., silver) line-up with this interpreted regional structure.

High conductivity is dominantly observed within the valley bottom along and across the stratigraphy. Part of the signal might be due to topographic effect and the intensity of the response should considered with in in mind. Another assumption would be that the higher value in the valley is caused by groundwater. In that case the swampy area may also represent recessive layer that could be prospective. Indeed, the sample assays from the saddle ridge tested in 2021 (presumably recessive) returned more elevated value in silver base and metals among other elements. However, the elongated shape of the high conductivity anomaly transverse the west-east trending ridge which suggest that the overall pattern is substantial. Conductivity can be attributed to graphitic units or sulphide bearing shales. Area of high magnetic and high conductivity are considered the most prospective.

The zinc shows a similar southeast-northwest trend but also significant concentration with the swampy area, at the bottom of the valley. Multiple assumptions can be made: 1. Mineralized units are more recessive, and the swamps are their landform expression. 2. The organic material concentration the selective elements. 3. The humps in between the swampy area are of glacial material and soil sample quality may explain the observed geochemical contrasts.

VTEM raw data re-interpretation is recommended paying a particular attention to the effect of topography, lithology changes and the folding.

6 BUDGET

The Table 4 details the 221 Ursa project expenditures.

The geophysics crew stayed at the Fireweed Zinc basecamp. The helicopter costs refer to fuel supply from the Forks Airstrip and include $650 per Jet A barrel.

Category	Person/Company	Activity	Units/Days	Rate ($)	Total ($)
Labour	Geotech	VTEM survey and report	1	93,460.00	93,460.00
	Geologist	Field visit/sampling	2	500	1,000
Helicopter costs		Fuel supply		7,395.00	7,395.00
Assays	ALS Minerals	Soil sample	18	80	1,440
		Rock sample	1	1	50
XRF rental	Rent		1	297.92	297.92
Camp costs	Fireweed Zinc Camp	Geophysics crew accommodation	1	8,727.00	8,727.60
Camp - *carpe diem*	Snowline Camp	Room, board	3	100	300
Total ($)					$ 112,670.52

Table 4: Ursa 2021 expenditures

7 STATEMENT OF QUALIFICATION

I, Jérôme de Pasquale, of:

Box 21201

Whitehorse, Yukon Territory

Y1A 6R8

do hereby certify that:

1. I am an independent geologist with over 11 years of experience working in Canada.

2. I am a graduate of Université d'Orléans-La-Source, with a Maitrise des Sciences de la Terre Option Géologie and have been involved in geology and mineral exploration continuously since 2011.

3. I worked for Snowline Gold Corp. during the 2021 field season, and I am currently a Snowline Gold Corp employee.

_____

March 9th, 2022

8 REFERENCES

Arehart, G. B. et al., 2013. A Comparison of Carlin-type Deposits in Nevada and Yukon, Tectonics, Metallogeny, and Discovery: The North American Cordillera and Similar Accretionary Settings, M. Colpron, T. Bissig, B. G. Rusk, J. F. H. Thompson.

Carne, R., Phillips, R., and Lane, J., 2013. An explorer's take on the Selwyn Basin ZTEM survey: Presented at Yukon airborne geophysics workshop, Yukon Geoscience Forum 2013, Yukon Chamber of Mines and Yukon Geo- logical Survey, Whitehorse, Canada.

Cecile, M.P., 2000. Geology of the northeastern Niddery Lake map area, east-central Yukon and adjacent Northwest Territories, Bulletin of the Geological Survey of Canada, 119 p.

Colpron, M., Israel, S., Murphy, D., Pigage, L. and Moynihan, D., 2016. Yukon bedrock geology map. Yukon Geological Survey, Open File 2016-1, scale 1:1 000 000, map and legend.

Distler, V. V., Yudovskaya, M. A., Mitrofanov, G. L., Prokofiev, V. Yu., Lishnevskii, E. N., 2004. Geology, composition, and genesis of the Sukhoi Log noble metals deposit, Russia, Ore Geology Reviews. 2004. V. 24, 1-2. P. 7-44.

Emsbo, P., 2000. Gold in Sedex Deposits, Gold in 2000, Steffen G. Hagemann, Philip E. Brown, Society of Economic Geologists.

Gadd, M. G., Layton-Matthews, D., Peter, J. M. et al., 2017. The world-class Howard's Pass SEDEX Zn-Pb district, Selwyn Basin, Yukon. Part II: the roles of thermochemical and bacterial sulfate reduction in metal fixation. Miner Deposita 52, 405–419 (2017).

Gardner, H.D. and Hutcheon, I., 1985. "Geochemistry, mineralogy, and geology of the Jason Pb-Zn deposits, Macmillan Pass, Yukon, Canada. Economic Geology (1985) 80 (5): 1257–1276.

Goodfellow, W. D. and Jonasson, I. R., 1987. Environment of formation of the Howards Pass (XY) Zn-Pb deposit, Selwyn Basin, Yukon. In: Proceedings Mineral Deposits of Northern Cordillera Symposium, Whitehorse, Yukon, Canada, 1987, Canadian Institute of Mining and Metallurgy, Special Volume 37, p. 19-50.

Goodfellow, W. D., 2007. Base metal metallogeny of the Selwyn Basin, Canada, in Goodfellow, W.D., ed., Mineral Deposits of Canada: A Synthesis of Major Deposit-Types, District Metallogeny, the Evolution of Geological Provinces, and Exploration Methods: Geological Association of Canada, Mineral Deposits Division, Special Publication 5, 553-579.

Goodfellow, W. D. and Lydon, J. W., 2007. Sedimentary exhalative (SEDEX) deposits. In: Mineral Deposits of Canada: A synthesis of major deposit types, district metallogeny, the evolution of geological provinces, and exploration methods, Goodfellow, W. D. (ed.), Geological Association of Canada, Special Publication No. 5, p. 163-183.

Jennings, D. S. and Jilson, G. A., 1986. Geology and Sulphide Deposits of Anvil Range, Yukon. In: Mineral Deposits of Northern Cordillera, Special Volume 37, J.A. Morin (ed.), Canadian Institute of Mining and Metallurgy, p. 319-361.

Jiang, X. and Broughton, D., 1997. 1997 Geological Assessment Report on Emerald Claims. AR093827.

Kirkham, G., Dunning, J., Schleiss, W., 2013. Update for Don deposit mineral resource estimate, Howard's Pass property, eastern Yukon, Selwyn Resources Ltd., NI 43-101 Technical Report. pp 145.

Lewis, L. L. and Bennett, V., 2011. Assessment Report. 2011 Surface Geochemical Exploration Program. AR096026.

Martel, E., Turner, E. C., Fischer, B., 2011. Geology of the central Mackenzie Mountains of the northern Canadian Cordillera, Sekwi Mountain (105P), Mount Eduni (106A) and northwestern Wrigley Lake (95M) map-areas, Northwest Territories, 423 p.

MINFILE 105O 040, - Ursa - Occurrence Details - Yukon Geological Survey (gov.yk.ca)

Moynihan, D., 2013. An introduction to the geology, tectonics and metallogeny of the Selwyn Basin area: Presented at Yukon airborne geophysics workshop, Yukon Geoscience Forum 2013, Yukon Chamber of Mines and Yukon Geological Survey, Whitehorse, Canada.

Paradis, S. and Goodfellow, W., 2012. SEDEX Deposits in the Cordillera: Currents concepts on their geology, genesis, and exploration, Geological Survey of Canada, Open File 7144.

Smith, C. A. S., Meikle, J. C., and Roots, C. F. (eds.), 2004. Ecoregions of the Yukon Territory: Biophysical properties of Yukon landscapes. Agriculture and Agri-Food Canada, PARC Technical Bulletin No. 04-01, Summerland, British Columbia, 313 p.

VTEM™

REPORT ON A HELICOPTER-BORNE VERSATILE TIME DOMAIN ELECTROMAGNETIC (VTEM™) AND AEROMAGNETIC GEOPHYSICAL SURVEY

JANUARY 2022

PROJECT: URSA PROJECT
LOCATION: FORKS AIRSTRIP, YUKON
FOR: SNOWLINE GOLD CORP
SURVEY FLOWN: SEPTEMBER 2021
PROJECT: GL210208

Geotech Ltd.
270 Industrial Parkway South Aurora,
ON Canada L4G 3T9

Tel: +1 905 841 5004
Web: www.geotech.ca Email:
info@geotech.ca

TABLE OF CONTENTS

LIST OF TABLES

APPENDICES

EXECUTIVE SUMMARY

URSA PROJECT
FORKS AIRSTRIP, YUKON

Between September 8th and September 14th, 2021, Geotech Ltd. carried out a helicopter-borne geophysical survey over the Ursa Project, situated near Forks Airstrip, Yukon.

Principal geophysical sensors included a versatile time domain electromagnetic (VTEM™) system, and a caesium magnetometer. Ancillary equipment included a GPS navigation system and a radar altimeter. A total of 461 line-kilometres of geophysical data were acquired during the survey.

In-field data quality assurance and preliminary processing were carried out on a daily basis during the acquisition phase. Preliminary and final data processing, including generation of final digital data and map products were undertaken from the office of Geotech Ltd. in Aurora, Ontario.

The processed survey results are presented as the following maps:

- Electromagnetic stacked profiles of the B-field Z Component,
- Electromagnetic stacked profiles of dB/dt Z Component,
- B-Field Z Component Channel grid,
- dB/dt Z Component Channel grid,
- Total Magnetic Intensity (TMI),
- Calculated Vertical Derivative (CVG) of Total Magnetic Intensity (TMI),
- Calculated Time Constant (Tau) with Calculated Vertical Derivative contours and
- Resistivity Depth Images (RDI) sections and plans are presented.

Digital data includes all electromagnetic and magnetic products, plus ancillary data including the waveform.

The survey report describes the procedures for data acquisition, equipment used, processing, final image presentation and the specifications for the digital data set.

1.   INTRODUCTION

1.1   GENERAL CONSIDERATIONS

Geotech Ltd. performed a helicopter-borne geophysical survey over the Ursa Project, situated near Forks Airstrip, Yukon (Figure 1 & Figure 2).

Scott Berdahl and Dan Meldrum represented Snowline Gold Corp during the data acquisition and data processing phases of this project.

The geophysical surveys consisted of helicopter borne EM using the versatile time-domain electromagnetic (VTEM™) system with Full-Waveform processing. Measurements consisted of Vertical (Z) component and aeromagnetics using a caesium magnetometer. A total of 461 line-km of geophysical data were acquired during the survey.

The crew was based out of Snowline Camp, Yukon (Figure 2) for the acquisition phase of the survey. Survey flying started on September 8th, 2021 and was completed on September 14th, 2021.

Data quality control and quality assurance, and preliminary data processing were carried out on a daily basis during the acquisition phase of the project. Final data processing followed immediately after the end of the survey. Final reporting, data presentation and archiving were completed from the Aurora office of Geotech Ltd. in December 2021.
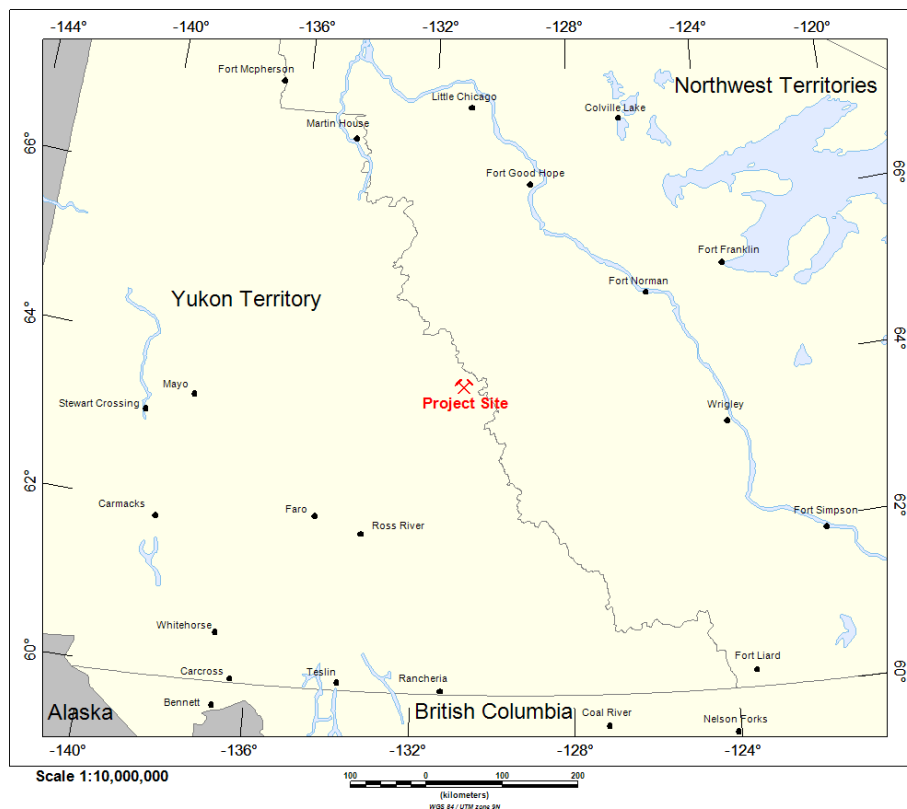
Figure 1: Survey location.

1.2   SURVEY AND SYSTEM SPECIFICATIONS

The Ursa Project survey area is situated approximately 13 km southeast of Forks Airstrip, Yukon (Figure 2).

Figure 2: Survey area locations on Google Earth.

The Ursa survey area was flown in a southwest to northeast (N 63° E azimuth) direction with traverse line spacing of 200 metres as depicted in Figure 3. Tie lines were flown perpendicular to the traverse lines at 2000 metre line spacing. For more detailed information on the flight spacing and direction see Table 1.

1.3   TOPOGRAPHIC RELIEF AND CULTURAL FEATURES

Topographically, the survey area exhibits rugged relief with elevations ranging from 1240 to 2106 metres above mean sea level over a total area of 82 square kilometres (Figure 3).

There are no visible signs of culture, such as roads, within the survey area.
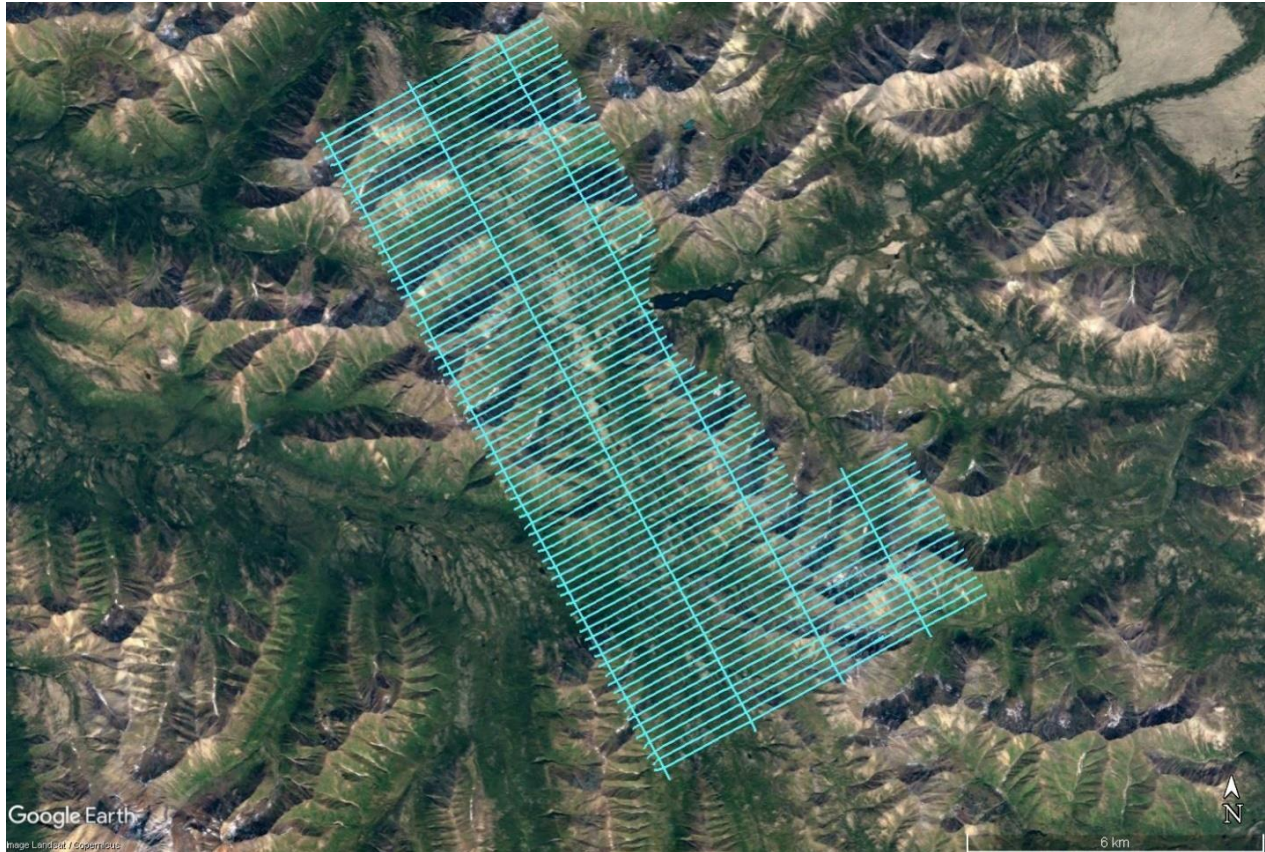
Figure 3: Flight path over a Google Earth Image.

2.   DATA ACQUISITION

2.1   SURVEY AREA

The survey area (see Figure 3 and Appendix A) and general flight specifications are as follows:

Table 1: Survey Specifications

Survey block	Line spacing (m)	Area (Km^2)	Planned Line-km	Actual[1] Line-km	Flight direction	Line numbers
Ursa Project	Traverse: 200	82	448	461	N63°E / N243°E	L1000 – L1720
	Tie: 2000				N153°E / N333°E	T2000 – T2030
TOTAL		82	448	461		

Survey area boundaries co-ordinates are provided in Appendix B.

2.2   SURVEY OPERATIONS

The following table shows the timing of the flying.

Table 2: Survey schedule

Date	Comments
08-September	Mobilization
09-September	Production Flight – 353.7 km flown
10-September	Weather day
11-September	Weather day
12-September	Weather day
13-September	Production Flight – 85.3 km flown
14-September	Demobilization

2.3   FLIGHT SPECIFICATIONS

During the survey, the helicopter was maintained at a mean altitude of 159 metres above the ground with an average survey speed of 79 km/hour. This allowed for an average Transmitter-Receiver loop terrain clearance of 122 metres and a magnetic sensor clearance of 146 metres.

The on-board operator was responsible for monitoring the system integrity. He also maintained a detailed flight log during the survey, tracking the times of the flight as well as any unusual geophysical or topographic features.

On return of the aircrew to the base camp the survey data was transferred from a compact flash card (PCMCIA) to the data processing computer. The data were then uploaded via ftp to the Geotech office in Aurora for daily quality assurance and quality control by qualified personnel.

[1] Note: Actual Line kilometres represent the total line kilometres in the final database. These line-km normally exceed the Planned Line-km, as indicated in the survey NAV files.

2.4   AIRCRAFT AND EQUIPMENT

2.4.1   SURVEY AIRCRAFT

The survey was flown using a Eurocopter Aerospatiale 350B3 helicopter, registration C-FKOI. The helicopter is owned and operated by Geotech Aviation. Installation of the geophysical and ancillary equipment was carried out by a Geotech Ltd crew.

2.4.2   ELECTROMAGNETIC SYSTEM

The electromagnetic system was a Geotech Time Domain EM (VTEM™) full receiver-waveform streamed data recorded system. The "full waveform VTEM system" uses the streamed half-cycle recording of transmitter and receiver waveforms to obtain a complete system response calibration throughout the entire survey flight. VTEM with the Serial number 25 had been used for the survey. The VTEM™ transmitter current waveform is shown diagrammatically in Figure 4.

The VTEM™ Receiver and transmitter coils were in concentric-coplanar and Z-direction oriented configuration. The Transmitter-receiver loop was towed at a mean distance of 37 metres below the aircraft as shown in Figure 5.

Figure 4: VTEM™ Transmitter Current Waveform.
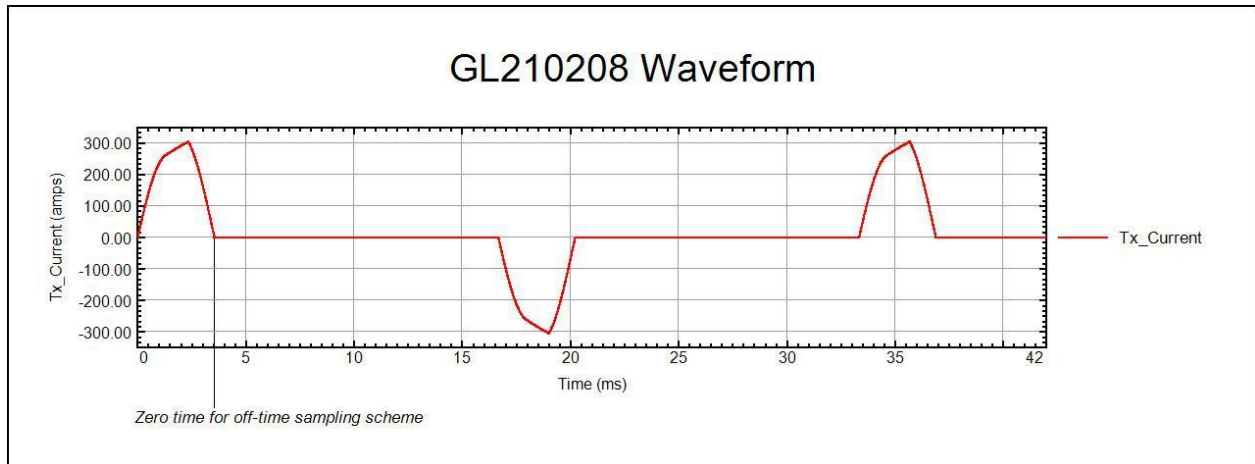
The VTEM™ decay sampling scheme is shown in Table 3 below. Forty-five-time measurement gates were used for the final data processing in the range from 0.021 to 10.667 msec. Zero time for the off- time sampling scheme is equal to the current pulse width and is defined as the time near the end of the turn-off ramp where the dI/dt waveform falls to 1/2 of its peak value.

Table 3: Off-Time Decay Sampling Scheme

VTEM™ Decay Sampling Scheme				
Index	Start	End	Middle	Width
Milliseconds				
4	0.018	0.023	0.021	0.005
5	0.023	0.029	0.026	0.005
6	0.029	0.034	0.031	0.005

VTEM™ Decay Sampling Scheme			
Index	Start	End	Middle	Width
Milliseconds			
7	0.034	0.039	0.036	0.005
8	0.039	0.045	0.042	0.006
9	0.045	0.051	0.048	0.007
10	0.051	0.059	0.055	0.008
11	0.059	0.068	0.063	0.009
12	0.068	0.078	0.073	0.010
13	0.078	0.090	0.083	0.012
14	0.090	0.103	0.096	0.013
15	0.103	0.118	0.110	0.015
16	0.118	0.136	0.126	0.018
17	0.136	0.156	0.145	0.020
18	0.156	0.179	0.167	0.023
19	0.179	0.206	0.190	0.027
20	0.206	0.236	0.220	0.030
21	0.236	0.271	0.253	0.035
22	0.271	0.312	0.290	0.040
23	0.312	0.358	0.333	0.046
24	0.358	0.411	0.383	0.053
25	0.411	0.472	0.440	0.061
26	0.472	0.543	0.505	0.070
27	0.543	0.623	0.580	0.081
28	0.623	0.716	0.667	0.093
29	0.716	0.823	0.766	0.107
30	0.823	0.945	0.880	0.122
31	0.945	1.086	1.010	0.141
32	1.086	1.247	1.161	0.161
33	1.247	1.432	1.333	0.185
34	1.432	1.646	1.531	0.214
35	1.646	1.891	1.760	0.245
36	1.891	2.172	2.021	0.281
37	2.172	2.1217	2.323	0.323
38	2.1217	2.865	2.667	0.370
39	2.865	3.290	3.063	0.427
40	3.290	3.781	3.521	0.490
41	3.781	4.341	4.042	0.560
42	4.341	4.987	4.641	0.646
43	4.987	5.729	5.333	0.742
44	5.729	6.581	6.125	0.852
45	6.581	7.560	7.036	0.979
46	7.560	8.685	8.083	1.125

VTEM™ Decay Sampling Scheme				
Index	Start	End	Middle	Width
Milliseconds				
47	8.685	9.977	9.286	1.290
48	9.977	11.458	10.667	1.482

Z Component: 4 - 48-time gates

VTEM™ system specifications:

Transmitter	Receiver
• Transmitter loop diameter: 17.6 m • Number of turns: 4 • Effective Transmitter loop area: 973 m^2 • Transmitter base frequency: 30 Hz • Peak current: 304.3 A • Pulse width: 3.55 ms • Waveform shape: Bi-polar trapezoid • Peak dipole moment: 296,126 nIA • Average transmitter-receiver loop terrain clearance: 122 metres above the ground	• Z-Coil diameter: 1.2 m • Number of turns: 100 • Effective coil area: 113.04 m^2
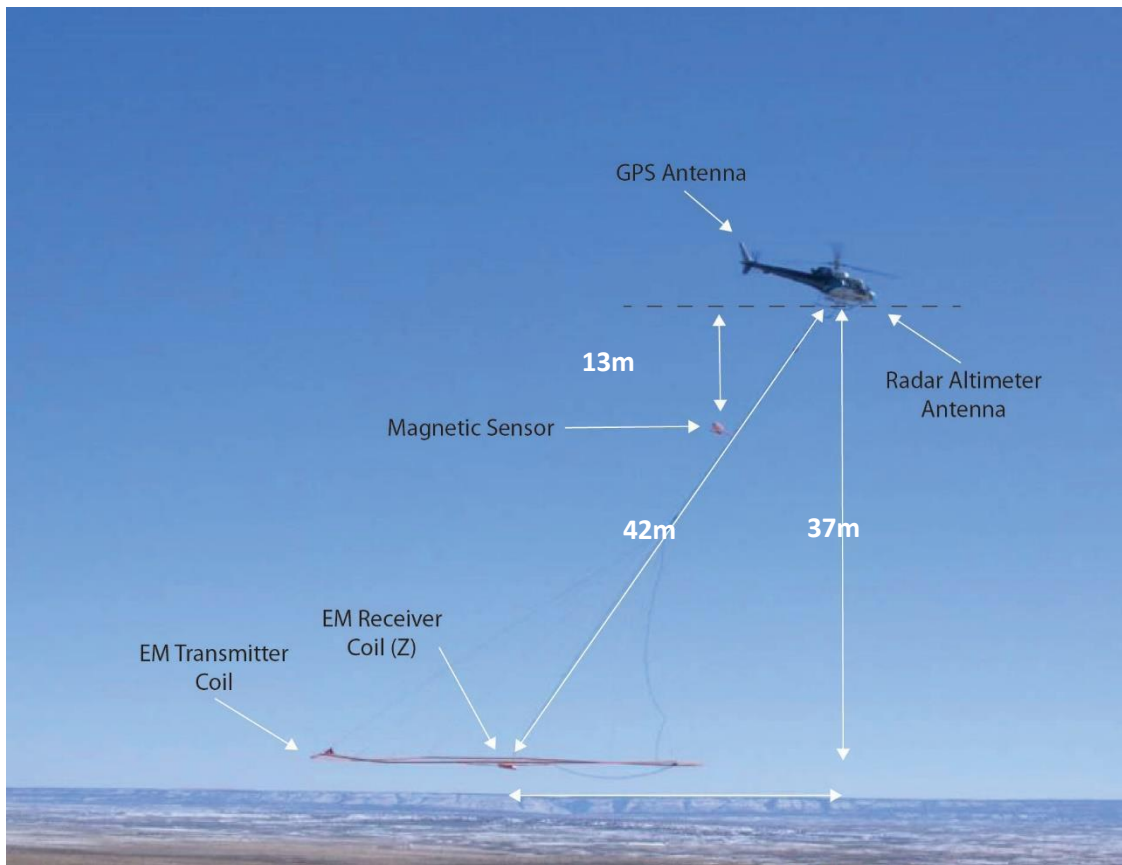
Figure 5: VTEM™ System Configuration.

2.4.3 FULL WAVEFORM VTEM™ SENSOR CALIBRATION

The calibration is performed on the complete VTEM™ system installed in and connected to the helicopter, using special calibration equipment. This calibration takes place on the ground at the start of the project prior to surveying.

The procedure takes half-cycle files acquired and calculates a calibration file consisting of a single stacked half-cycle waveform. The purpose of the stacking is to attenuate natural and man-made magnetic signals, leaving only the response to the calibration signal.

This calibration allows the transfer function between the EM receiver and data acquisition system and also the transfer function of the current monitor and data acquisition system to be determined. These calibration results are then used in VTEM full waveform processing.

2.4.4 RADAR ALTIMETER

A Terra TRA 3000/TRI 40 radar altimeter was used to record terrain clearance. The antenna was mounted beneath the bubble of the helicopter cockpit (Figure 5).

2.4.5 GPS NAVIGATION SYSTEM

The navigation system used was a Geotech PC104 based navigation system utilizing a NovAtel's WAAS (Wide Area Augmentation System) enabled GPS receiver, Geotech navigate software, a full screen display with controls in front of the pilot to direct the flight and a NovAtel GPS antenna mounted on the helicopter tail (Figure 5). As many as 11 GPS and two WAAS satellites may be monitored at any one time. The positional accuracy or circular error probability (CEP) is 1.8 m, with WAAS active, it is 1.0 m. The co-ordinates of the survey area were set-up prior to the survey and the information was fed into the airborne navigation system. The second GPS antenna is installed on the additional magnetic loop together with Gyro Inclinometer.

2.4.6 DIGITAL ACQUISITION SYSTEM

A Geotech data acquisition system recorded the digital survey data on an internal compact flash card. Data is displayed on an LCD screen as traces to allow the operator to monitor the integrity of the system. The data type and sampling interval as provided in Table 4.

Table 4: Acquisition Sampling Rates

Data Type	Sampling
TDEM	0.1 sec
Magnetometer	0.1 sec
GPS Position	0.2 sec
Radar Altimeter	0.2 sec

2.5   BASE STATION

A combined magnetometer/GPS base station was utilized on this project. A Geometrics Caesium vapour magnetometer was used as a magnetic sensor with a sensitivity of 0.001 nT. The base station was recording the magnetic field together with the GPS time at 1 Hz on a base station computer.

The base station magnetometer sensor was installed away from electric transmission lines and moving ferrous objects such as motor vehicles. The base station data were backed-up to the data processing computer at the end of each survey day.

3.   PERSONNEL

The following Geotech Ltd. personnel were involved in the project. <u>FIELD:</u>

Project Manager: Steven Cargnello (Office)

Data QC: Nick Venter (Office)

Crew chief: Colin Lennox

Operator: n/a

The survey pilot and the mechanical engineer were employed directly by the helicopter operator – Geotech Aviation.

Pilot: Robert Gerrard

Mechanical Engineer: n/a

<u>OFFICE</u>:

Preliminary Data Processing: Nick Venter

Final Data Processing: Marta Orta

Data QA/QC: TaiChyi Shei
                                       Jean M. Legault

Reporting/Mapping: Oreva Oputeh

Processing phase was carried out under the supervision of TaiChyi Shei and Jean M. Legault, Chief Geophysicist. The customer relations were looked after by David Hitz.

4.   DATA PROCESSING AND PRESENTATION

Data compilation and processing were carried out by the application of Geosoft OASIS Montaj and programs proprietary to Geotech Ltd.

4.1   FLIGHT PATH

The flight path, recorded by the acquisition program as WGS 84 latitude/longitude, was converted into the WGS84 Datum, UTM Zone 9 North coordinate system in Oasis Montaj.

The flight path was drawn using linear interpolation between x, y positions from the navigation system. Positions are updated every second and expressed as UTM easting's (x) and UTM northing's (y).

4.2   ELECTROMAGNETIC DATA

The Full Waveform EM specific data processing operations included:

- Half cycle stacking (performed at time of acquisition).
- System response correction.
- Parasitic and drift removal.

A three-stage digital filtering process was used to reject major sferic events and to reduce noise levels. Local sferic activity can produce sharp, large amplitude events that cannot be removed by conventional filtering procedures. Smoothing or stacking will reduce their amplitude but leave a broader residual response that can be confused with geological phenomena. To avoid this possibility, a computer algorithm searches out and rejects the major sferic events.

The signal to noise ratio was further improved by the application of a low pass linear digital filter. This filter has zero phase shift which prevents any lag or peak displacement from occurring, and it suppresses only variations with a wavelength less than about 1 second or 15 metres. This filter is a symmetrical 1 sec linear filter.

The results are presented as stacked profiles of EM voltages for the time gates, in linear - logarithmic scale for the B-field and dB/dt responses in the Z component. B-field Z component time channel recorded at 2.021 milliseconds after the termination of the impulse is also presented as a colour image. Calculated Time Constant (TAU) with Calculated Vertical Derivative contours is presented in Appendix C. Resistivity Depth Image (RDI) is also presented in Appendix F and G.

VTEM™ receiver coil orientation Z-axis coil is oriented parallel to the transmitter coil axis, and both are horizontal to the ground. Generalized modeling results of VTEM data, are shown in Appendix D.

Z component data produce double peak type anomalies for "thin" sub vertical targets and single peak for "thick" targets.

The limits and change-over of "thin-thick" depends on dimensions of a TEM system (Appendix D, Figure D-16).

4.3 MAGNETIC DATA

The processing of the magnetic data involved the correction for diurnal variations by using the digitally recorded ground base station magnetic values. The base station magnetometer data was edited and merged into the Geosoft GDB database on a daily basis. The aeromagnetic data was corrected for diurnal variations by subtracting the observed magnetic base station deviations.

Tie line levelling was carried out by adjusting intersection points along traverse lines. A micro- levelling procedure was applied to remove persistent low-amplitude components of flight-line noise remaining in the data.

The corrected magnetic data was interpolated between survey lines using a random point gridding method to yield x-y grid values for a standard grid cell size of 50 metres at the mapping scale. The Minimum Curvature algorithm was used to interpolate values onto a rectangular regular spaced grid.

5. DELIVERABLES

5.1 SURVEY REPORT

The survey report describes the data acquisition, processing, and final presentation of the survey results. The survey report is provided in two paper copies and digitally in PDF format.

5.2 MAPS

Final maps were produced at scale of 1:25,000 for best representation of the survey size and line spacing. The coordinate/projection system used was WGS84 Datum, UTM Zone 9 North. All maps show the flight path trace and topographic data; latitude and longitude are also noted on maps.

The results of the survey are presented as EM profiles, a late-time gate gridded EM channel, and a colour magnetic TMI contour map.

- Maps at 1:25,000 in Geosoft MAP format, as follows:

GL210208_25k_dBdt:	dB/dt profiles Z Component, Time Gates 0.220 – 7.036 ms in linear – logarithmic scale.
GL210208_25k _BField:	B-field profiles Z Component, Time Gates 0.220 – 7.036 ms in linear – logarithmic scale.
GL210208_25k _BFz36:	B-field late time Z Component Channel 36, Time Gate 2.021 ms colour image.
GL210208_25k _SFz31:	VTEM dB/dt Z Component Channel 31, Time Gate 1.010 ms.
GL210208_25k _TMI:	Total Magnetic Intensity (TMI)
GL210208_25k _CVG:	Calculated Vertical Gradient of Total Magnetic Intensity (TMI)
GL210208_25k _TauSF:	dB/dt Z Component Calculated Time Constant (Tau) with Calculated Vertical Derivative (CVG) contours

- Maps are also presented in PDF format.

- The topographic data and background shading were derived from ASTER GDEM: https://gdex.cr.usgs.gov/gdex.

- A Google Earth file *GL210208_Snowline.kmz* showing the flight path of the block is included. Free versions of Google Earth software from: http://earth.google.com/download-earth.html

5.3 DIGITAL DATA

Two copies of the data and maps on DVD were prepared to accompany the report. Each DVD contains a digital file of the line data in GDB Geosoft Montaj format as well as the maps in Geosoft Montaj Map and PDF format.

5.3.1 DVD STRUCTURE
Data   contains databases, grids and maps, as described below. Report contains a copy of the report and appendices in PDF format.

Databases in Geosoft GDB format, containing the channels listed in Table 5.

Table 5: Geosoft GDB Data Format

Channel name	Units	Description
X	metres	UTM Easting WGS84 Zone 9 North
Y	metres	UTM Northing WGS84 Zone 9 North
Longitude	Decimal Degrees	WGS 84 Longitude data
Latitude	Decimal Degrees	WGS 84 Latitude data
Z	metres	GPS antenna elevation (above Geoid)
Zb	metres	EM bird elevation (above Geoid)
Radar	metres	helicopter terrain clearance from radar altimeter
Radarb	metres	Calculated EM transmitter-receiver loop terrain clearance from radar altimeter
DEM	metres	Digital Elevation Model
Gtime	Seconds of the day	GPS time
Mag1	nT	Magnetic diurnal variation data
Basemag	nT	Magnetic diurnal variation data
Mag2	nT	Diurnal corrected Total Magnetic field data
Mag3	nT	Levelled Total Magnetic field data
CVG	nT/m	Calculated Magnetic Vertical Gradient
SFz[4]	$pV/(A*m^4)$	Z dB/dt 0.021 millisecond time channel
SFz[5]	$pV/(A*m^4)$	Z dB/dt 0.026 millisecond time channel
SFz[6]	$pV/(A*m^4)$	Z dB/dt 0.031 millisecond time channel
SFz[7]	$pV/(A*m^4)$	Z dB/dt 0.036 millisecond time channel
SFz[8]	$pV/(A*m^4)$	Z dB/dt 0.042 millisecond time channel
SFz[9]	$pV/(A*m^4)$	Z dB/dt 0.048 millisecond time channel
SFz[10]	$pV/(A*m^4)$	Z dB/dt 0.055 millisecond time channel
SFz[11]	$pV/(A*m^4)$	Z dB/dt 0.063 millisecond time channel
SFz[12]	$pV/(A*m^4)$	Z dB/dt 0.073 millisecond time channel
SFz[13]	$pV/(A*m^4)$	Z dB/dt 0.083 millisecond time channel
SFz[14]	$pV/(A*m^4)$	Z dB/dt 0.096 millisecond time channel
SFz[15]	$pV/(A*m^4)$	Z dB/dt 0.110 millisecond time channel
SFz[16]	$pV/(A*m^4)$	Z dB/dt 0.126 millisecond time channel
SFz[17]	$pV/(A*m^4)$	Z dB/dt 0.145 millisecond time channel
SFz[18]	$pV/(A*m^4)$	Z dB/dt 0.167 millisecond time channel
SFz[19]	$pV/(A*m^4)$	Z dB/dt 0.190 millisecond time channel
SFz[20]	$pV/(A*m^4)$	Z dB/dt 0.220 millisecond time channel
SFz[21]	$pV/(A*m^4)$	Z dB/dt 0.253 millisecond time channel

Channel name	Units	Description
SFz[22]	$pV/(A*m^4)$	Z dB/dt 0.290 millisecond time channel
SFz[23]	$pV/(A*m^4)$	Z dB/dt 0.333 millisecond time channel
SFz[24]	$pV/(A*m^4)$	Z dB/dt 0.383 millisecond time channel
SFz[25]	$pV/(A*m^4)$	Z dB/dt 0.440 millisecond time channel
SFz[26]	$pV/(A*m^4)$	Z dB/dt 0.505 millisecond time channel
SFz[27]	$pV/(A*m^4)$	Z dB/dt 0.580 millisecond time channel
SFz[28]	$pV/(A*m^4)$	Z dB/dt 0.667 millisecond time channel
SFz[29]	$pV/(A*m^4)$	Z dB/dt 0.766 millisecond time channel
SFz[30]	$pV/(A*m^4)$	Z dB/dt 0.880 millisecond time channel
SFz[31]	$pV/(A*m^4)$	Z dB/dt 1.010 millisecond time channel
SFz[32]	$pV/(A*m^4)$	Z dB/dt 1.161 millisecond time channel
SFz[33]	$pV/(A*m^4)$	Z dB/dt 1.333 millisecond time channel
SFz[34]	$pV/(A*m^4)$	Z dB/dt 1.531 millisecond time channel
SFz[35]	$pV/(A*m^4)$	Z dB/dt 1.760 millisecond time channel
SFz[36]	$pV/(A*m^4)$	Z dB/dt 2.021 millisecond time channel
SFz[37]	$pV/(A*m^4)$	Z dB/dt 2.323 millisecond time channel
SFz[38]	$pV/(A*m^4)$	Z dB/dt 2.667 millisecond time channel
SFz[39]	$pV/(A*m^4)$	Z dB/dt 3.063 millisecond time channel
SFz[40]	$pV/(A*m^4)$	Z dB/dt 3.521 millisecond time channel
SFz[41]	$pV/(A*m^4)$	Z dB/dt 4.042 millisecond time channel
SFz[42]	$pV/(A*m^4)$	Z dB/dt 4.641 millisecond time channel
SFz[43]	$pV/(A*m^4)$	Z dB/dt 5.333 millisecond time channel
SFz[44]	$pV/(A*m^4)$	Z dB/dt 6.125 millisecond time channel
SFz[45]	$pV/(A*m^4)$	Z dB/dt 7.036 millisecond time channel
SFz[46]	$pV/(A*m^4)$	Z dB/dt 8.083 millisecond time channel
SFz[47]	$pV/(A*m4)$	Z dB/dt 9.286 millisecond time channel
SFz[48]	$pV/(A*m4)$	Z dB/dt 10.667 millisecond time channel
BFz	$(pV*ms)/(A*m^4)$	Z B-Field data for time channels 4 to 48
NchanBF		Latest time channels of TauBF calculation
TauBF	ms	Time constant B-Field
NchanSF		Latest time channels of TAU calculations
TauSF	ms	Time constant dB/dt
PLM		60 Hz power line monitor

Electromagnetic B-field and dB/dt Z component data is found in array channel format between indexes 4 – 48, as described above.

5.3.2   DATABASE OF THE APPARENT RESISTIVITY DEPTH IMAGING PRODUCTS

- in Geosoft GDB format, containing the following channels:

Table 6: Geosoft Resistivity Depth Image GDB Data Format

Channel name	Units	Description
Xg	metres	UTM Easting WGS84 Zone 9 North
Yg	metres	UTM Northing WGS84 Zone 9 North
Dist	metres	Distance from the beginning of the line
Depth	metres	array channel, depth from the surface
Z	metres	array channel, depth from sea level

Channel name	Units	Description
AppRes	Ohm-m	array channel, Apparent Resistivity
TR	metres	EM system height from sea level
Topo	metres	digital elevation model
Radarb	metres	Calculated EM transmitter-receiver loop terrain clearance from radar altimeter
SF	pV/(A*m^4)	array channel, Z dB/dT
MAG	nT	Total Magnetic Intensity
CVG	nT/m	Calculated Vertical Derivative
DOI	metres	Depth of Investigation: a measure of VTEM depth effectiveness
PLM		60Hz Power Line Monitor

5.3.3   DATABASE OF THE VTEM WAVEFORM

- "GL210208_Waveform.gdb" in Geosoft GDB format, containing the following channels:

Table 7: Geosoft database for the VTEM waveform

Channel name	Units	Description
Time	milliseconds	Sampling rate interval, 5.2083 microseconds
Tx_Current	amps	Output current of the transmitter

5.3.4   GEOSOFT RESISTIVITY DEPTH IMAGE PRODUCTS:

Sections: Apparent resistivity sections along each line in .GRD and .PDF format Slices: Apparent resistivity slices at selected depths from 25m to depth of investigation, at an increment of 25m in .GRD and .PDF format Voxel: 3D Voxel imaging of apparent resistivity data clipped by digital elevation and depth of investigation

5.3.5   GRIDS IN GEOSOFT GRD AND GEOTIFF FORMAT

- Grids in Geosoft GRD and GeoTIFF format, as follows:

BFz36:   B-Field Z Component Channel 36 (Time Gate 2.021ms) CVG: Calculated Vertical Derivative (nT/m)
DEM: Digital Elevation Model (metres) Mag3: Total Magnetic Intensity (nT)
SFz10:   dB/dt Z Component Channel 10 (Time Gate 0.055 ms) SFz31: dB/dt Z Component Channel 31 (Time Gate 1.010 ms) SFz41: dB/dt Z Component Channel 41 (Time Gate 4.042 ms) TauBF: B-Field Z Component, Calculated Time Constant (ms) TauSF: dB/dt Z Component, Calculated Time Constant (ms) PLM: 60Hz Power Line Monitor

A Geosoft .GRD file has a .GI metadata file associated with it, containing grid projection information. A grid cell size of 50 metres was used.

6. CONCLUSIONS AND RECOMMENDATIONS

A helicopter-borne versatile time domain electromagnetic (VTEM™) geophysical survey has been completed over the Ursa Project situated near Forks Airstrip, Yukon.

The total area coverage is 82 km^2 and the total survey line coverage is 461 line-kilometres on one(1) survey block. The principal sensors included a Time Domain EM system, and a magnetometer system. Results have been presented as stacked profiles, and contour colour images at a scale of 1:25,000. There is no formal interpretation included in this study, however RDI resistivity-depth imaging has been performed in support of the VTEM data.

The relatively rugged topography and the flight lines that follow alternating NE-SW trending valleys and hills, likely coupled with the nature of the geology at Ursa, have resulted in corrugation-like, cross-cutting NE-SW trending patterns that overprint the NW-SE geologic trends and impact the magnetic data, in particular, due to the relatively weak magnetic field strengths, as well the EM data channels. We therefore note that additional processing has been applied to some of the final grid contour maps to help minimize this effect for mapping purposes (see Appendix C).

Based on the geophysical results obtained, a number of geophysical anomalies have been identified across the survey area. The block features weak magnetic responses, with a measured range of only 90nT, highlighting a prominent, long wavelength, intrusion-like, weak magnetic high in the northeast corner of the block and a decreasing regional trend from north to south. Magnetic derivatives (CVG) accentuate multiple, weak, sinuous NW-SE oriented magnetic lineament trends that are widespread cross the property and potentially represent the basement geology. In particular, a prominent, structural-like, long-strike length and narrow magnetic low lineament is highlighted in the CVG plan (Appendix C) on the western edge of the block.

Electromagnetically, a number of EM anomalies are identified in the block, including a major, NW-SE trending, long strike length (>15km), variably conductive, stratigraphic-like horizon that extends along west central part of Ursa block. Consisting of multiple (>2-3), closely spaced, subparalleling, steeply-dipping conductive horizons, this unit lies along the eastern contact with the prominent, NW- SE trending structural-like magnetic low lineament mentioned previously. This stratigraphic like conductive unit is ~4km wide in the northern half of the block, but narrows to ~1.5km wide at the southern end. As mentioned earlier, the cross-cutting NE-SW conductive trends that are visible in the VTEM data also correlate with lines flown at lower elevations along incised valleys and may instead reflect depth to basement artifacts.
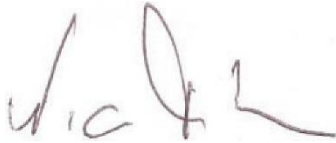
The relationship between the EM resistivity and magnetic data are highlighted in the TAU dB$_Z$/dt EM decay constant image with magnetic CVG contour map (Appendix C) and the RDI resistivity-depth sections with profiles (Appendix G). Measured dB$_Z$/dt time-constants (TauSF) for conductors range from ~ 1.0-3.6 ms, indicating induced responses from relatively moderate to highly conductive targets. Based on RDI imaging, apparent resistivities range from lows of ~1-3 ohm-m to highs of
~2200-5000 ohm-m. Based on the EM profiles and RDI sections, anomalies exhibit top depths varying from ~50 m in valleys and deepening to >200 m below topographic highs . Depths of investigation (DOI) are indicated to vary between ~175m to >650m.

The Ursa Project is known to be prospective for shale-hosted base metals (Zn-Ni-Cu-V-Ag) and Carlin- style gold mineralization (https://snowlinegold.com/ursa). As a result, both EM and magnetic results

are likely to be of exploration interest. We recommend that EM anomaly picking be performed along with Maxwell EM plate modeling of major anomalies of interest. More advanced 1D layered earth modeling of the EM data be performed to highlight anomalous resistivity features of interest, both in plan and in cross-section, prior to ground follow up and drill testing. CET-type magnetic structural / lineament analysis and 3D MVI magnetic inversions will be useful for mapping structure, alteration, and lithology in 2D-3D spatially distributed across the block. We recommend that more advanced, integrated interpretation be performed on these geophysical data and these results further evaluated against the known geology for future targeting.

Respectfully submitted[2],

_____
Nick Venter

Geotech Ltd.

_____
Jean Legault, M.Sc.A., P.Eng, P.Geo

Geotech Ltd.

_____

_____
Geotech Ltd.

January 2022

---

[2] Final data processing of the EM and magnetic data were carried out by Marta Orta, from the office of Geotech Ltd. in Aurora, Ontario, under the supervision of TaiChyi Shei and Jean Legault, Chief Geophysicist.

9   APPENDIX A

SURVEY AREA LOCATION MAP

Overview of the Survey Area

10 APPENDIX B

10.1 SURVEY AREA COORDINATES

(WGS 84, UTM Zone 9 North)

Ursa	
X	Y
407494	7061433
400968	7074443
405362	7076647
410245	7066914
412374	7067982
414018	7064705

APPENDIX C - GEOPHYSICAL MAPS[1]

Profiles scale 1 mm = 0.045 (pV*ms)/(A*m^4)
(Linear between +/- 0.5 (pV*ms)/(A*m^4)
logarithmic above 0.5 (pV*ms)/(A*m^4)

0.220 ms (B-field)
0.253 ms (B-field)
0.290 ms (B-field)
0.333 ms (B-field)
0.383 ms (B-field)
0.440 ms (B-field)
0.505 ms (B-field)
0.580 ms (B-field)
0.667 ms (B-field)
0.766 ms (B-field)
0.880 ms (B-field)
1.010 ms (B-field)
1.161 ms (B-field)
1.333 ms (B-field)
1.531 ms (B-field)
1.760 ms (B-field)
2.021 ms (B-field)
2.323 ms (B-field)
2.667 ms (B-field)
3.063 ms (B-field)
3.521 ms (B-field)
4.042 ms (B-field)
4.641 ms (B-field)
5.333 ms (B-field)
6.125 ms (B-field)
7.036 ms (B-field)

57133.53
57130.39
57128.34
57125.93
57122.49
57120.41
57118.50
57116.67
57114.88
57112.71
57110.98
57108.60
57106.24
57103.54
57101.15
57099.39
57096.64
57091.28
57079.66

TMI
(nT)

Scale 1:50000

VTEM B-Field Z Component Profiles, Time Gates 0.220 to 7.036 ms, over total magnetic intensity (TMI) grid

---

[1] Complete full size geophysical maps are also available in PDF format located in the final data maps folder
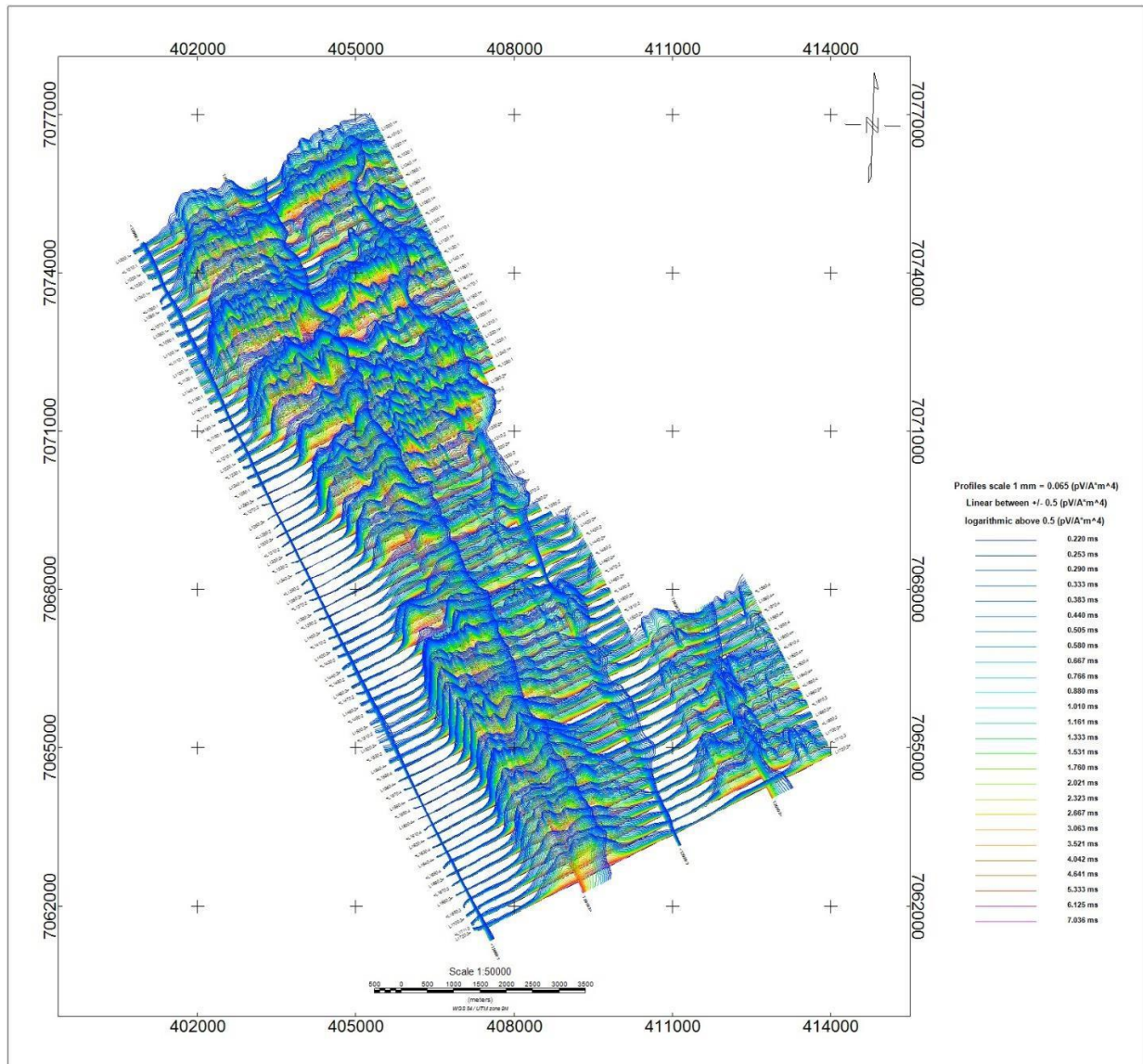
VTEM dB/dt Z Component Profiles, Time Gates 0.220 to 7.036 ms
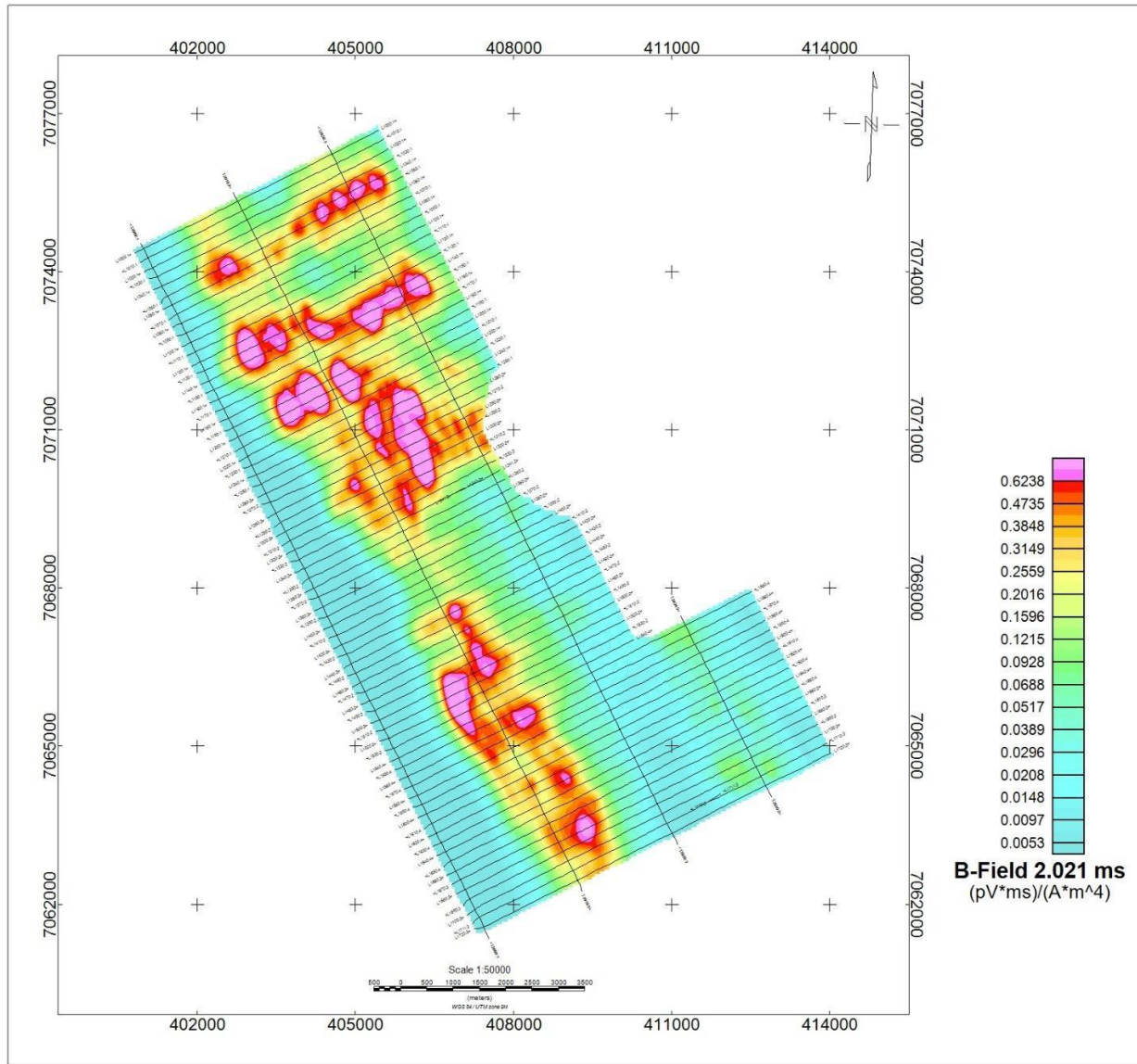
VTEM B-Field Z Component Channel 36, Time Gate 2.021 ms
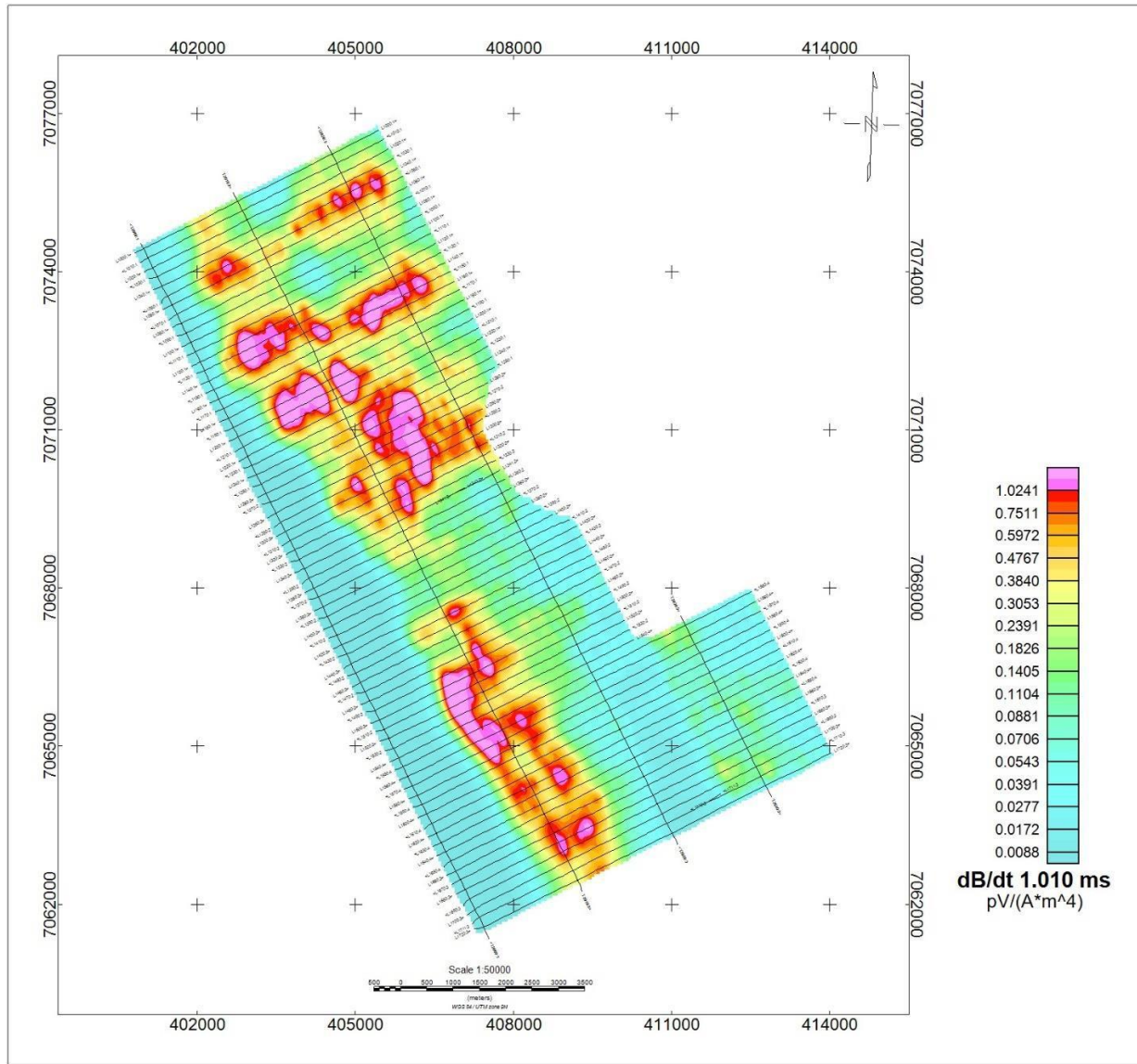
VTEM dB/dt Z Component Channel 31, Time Gate 1.010 ms.
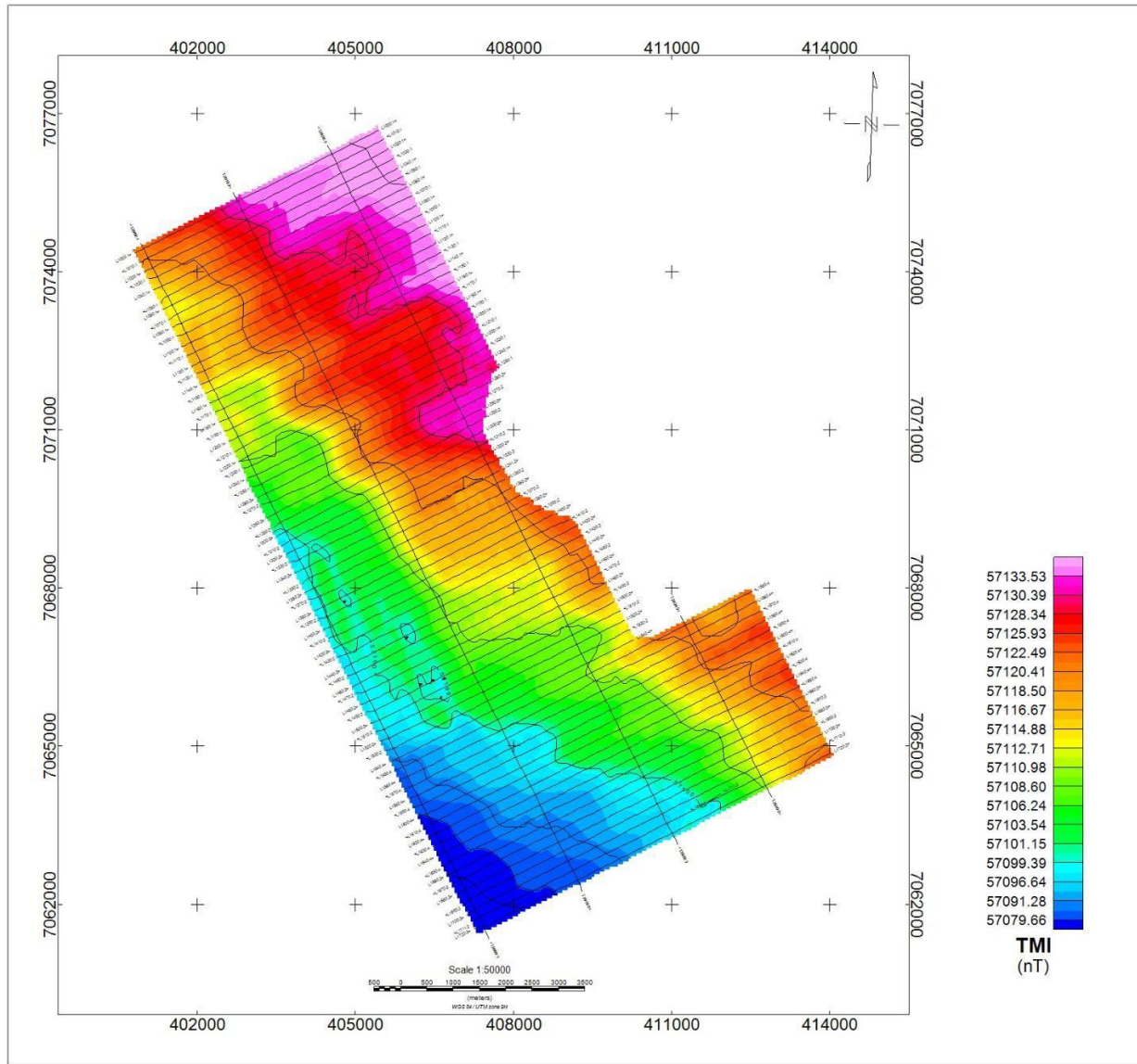
Total Magnetic Intensity (TMI)
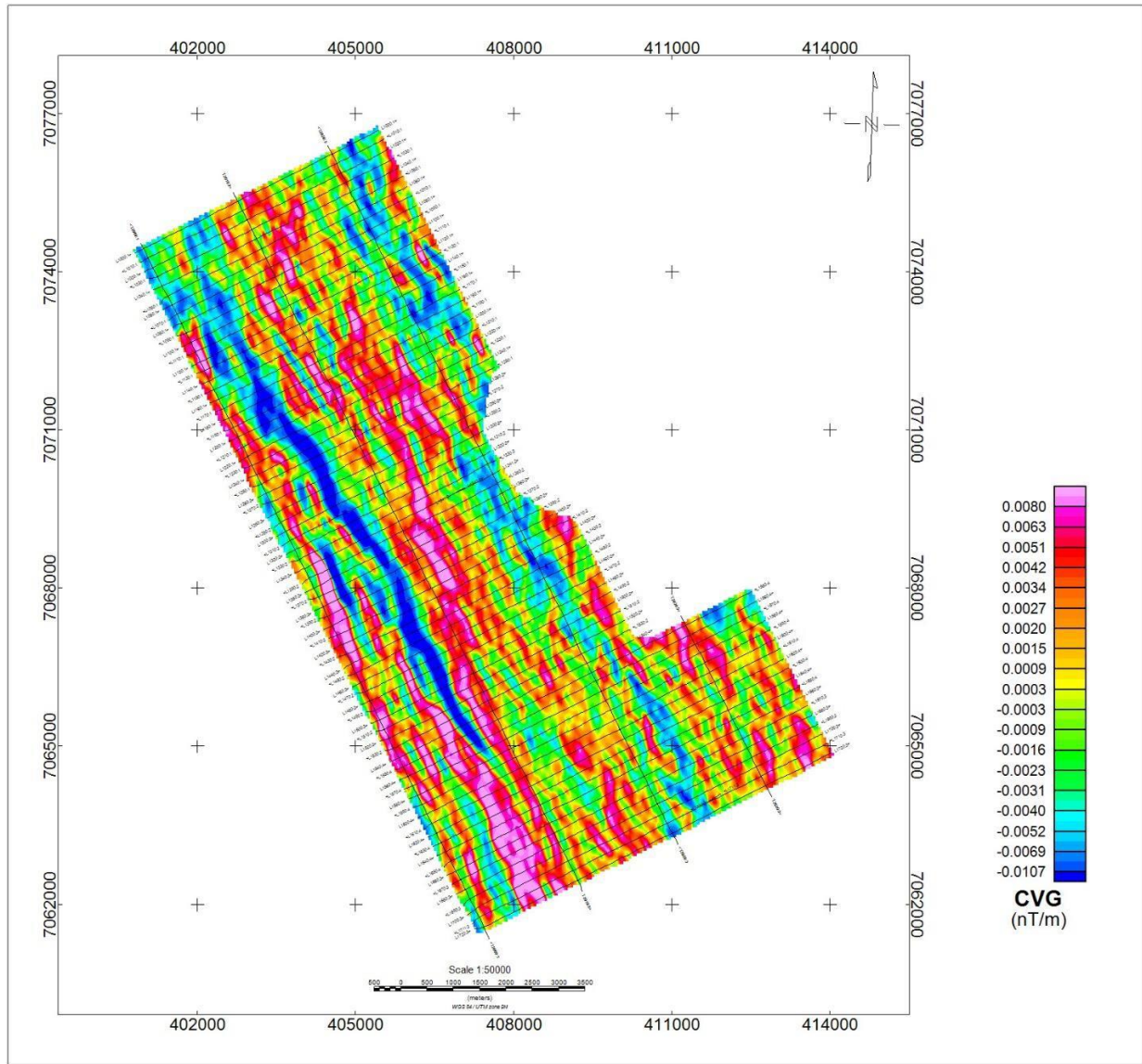
Calculated Vertical Derivative (CVG) of Total Magnetic Intensity (TMI)
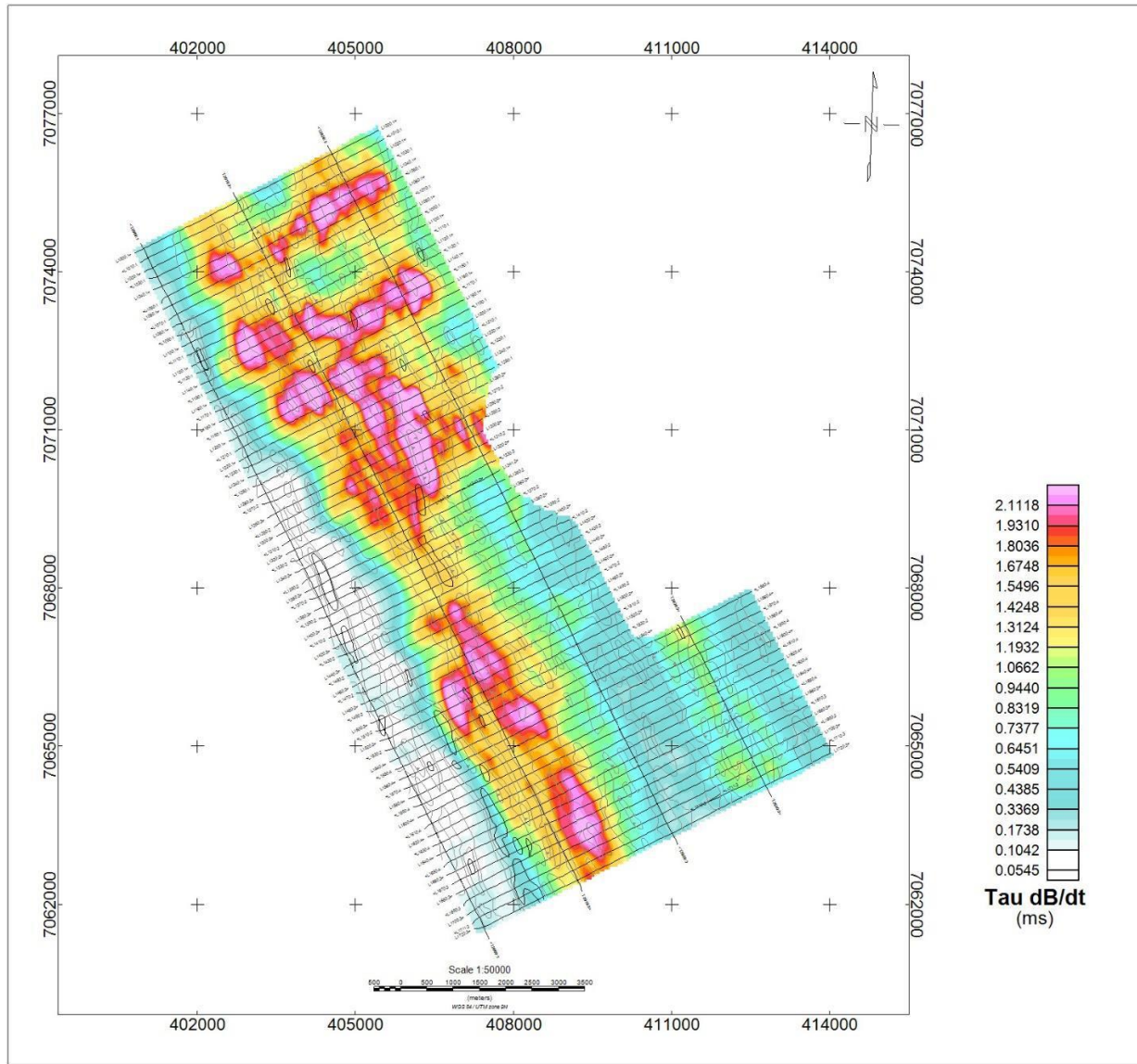
dB/dt Z Component Calculated Time Constant (Tau), with Calculated Vertical Derivative (CVG) contours

10.2 RESISTIVITY DEPTH IMAGE (RDI) MAPS

3D View of the RDI Apparent Resistivity Voxel
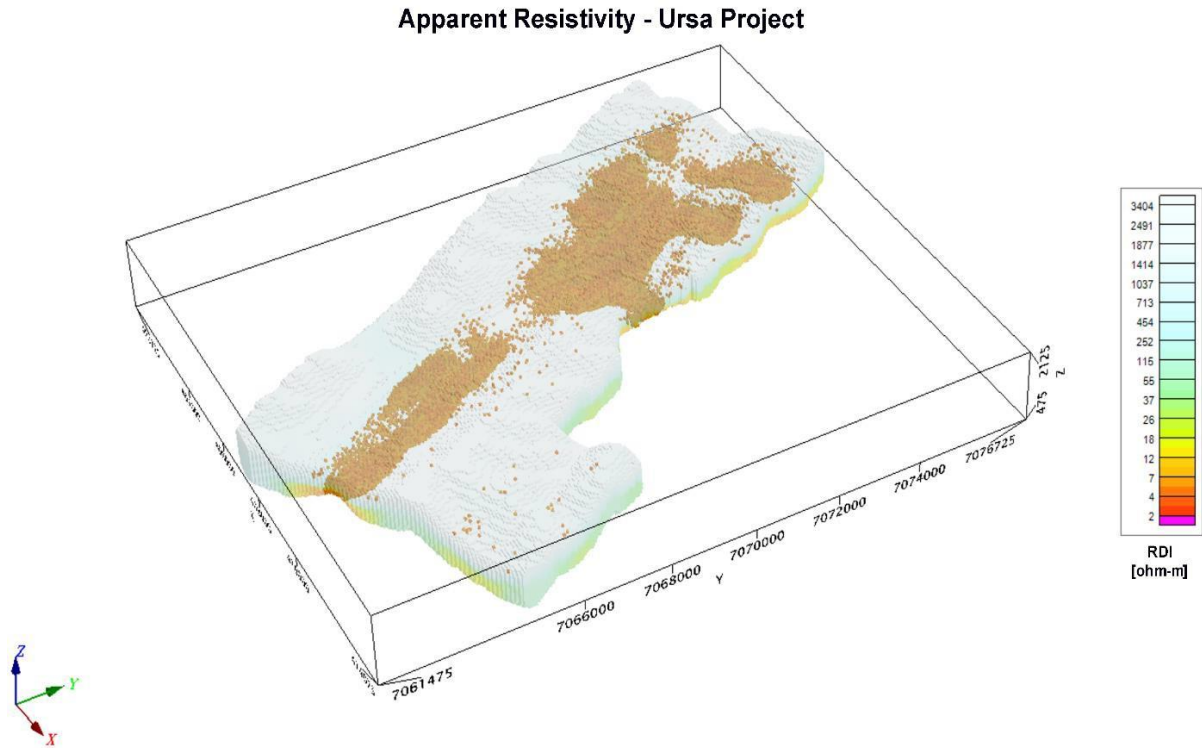
11 APPENDIX D

11.1 GENERALIZED MODELING RESULTS OF THE VTEM SYSTEM INTRODUCTION

The VTEM system is based on a concentric or central loop design, whereby, the receiver is positioned at the centre of a transmitter loop that produces a primary field. The wave form is a bi-polar, modified square wave with a turn-on and turn-off at each end.

During turn-on and turn-off, a time varying field is produced (dB/dt) and an electro-motive force (emf) is created as a finite impulse response. A current ring around the transmitter loop moves outward and downward as time progresses. When conductive rocks and mineralization are encountered, a secondary field is created by mutual induction and measured by the receiver at the centre of the transmitter loop.

Efficient modeling of the results can be carried out on regularly shaped geometries, thus yielding close approximations to the parameters of the measured targets. The following is a description of a series of common models made for the purpose of promoting a general understanding of the measured results.

A set of models has been produced for the Geotech VTEM™ system dB/dT Z and X components (see models D1 to D15). The Maxwell ™ modeling program (EMIT Technology Pty. Ltd. Midland, WA, AU) used to generate the following responses assumes a resistive half-space. The reader is encouraged to review these models, so as to get a general understanding of the responses as they apply to survey results. While these models do not begin to cover all possibilities, they give a general perspective on the simple and most commonly encountered anomalies.

As the plate dips and departs from the vertical position, the peaks become asymmetrical.

As the dip increases, the aspect ratio (Min/Max) decreases and this aspect ratio can be used as an empirical guide to dip angles from near 90º to about 30º. The method is not sensitive enough where dips are less than about 30º.
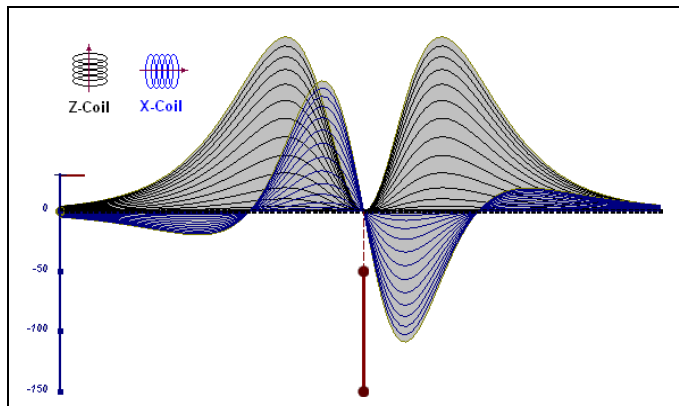
Figure D-1: vertical thin plate
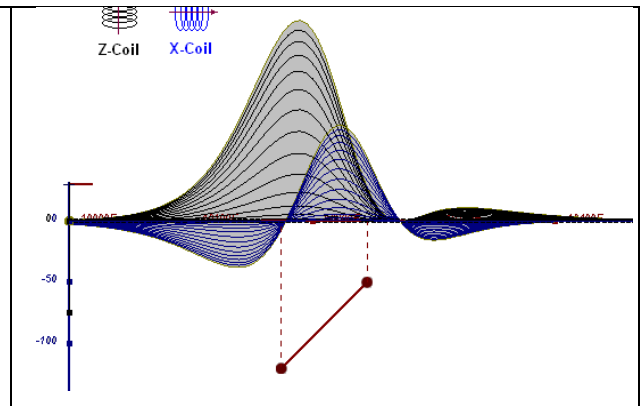
Figure D-2: inclined thin plate
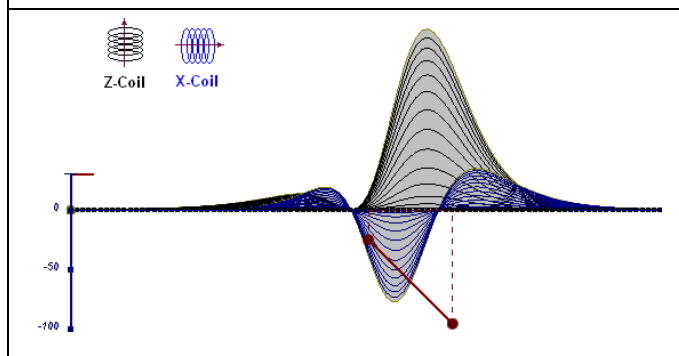
Figure D-3: inclined thin plate
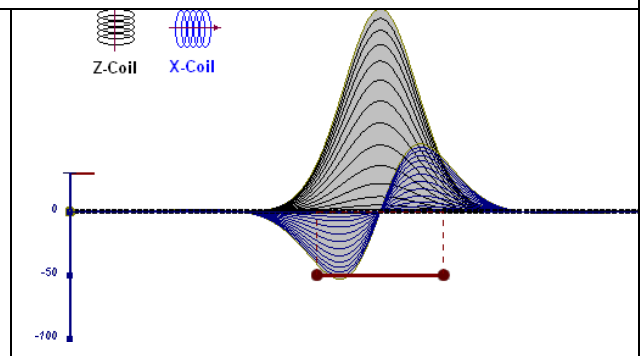
Figure D-4: horizontal thin plate
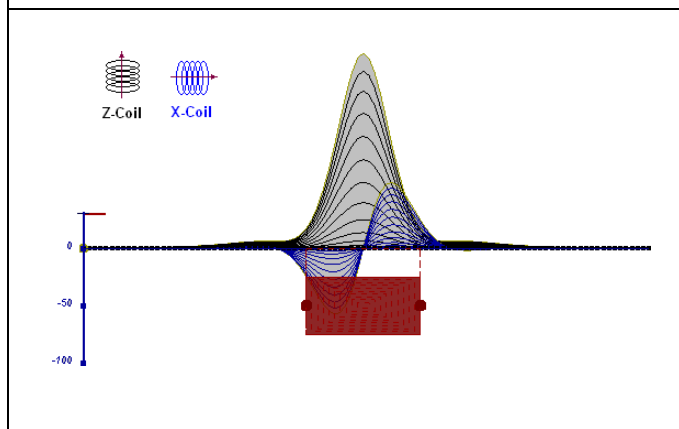
Figure D-5: horizontal thick plate (linear scale of the response)
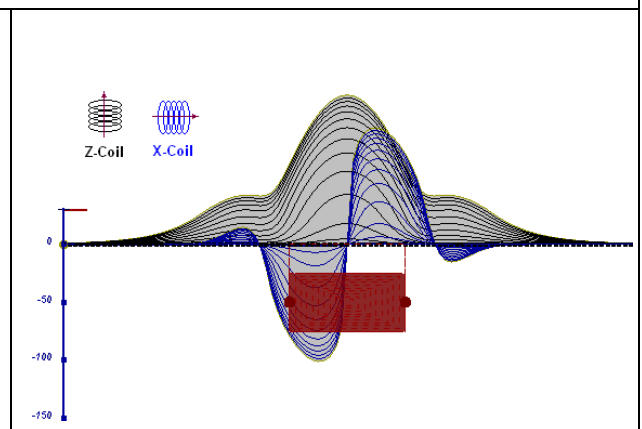
Figure D-6: horizontal thick plate (log scale of the response)
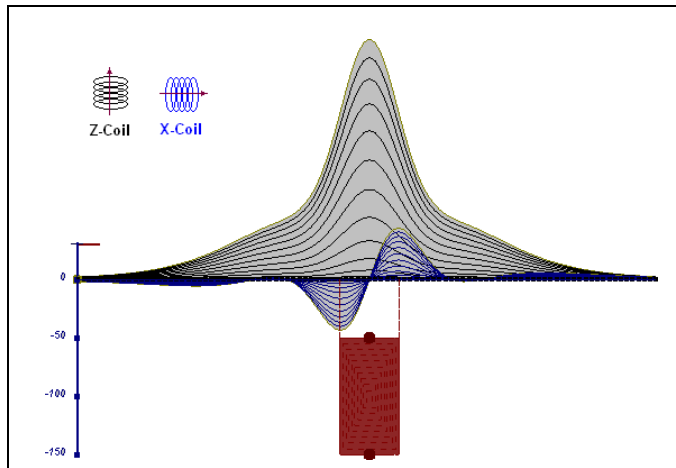
Figure D-7: vertical thick plate (linear scale of the response). 50 m depth
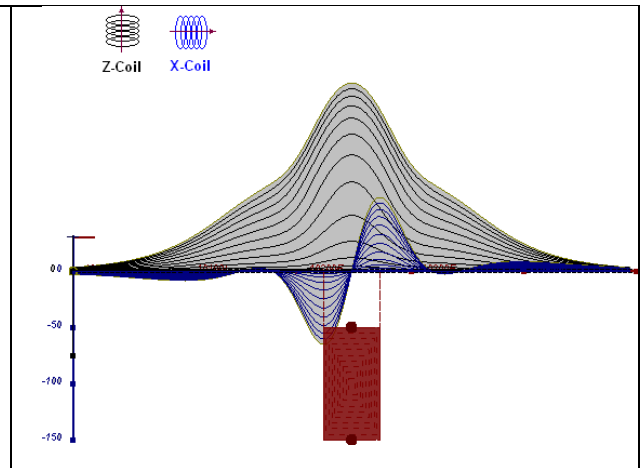
Figure D-8: vertical thick plate (log scale of the response). 50 m depth
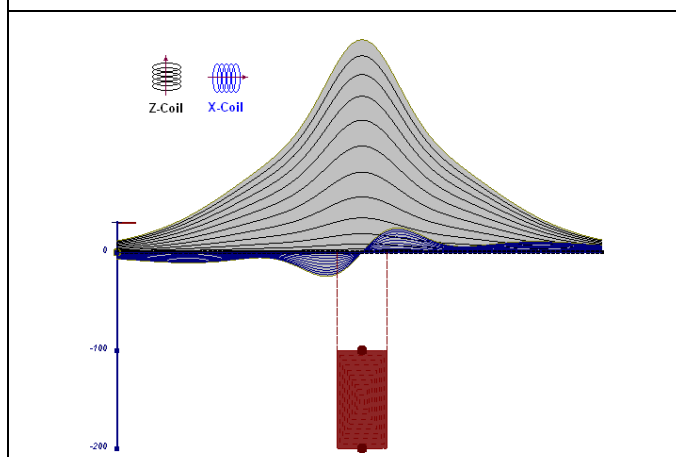
Figure D-9: vertical thick plate (linear scale of the response). 100 m depth
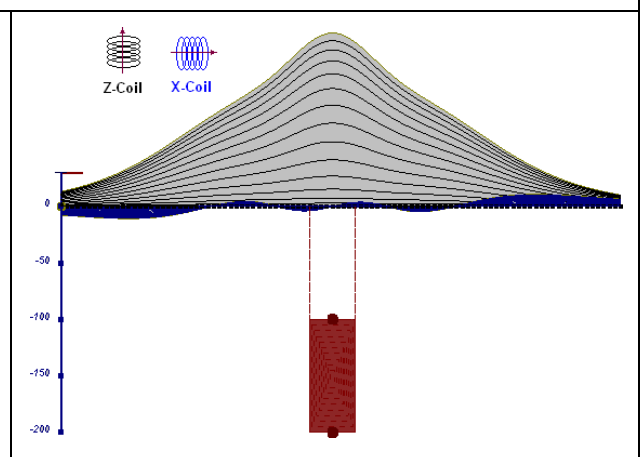
Figure D-10: vertical thick plate (linear scale of the response). Depth / horizontal thickness=2.5
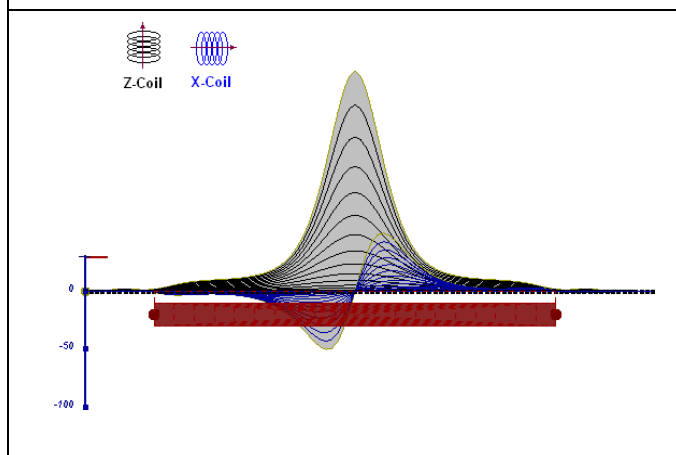
Figure D-11: horizontal thick plate (linear scale of the response)
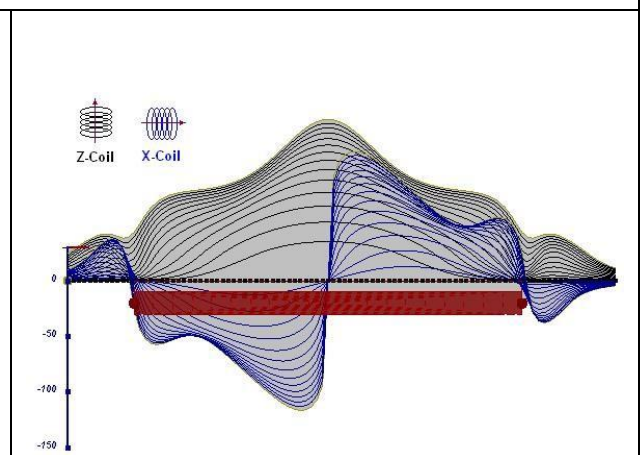
Figure D-12: horizontal thick plate (log scale of the response)
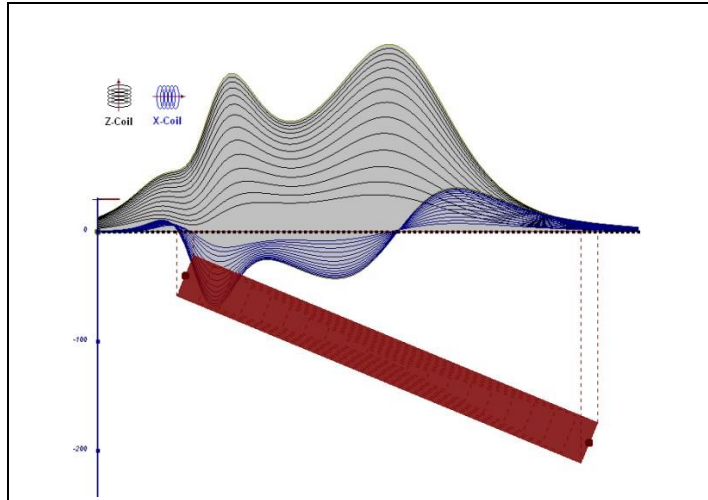
Figure D-13: inclined long thick plate
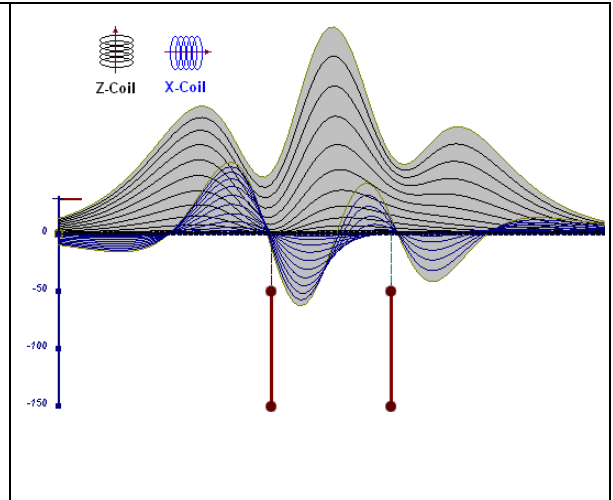
Figure D-14: two vertical thin plates
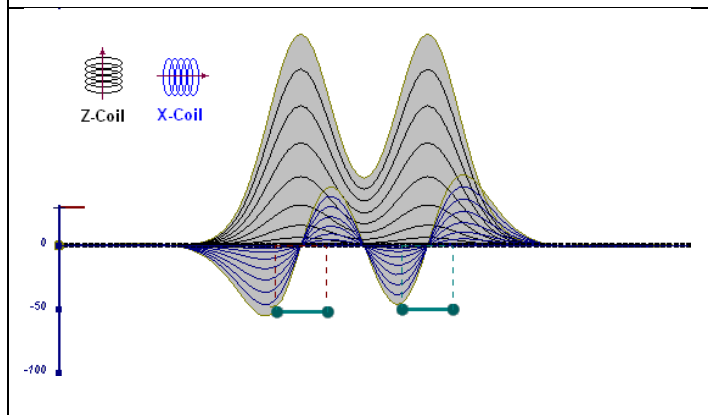
Figure D-15: two horizontal thin plates
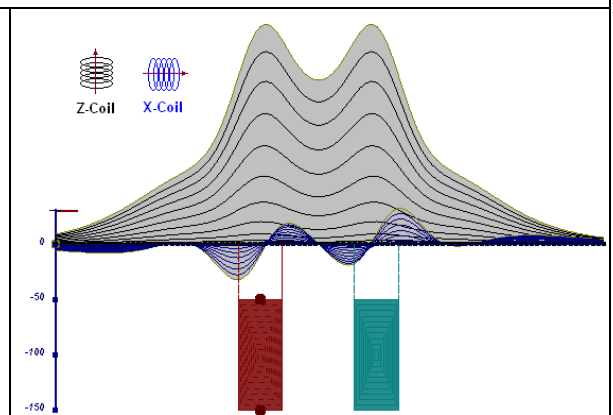
Figure D-16: two vertical thick plates

The same type of target but with different thickness, for example, creates different form of the response:
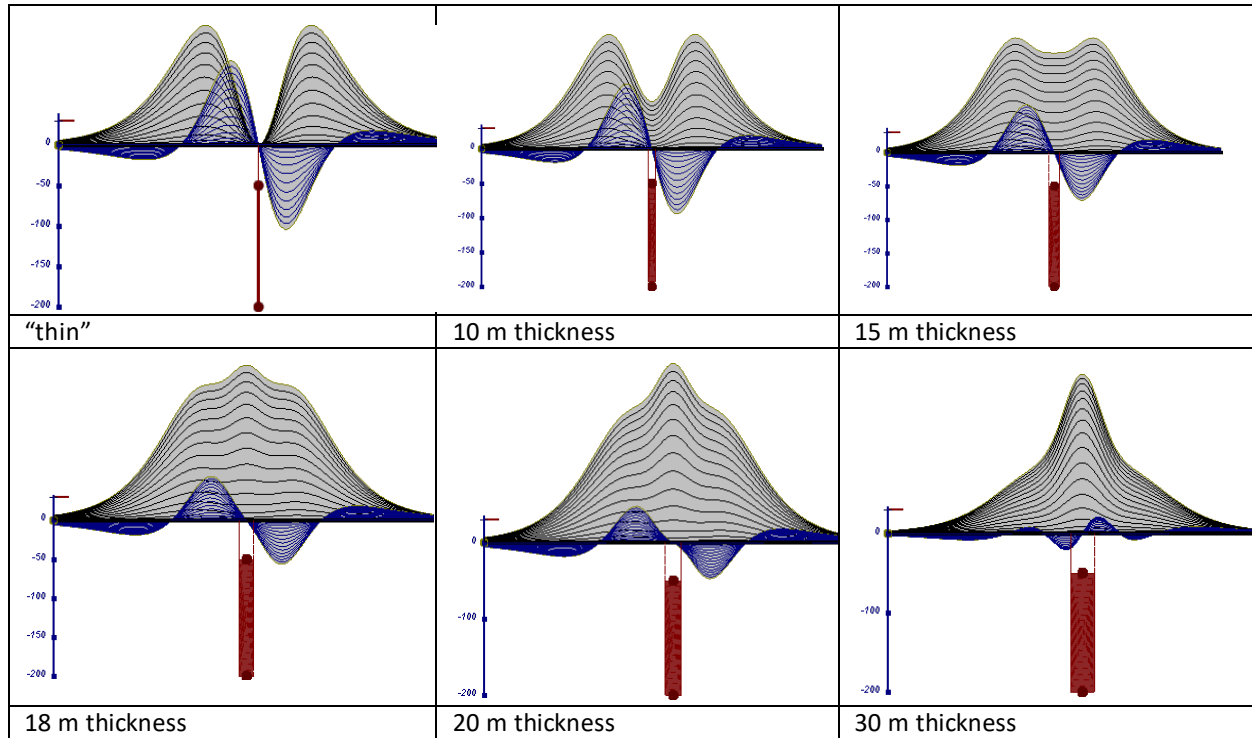
Figure D-17: Conductive vertical plate, depth 50 m, strike length 200 m, depth extends 150 m. September 2010

12 APPENDIX E

12.1 EM TIME CONSTANT (TAU) ANALYSIS

Estimation of time constant parameter[1] in transient electromagnetic method is one of the steps toward the extraction of the information about conductances beneath the surface from TEM measurements.

The most reliable method to discriminate or rank conductors from overburden, background or one and other is by calculating the EM field decay time constant (TAU parameter), which directly depends on conductance despite their depth and accordingly amplitude of the response.

12.2 THEORY

As established in electromagnetic theory, the magnitude of the electro-motive force (emf) induced is proportional to the time rate of change of primary magnetic field at the conductor. This emf causes eddy currents to flow in the conductor with a characteristic transient decay, whose Time Constant (Tau) is a function of the conductance of the survey target or conductivity and geometry (including dimensions) of the target. The decaying currents generate a proportional secondary magnetic field, the time rate of change of which is measured by the receiver coil as induced voltage during the Off time.

The receiver coil output voltage (e_0) is proportional to the time rate of change of the secondary magnetic field and has the form,

$$e_0 \propto (1 / \tau) \, e^{-(t / \tau)}$$

Where,
τ = L/R is the characteristic time constant of the target (TAU) R = resistance
L = inductance

From the expression, conductive targets that have small value of resistance and hence large value of τ yield signals with small initial amplitude that decays relatively slowly with progress of time. Conversely, signals from poorly conducting targets that have large resistance value and small τ, have high initial amplitude but decay rapidly with time[1] (Fig. E1).
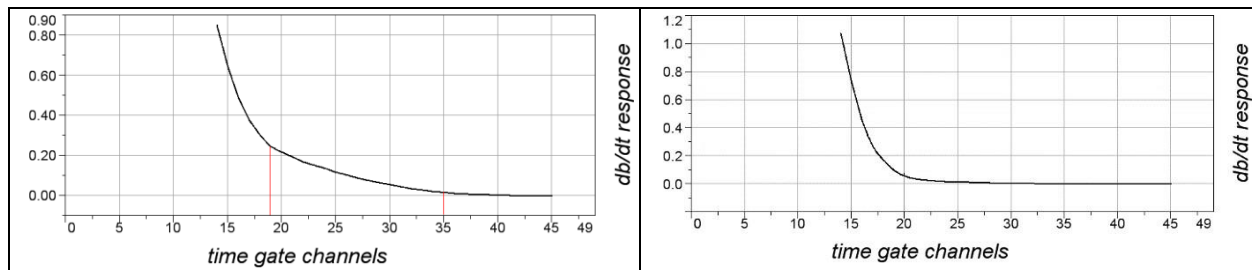
Figure E-1: Left – presence of good conductor, right – poor conductor.

---

[1] McNeill, JD, 1980, "Applications of Transient Electromagnetic Techniques", Technical Note TN-7 page 5, Geonics Limited, Mississauga, Ontario.

12.3 EM TIME CONSTANT (TAU) CALCULATION

The EM Time-Constant (TAU) is a general measure of the speed of decay of the electromagnetic response and indicates the presence of eddy currents in conductive sources as well as reflecting the "conductance quality" of a source. Although TAU can be calculated using either the measured dB/dt decay or the calculated B-field decay, dB/dt is commonly preferred due to better stability (S/N) relating to signal noise. Generally, TAU calculated on base of early time response reflects both near surface overburden and poor conductors whereas, in the late ranges of time, deep and more conductive sources, respectively. For example, early time TAU distribution in an area that indicates conductive overburden is shown in Figure 2.
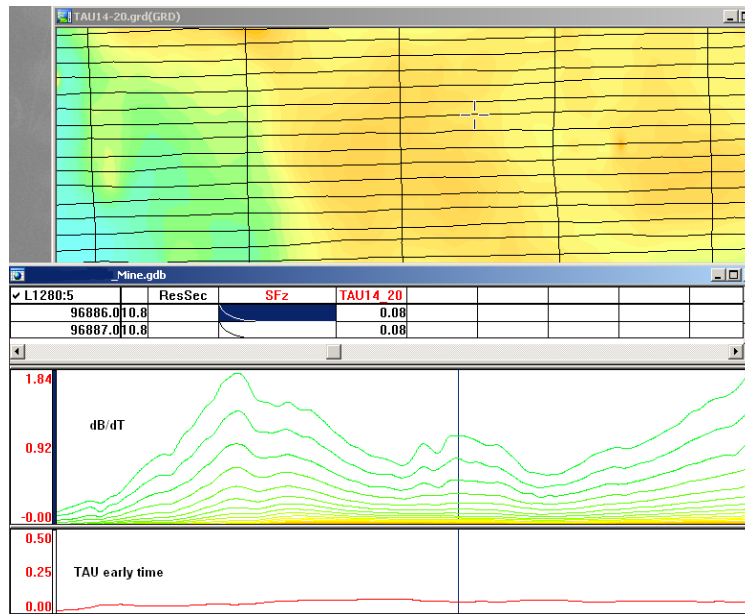
Figure E-2: Map of early time TAU. Area with overburden conductive layer and local sources.
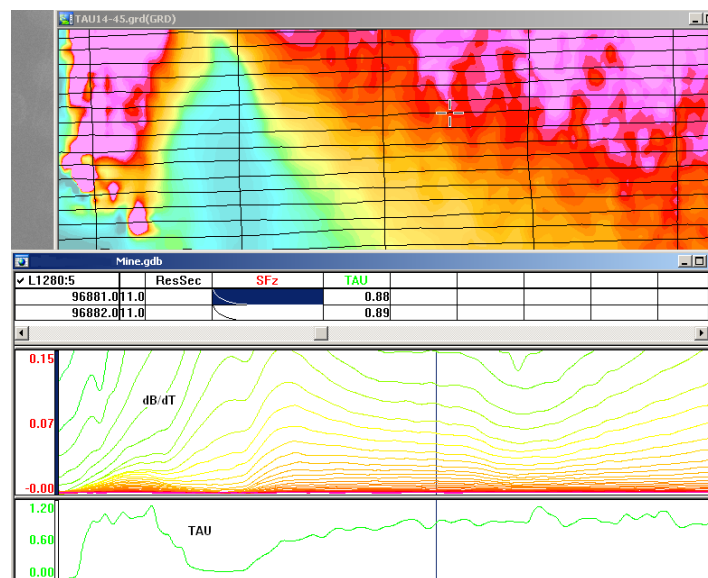
Figure E-3: Map of full time range TAU with EM anomaly due to deep highly conductive target.

There are many advantages of TAU maps:

- TAU depends only on one parameter (conductance) in contrast to response magnitude.
- TAU is an integral parameter, which covers the time range, and all conductive zones and targets are displayed independently of their depth and conductivity on a single map.
- Very good differential resolution in complex conductive places with many sources with different conductivity.
- Signs of the presence of good conductive targets are amplified and emphasized independently of their depth and level of response accordingly.

In the example shown in Figure 4 and 5, three local targets are defined, each of them with a different depth of burial, as indicated on the resistivity depth image (RDI). All are very good conductors, but the deeper target (number 2) has a relatively weak dB/dt signal yet also features the strongest total TAU (Figure 4). This example highlights the benefit of TAU analysis in terms of an additional target discrimination tool.
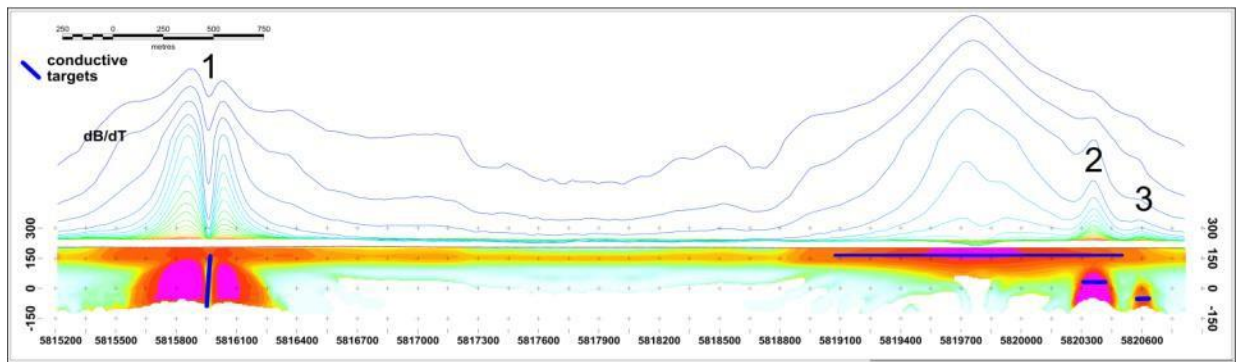
Figure E-4: dB/dt profile and RDI with different depths of targets.
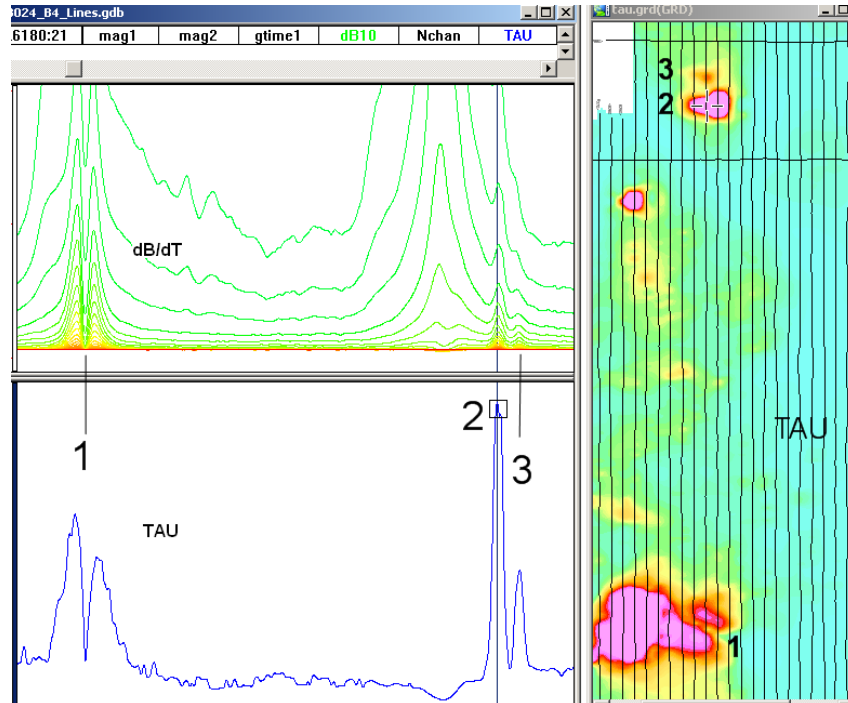
Figure E-5: Map of total TAU and dB/dt profile.

The EM Time Constants for dB/dt and B-field were calculated using the "sliding Tau" in-house program developed at Geotech2. The principle of the calculation is based on using of time window (4 time channels) which is sliding along the curve decay and looking for latest time channels which have a response above the level of noise and decay. The EM decays are obtained from all available decay channels, starting at the latest channel. Time constants are taken from a least square fit of a straight- line (log/linear space) over the last 4 gates above a pre-set signal threshold level (Figure F6). Threshold settings are pointed in the "label" property of TAU database channels. The sliding Tau method determines that, as the amplitudes increase, the time-constant is taken at progressively later times in the EM decay. Conversely, as the amplitudes decrease, Tau is taken at progressively earlier times in the decay. If the maximum signal amplitude falls below the threshold or becomes negative for any of the 4 time gates, then Tau is not calculated and is assigned a value of "dummy" by default.
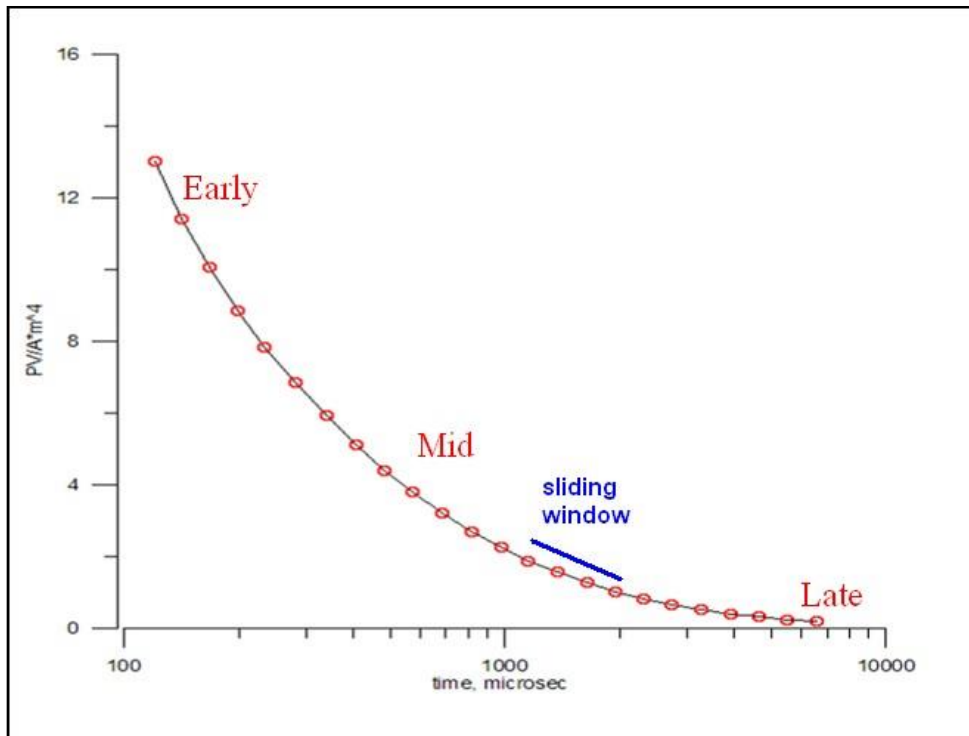
Figure E-6: Typical dB/dt decays of VTEM data

September 2010

---

[2] by A.Prikhodko

---

13 APPENDIX F

13.1 TEM RESISTIVITY DEPTH IMAGING (RDI)

Resistivity depth imaging (RDI) is technique used to rapidly convert EM profile decay data into an equivalent resistivity versus depth cross-section, by deconvolving the measured TEM data.
The used RDI algorithm of Resistivity-Depth transformation is based on scheme of the apparent resistivity transform of Maxwell A.Meju (1998)[1] and TEM response from conductive half-space. The program is developed by Geotech Ltd. and depth calibrated based on forward plate modeling for VTEM system configuration (Fig. 1-10).

RDIs provide reasonable indications of conductor relative depth and vertical extent, as well as accurate 1D layered-earth apparent conductivity/resistivity structure across VTEM flight lines. Approximate depth of investigation of a TEM system, image of secondary field distribution in half space, effective resistivity, initial geometry and position of conductive targets is the information obtained on base of the RDIs.

Maxwell plate forward modeling with RDI sections from the synthetic responses (VTEM system) are presented below:
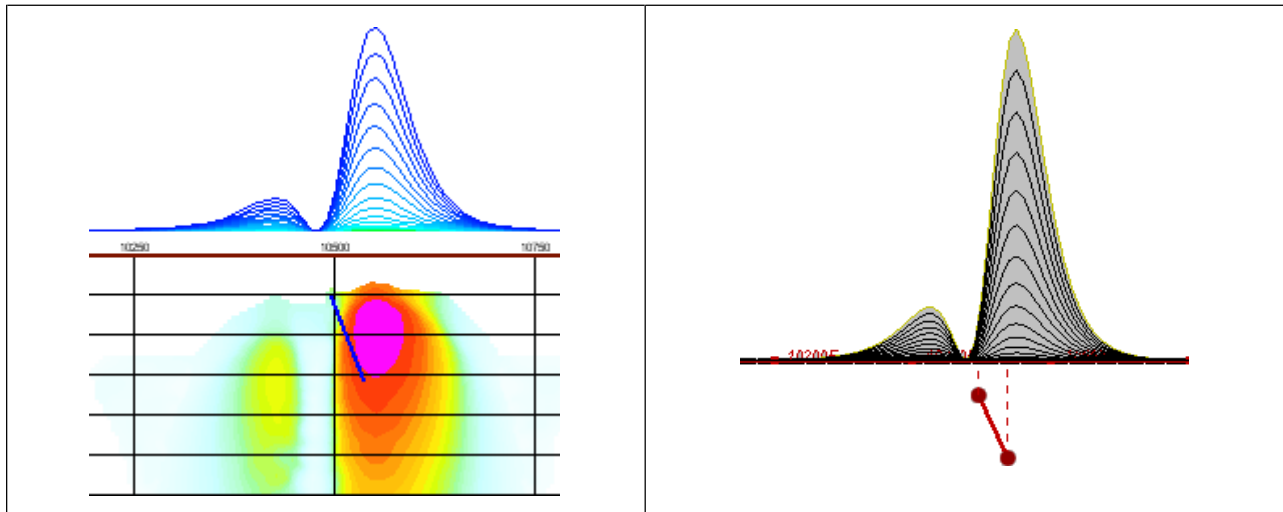
Figure F-1: Maxwell plate model and RDI from the calculated response for conductive "thin" plate (depth 50 m, dip 65 degree, depth extend 100 m).

---

[1] Maxwell A.Meju, 1998. Short Note: A simple method of transient electromagnetic data analysis. Geophysics, **63**.405–410.
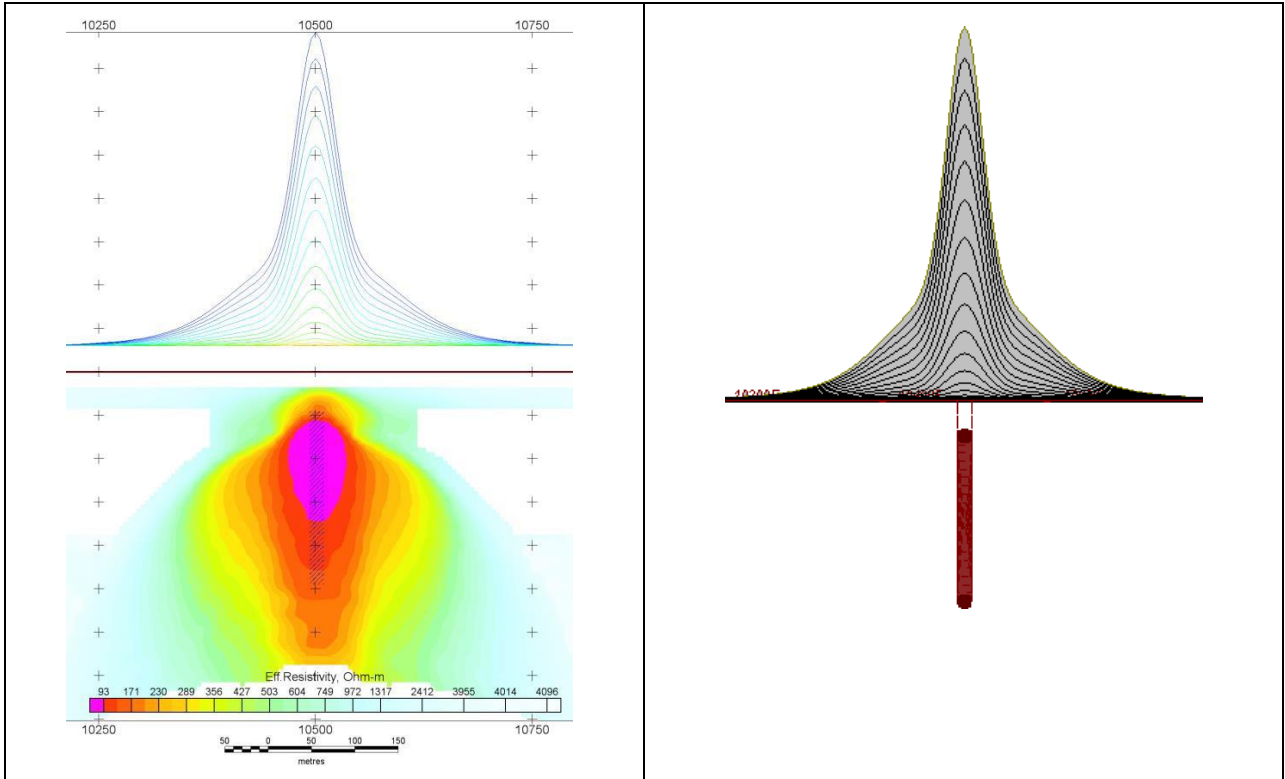
Figure F-2: Maxwell plate model and RDI from the calculated response for "thick" plate 18 m thickness,

depth 50 m, depth extend 200 m).
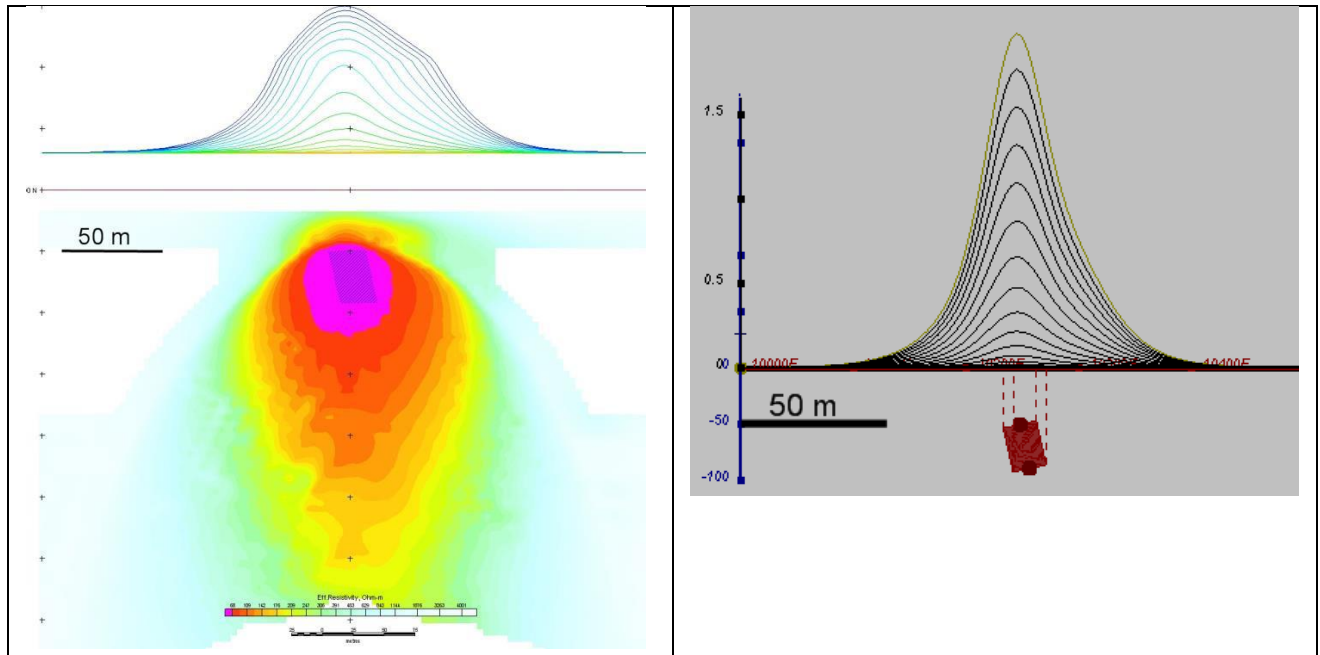
Figure F-3: Maxwell plate model and RDI from the calculated response for bulk ("thick") 100 m length,

40 m depth extend, 30 m thickness
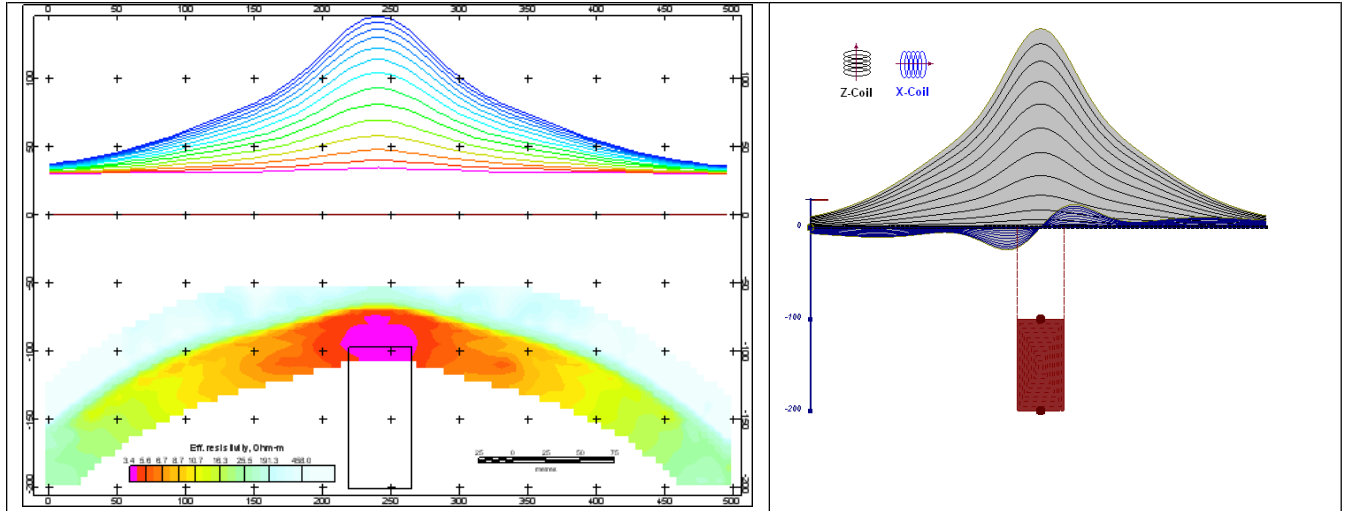
Figure F-4: Maxwell plate model and RDI from the calculated response for "thick" vertical target (depth 100 m, depth extend 100 m). 19-44 chan.
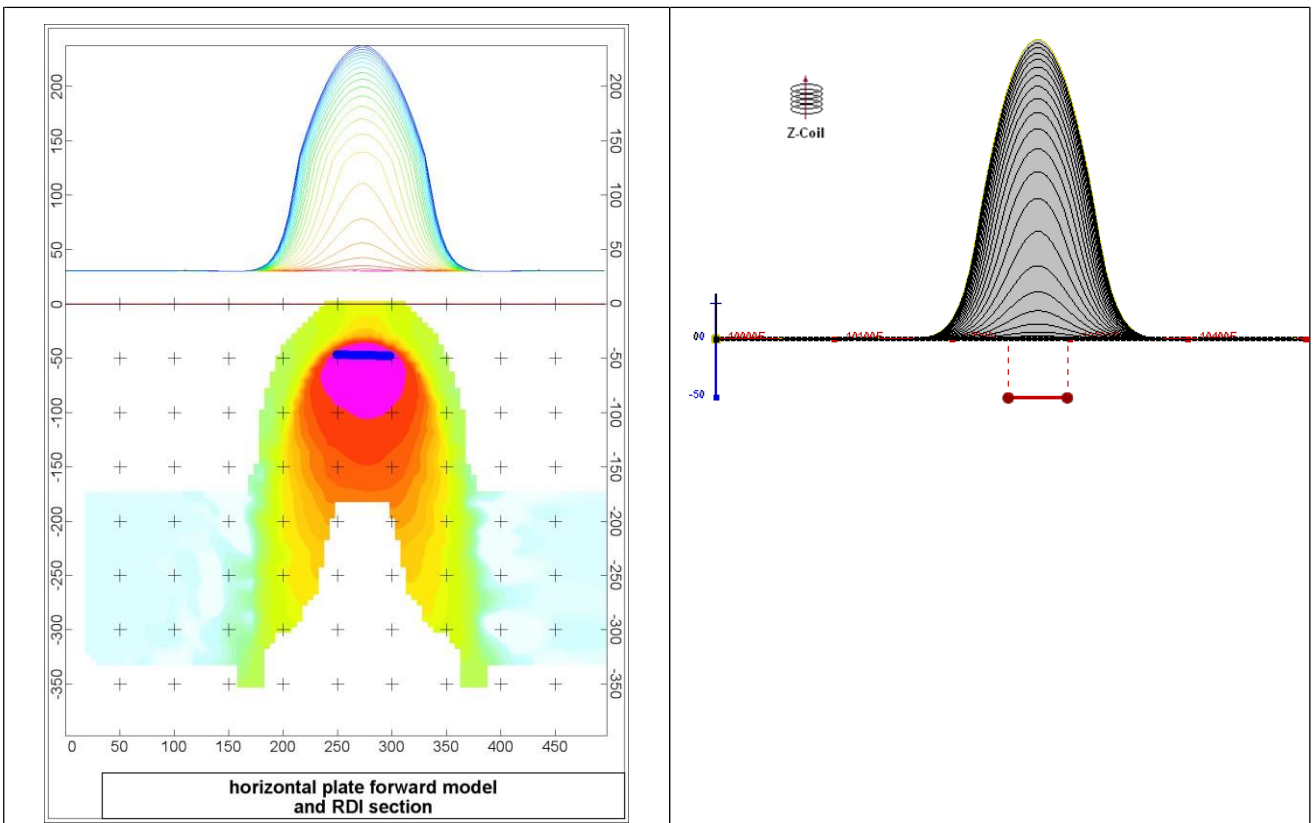
Figure F-5: Maxwell plate model and RDI from the calculated response for horizontal thin plate (depth 50 m, dim 50x100 m). 15-44 chan.
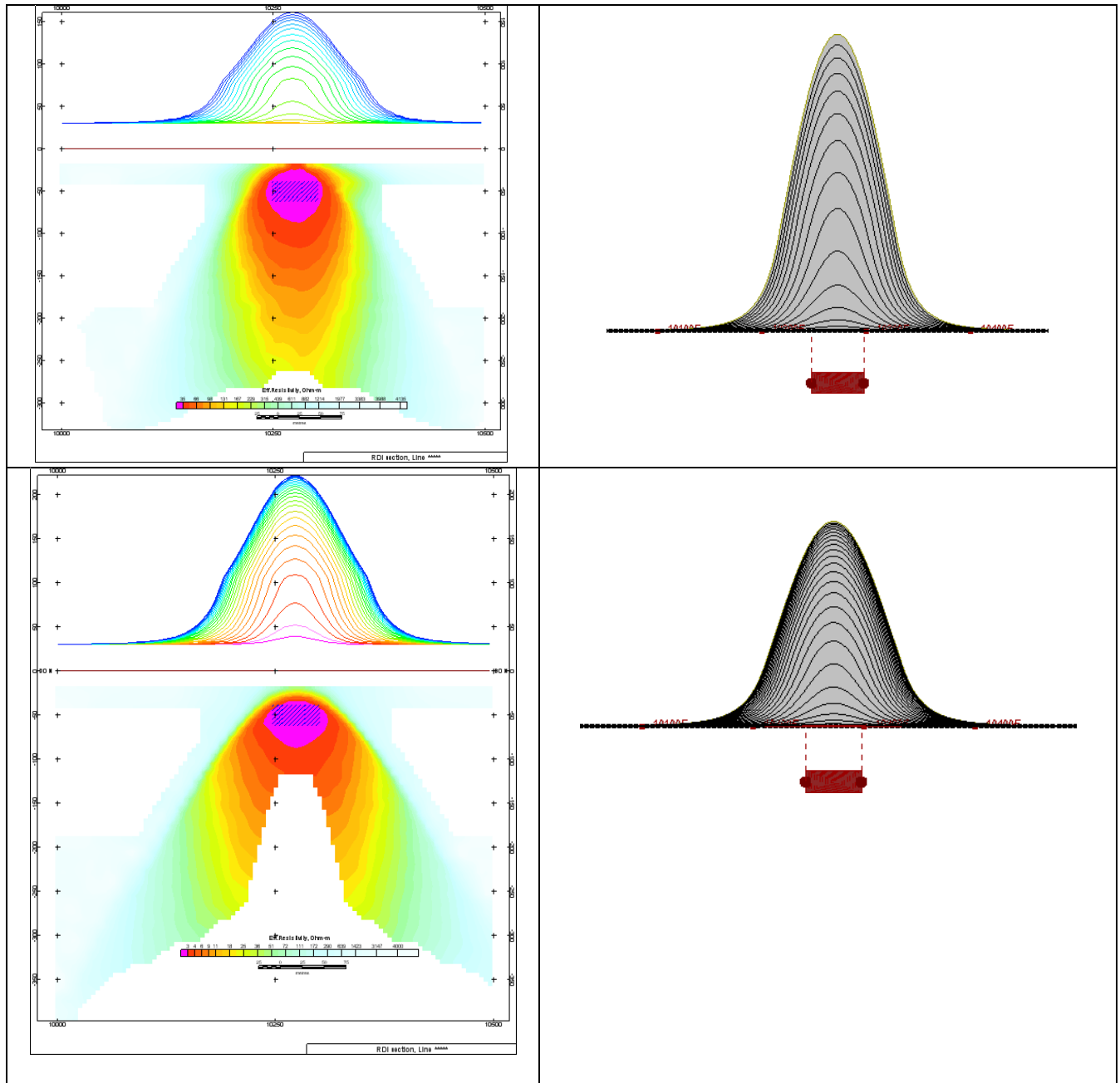
Figure F-6: Maxwell plate model and RDI from the calculated response for horizontal thick (20m) plate –

less conductive (on the top), more conductive (below).
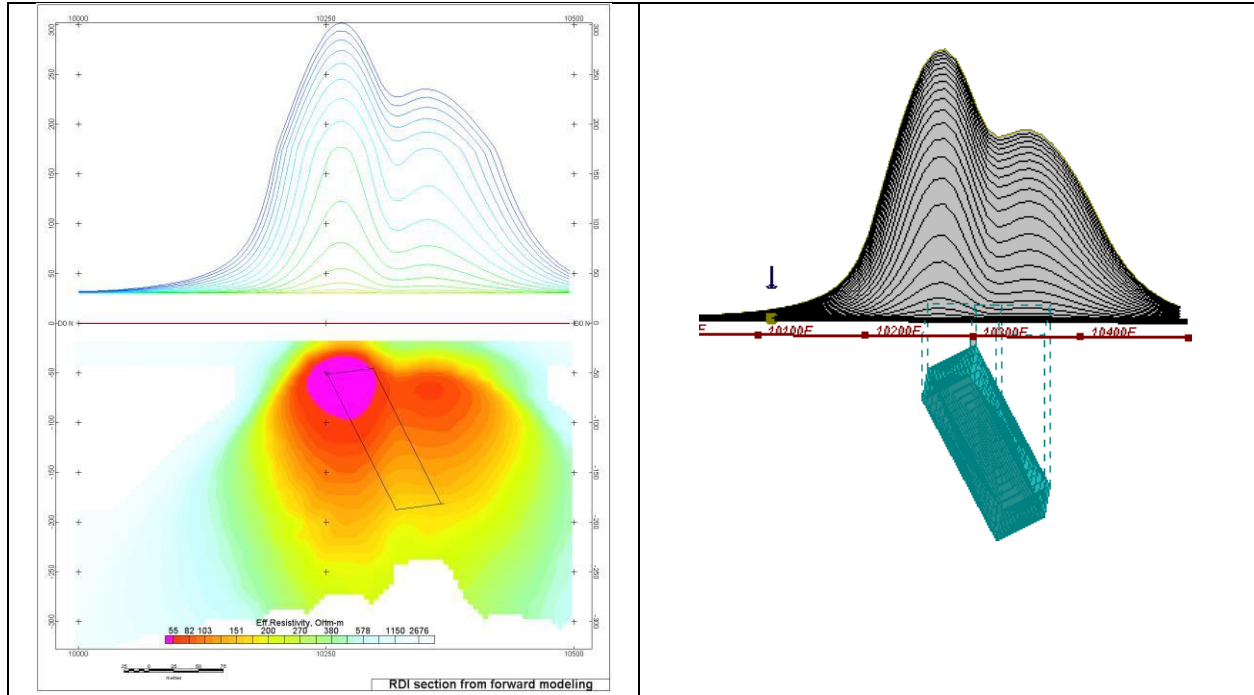
Figure F-7: Maxwell plate model and RDI from the calculated response for inclined thick (50m) plate. Depth extends 150 m, depth to the target 50 m.
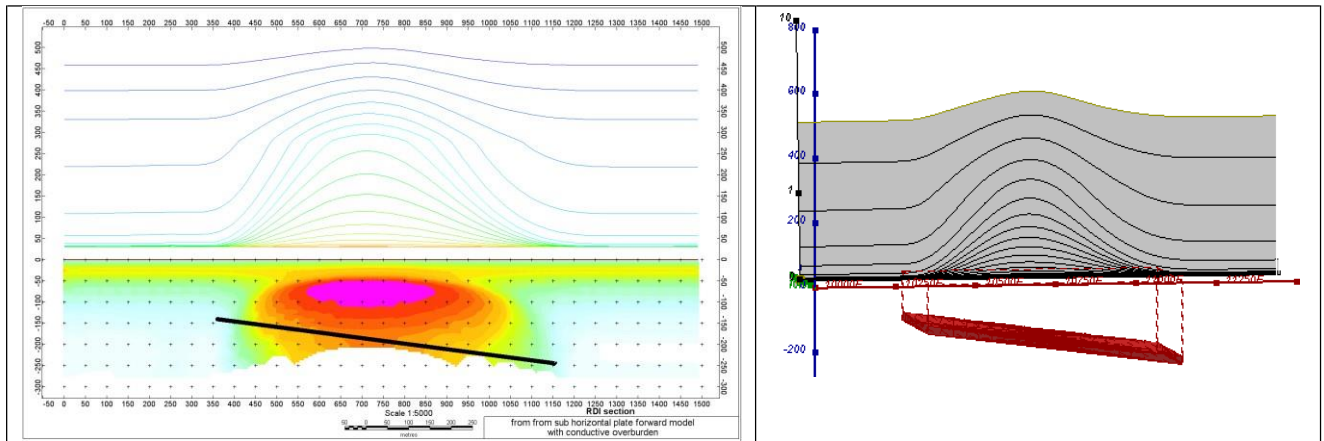
Figure F-8: Maxwell plate model and RDI from the calculated response for the long, wide and deep subhorizontal plate (depth 140 m, dim 25x500x800 m) with conductive overburden.
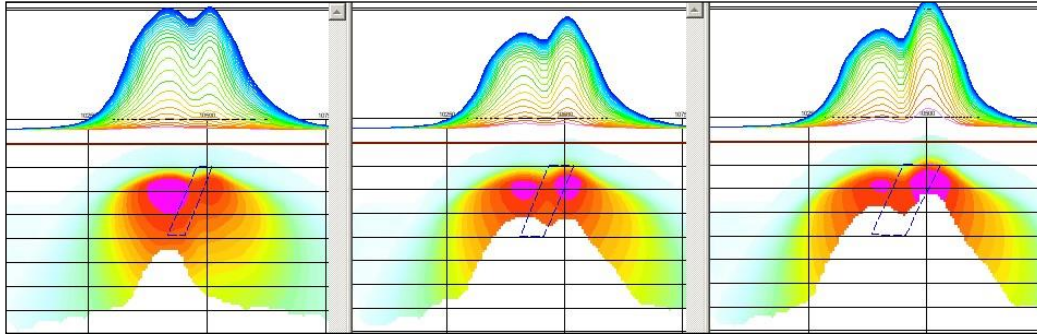
Figure F-9: Maxwell plate models and RDIs from the calculated response for "thick" dipping plates (35, 50, 75 m thickness), depth 50 m, conductivity 2.5 S/m.
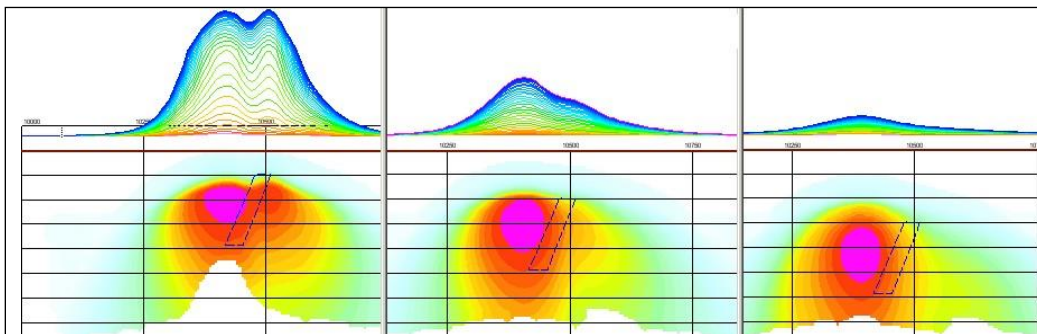
Figure F-10: Maxwell plate models and RDIs from the calculated response for "thick" (35 m thickness) dipping plate on different depth (50, 100, 150 m), conductivity 2.5 S/m.
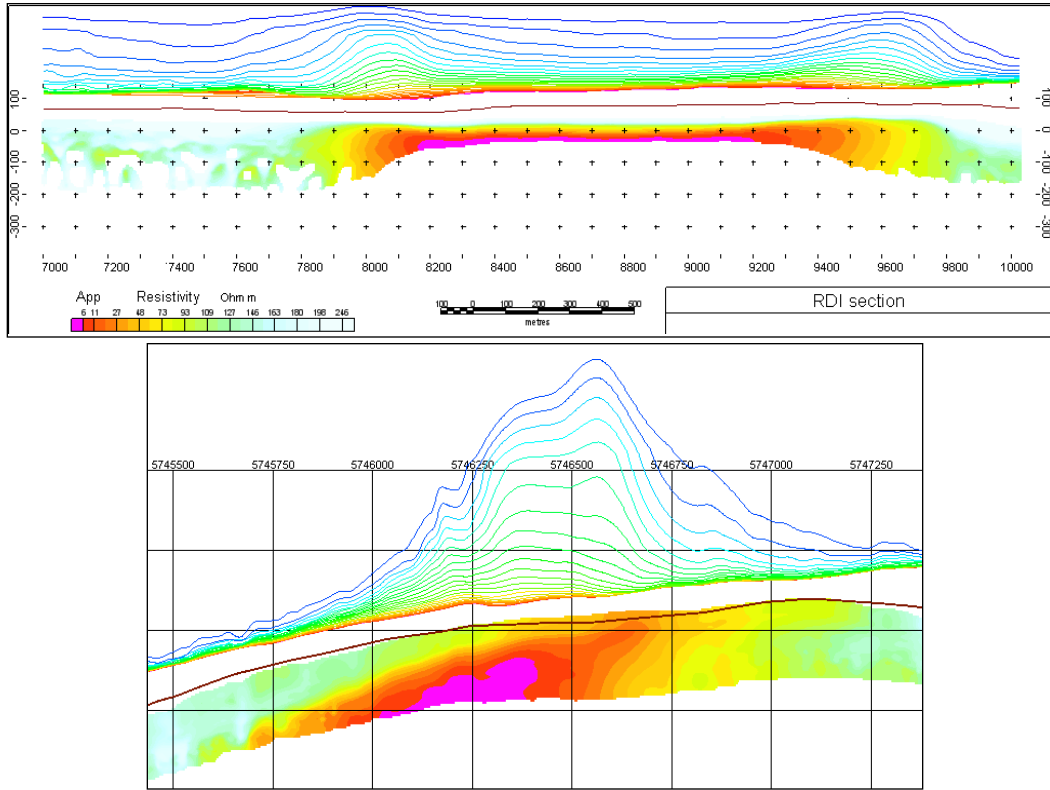
Figure F-11: RDI section for the real horizontal and slightly dipping conductive layers
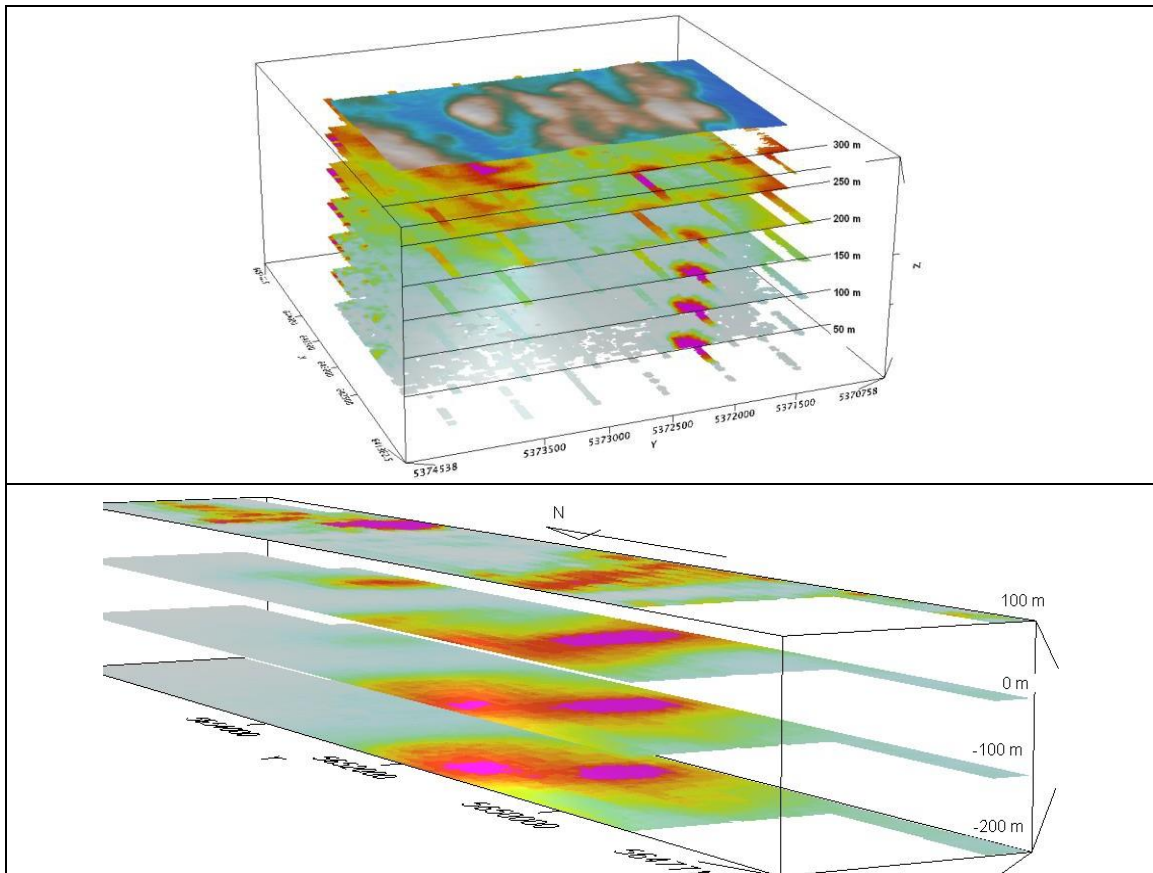
14 FORMS OF RDI PRESENTATION

14.1 PRESENTATION OF SERIES OF LINES
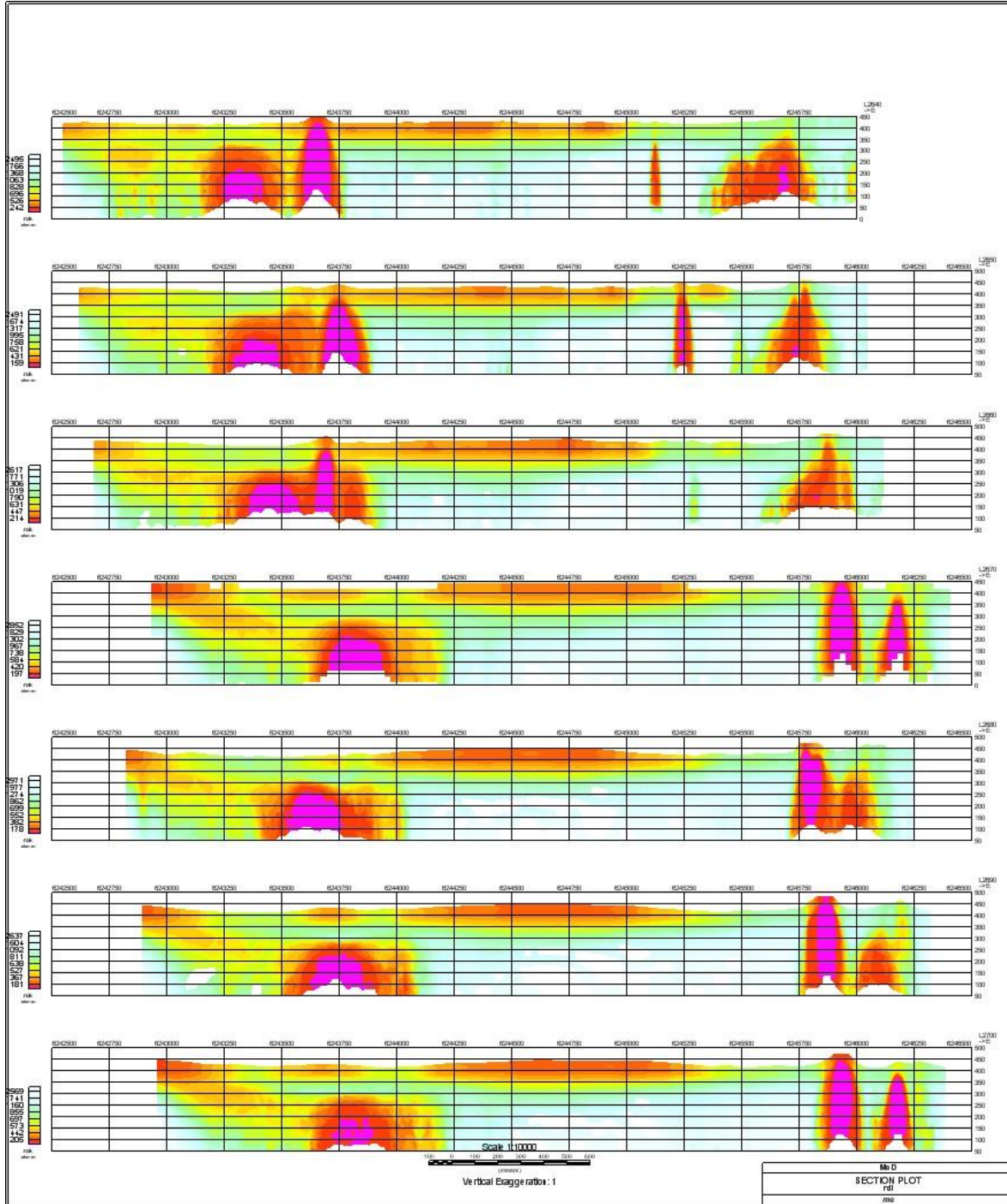
3D PRESENTATION OF RDIS
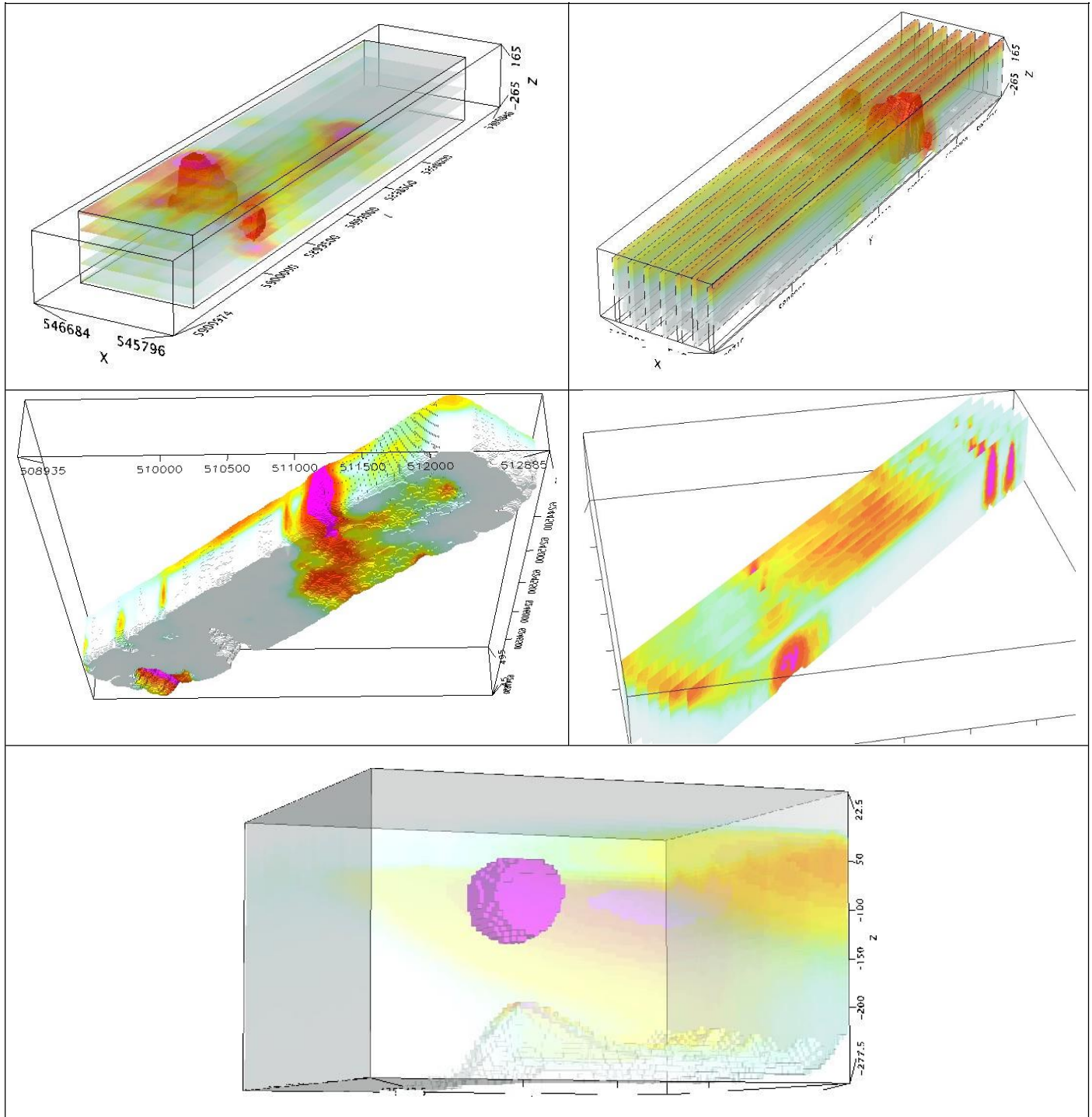
APPARENT RESISTIVITY DEPTH SLICES PLANS:
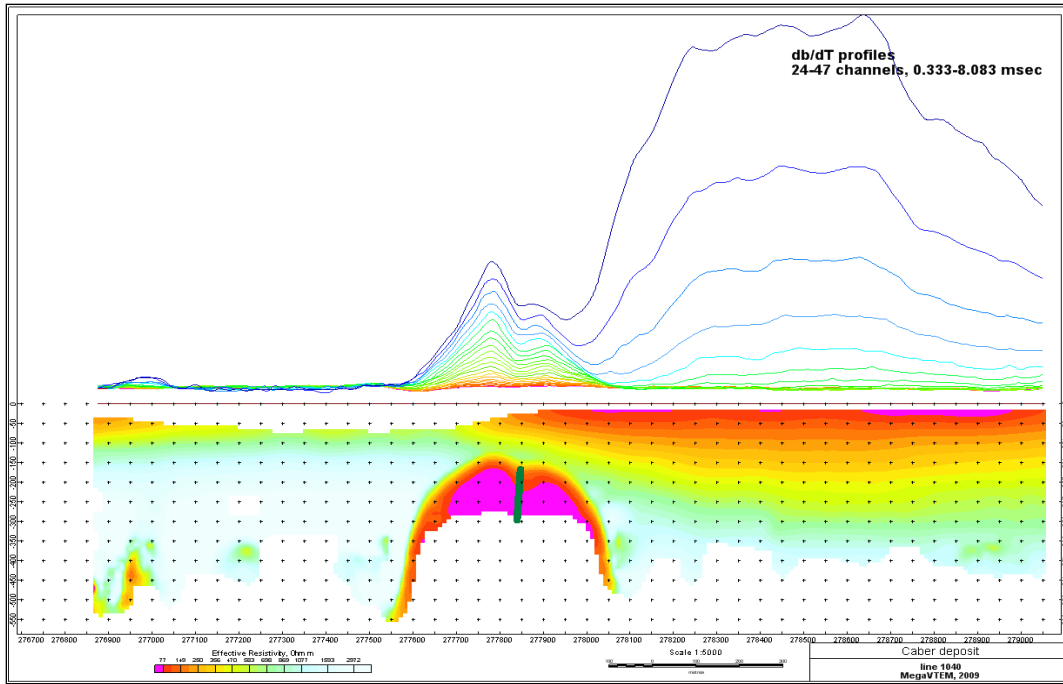

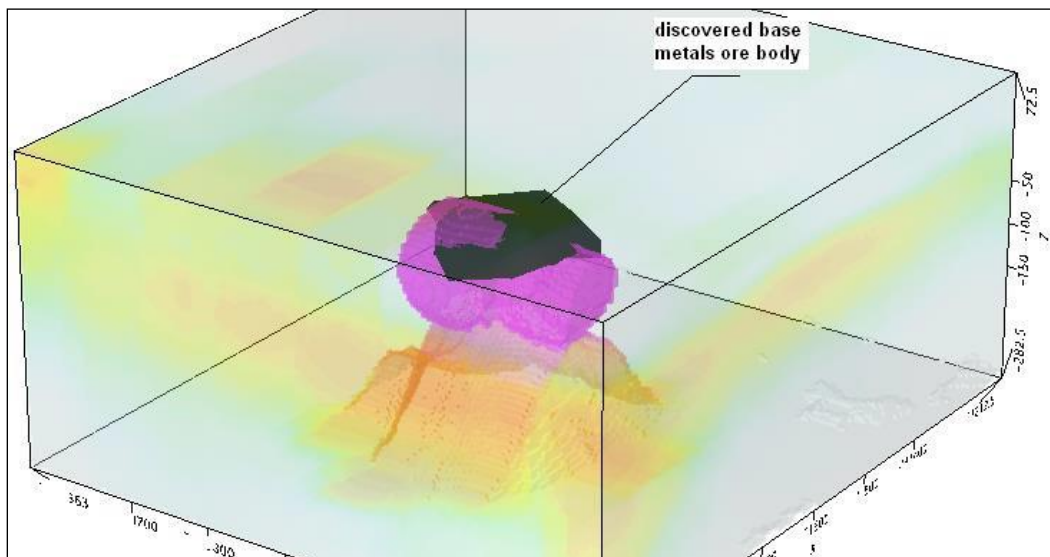| 0 m (surface) | –100 m | –200 m |
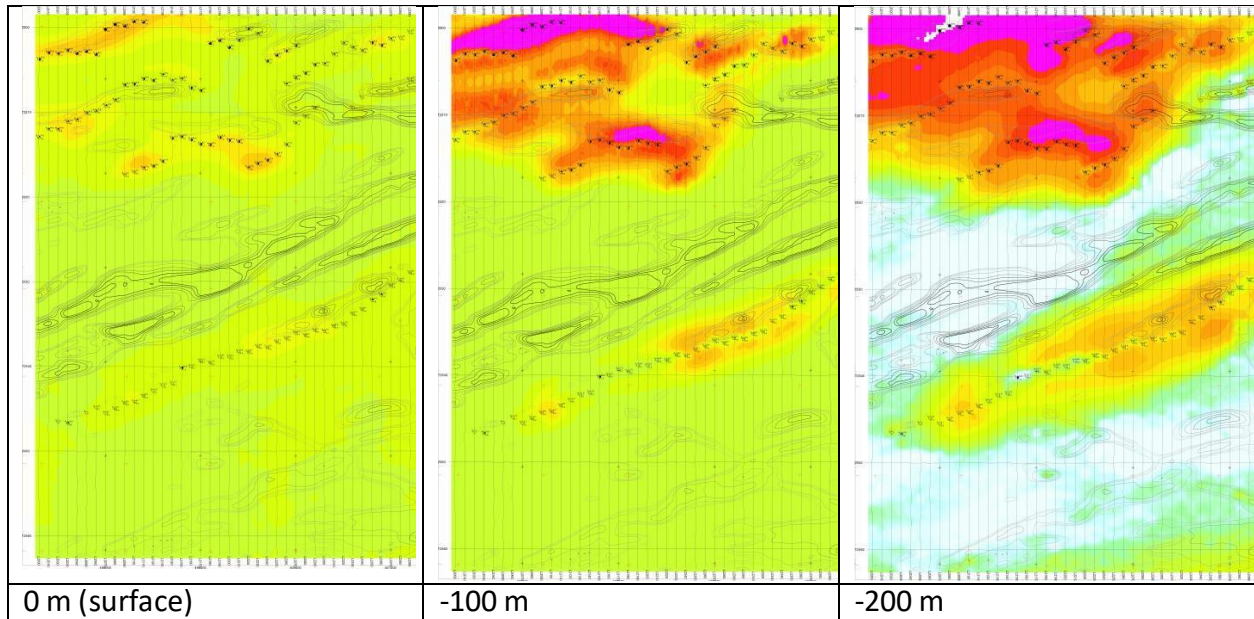
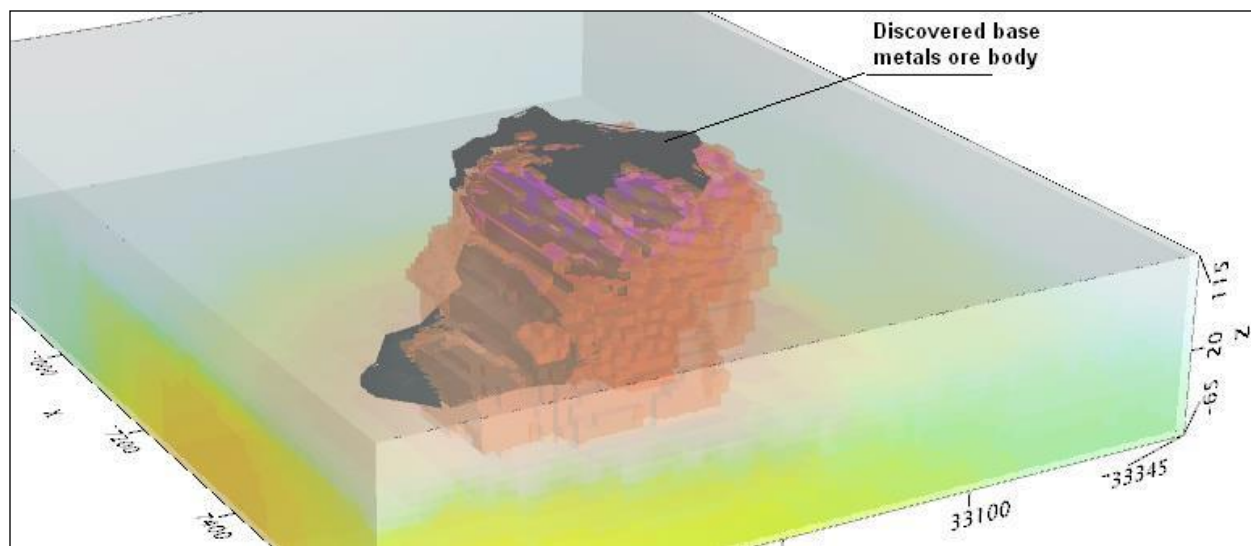3D VIEWS OF APPARENT RESISTIVITY DEPTH SLICES:

REAL BASE METAL TARGETS IN COMPARISON WITH RDIS:

RDI section of the line over Caber deposit ("thin" subvertical plate target and conductive overburden.

14.2 3D RDI VOXELS WITH BASE METALS ORE BODIES (MIDDLE EAST):

April 2011

15 APPENDIX G

15.1 RESISTIVITY DEPTH IMAGES (RDI)

Please see RDI Folder on DVD for the PDF's